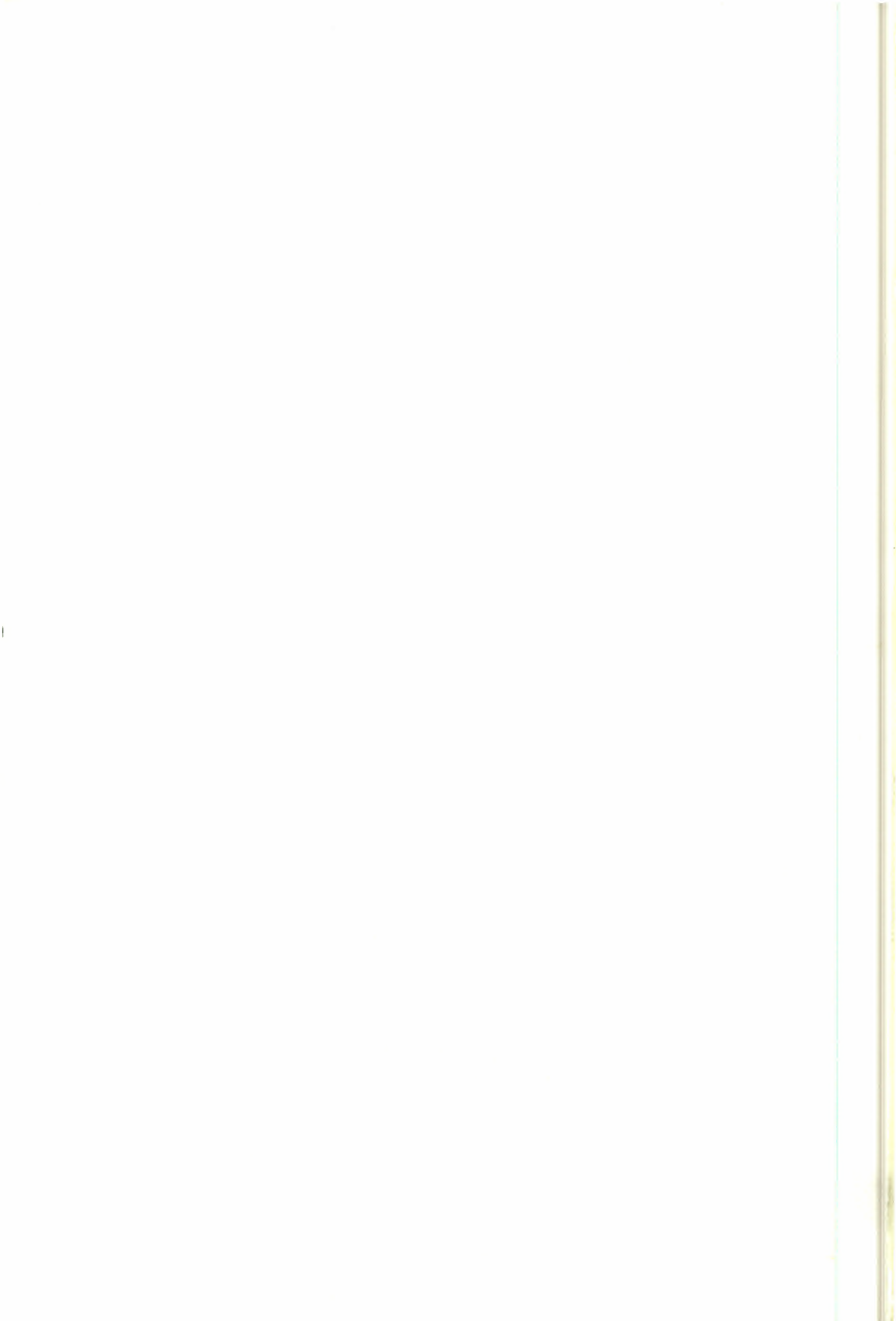


# Envisat

## GOMOS

An Instrument for  
Global Atmospheric Ozone Monitoring





**Envisat**

**GOMOS**

**An Instrument for  
Global Atmospheric Ozone Monitoring**

*Short Title:* **SP-1244 'Envisat - GOMOS'**

*Published by:* ESA Publications Division  
ESTEC, P.O. Box 299  
2200 AG Noordwijk  
The Netherlands  
Tel: +31 71 565 3400  
Fax: +31 71 565 5433

*Technical Coordinators:* C. Readings & T. Wehr  
*Editor:* R.A. Harris  
*Layout:* Isabel Kenny  
*Copyright:* © European Space Agency 2001  
*Price:* 30 Euros  
*ISBN No:* 92-9092-572-8  
*Printed in:* The Netherlands

# Foreword

This report is one of a series being published to help publicise the European Space Agency's environmental research satellite Envisat, which is due to be launched in the year 2001. It is intended to support the preparation of the Earth Observation community to utilise the measurements of the GOMOS (Global Ozone Monitoring by Occultation of Stars) instrument, which forms an important part of the Envisat payload. The heritage of the GOMOS instrument is outlined here and its scientific objectives, instrument concept, technical characteristics and scientific data products are described. Furthermore the in-flight calibration and validation, and aspects of the mission planning are also presented.

GOMOS is one of three instruments intended for atmospheric composition measurements onboard the Envisat satellite. The other two instruments are MIPAS (Michelson Interferometer for Passive Atmospheric Sounding) and SCIAMACHY (Scanning Imaging Absorption Spectrometer for Atmospheric Chartography). Further information may be found in [ESA 1998a] and on the ESA web page

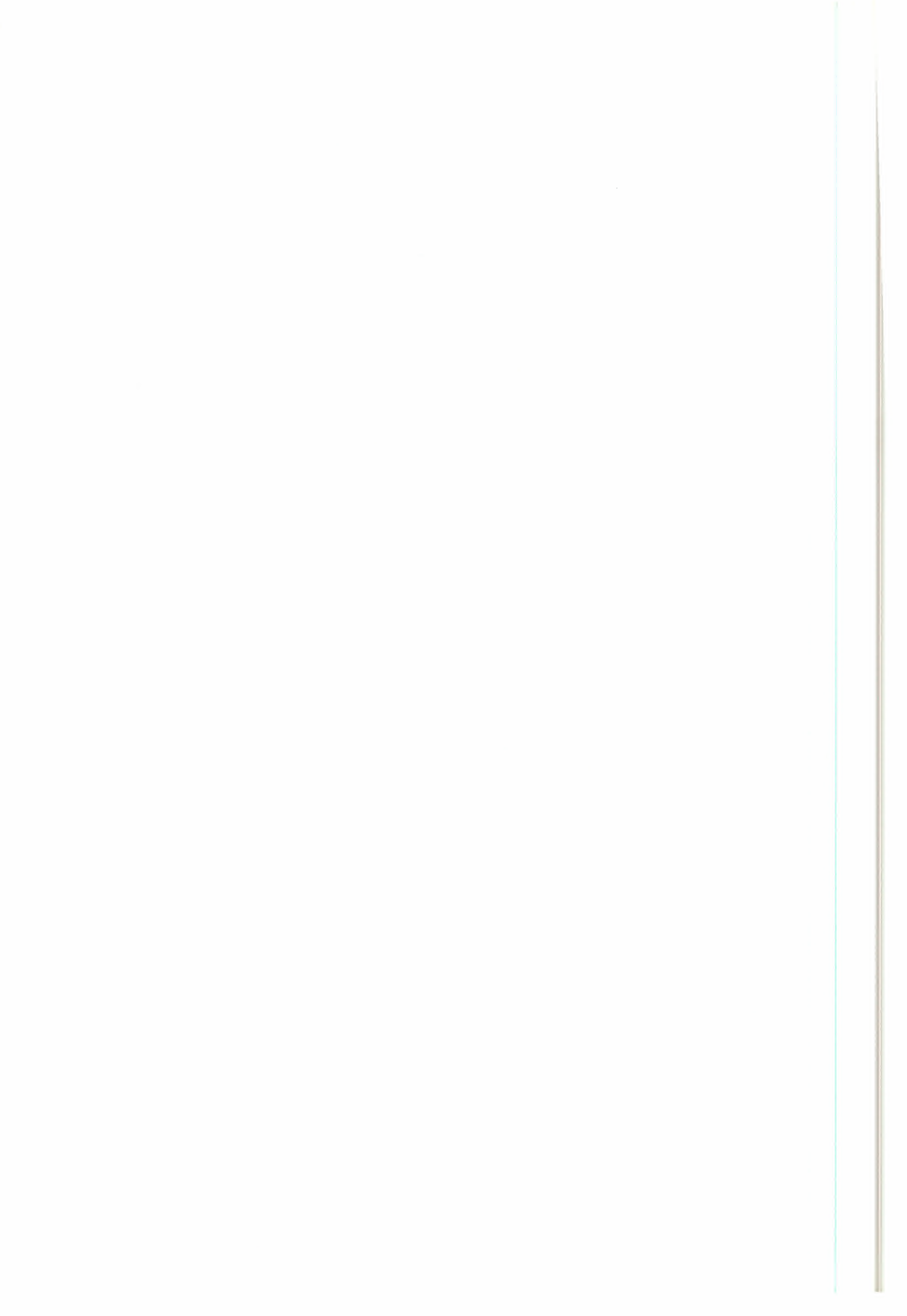
<<http://envisat.estec.esa.nl>>. A full listing of all the products planned to be made available shortly after the end of the commissioning phase (six months after launch) can be found in [ESA 1998b].

The principal authors of this report are:

J.-L. Bertaux, F. Dalaudier and A. Hauchecorne of the Service d'Aéronomie du CNRS, Verrières-le-Buisson, France, M. Chipperfield of the University of Leeds, Leeds, UK, D. Fussen of IASB, Brussels, Belgium, E. Kyrölä and G. Leppelmeier of the Finnish Meteorological Institute, Helsinki, Finland, and H. Roscoe of the British Antarctic Survey, Cambridge, UK.

The report was technically coordinated by C.J. Readings and T. Wehr; additional contributions were provided by: S. Fahmy, J. Langen and T. Paulsen.

The Agency would like to thank all those involved for their endeavours in helping to produce this report.



# Contents

<b>Foreword</b>	.iii
<b>List of Acronyms</b>	.ix
<b>Chapter 1: Introduction</b>	
1.1 The European Space Agency's Present Atmospheric Chemistry	1
Sounding Missions	
1.1.1 Upcoming Mission: Envisat	1
1.1.2 Ongoing and Future Mission: The GOME Instrument on ERS-2 and Metop	2
1.2 GOMOS Short History	3
1.3 Scientific Rationale	3
1.4 The Observation Principle	5
1.4.1 Vertical distribution, resolution and accuracy	5
1.4.2 Geographical coverage	7
1.4.3 A short history of the stellar occultation technique	7
1.4.4 Difficulties associated with stellar occultation	8
1.4.5 This Report	8
<b>Chapter 2: Scientific Objectives</b>	
2.1 Motivation	11
2.2 Current Science Issues	12
2.2.1 Monitoring Profiles of O <sub>3</sub> and Trends	13
2.2.2 Increasing Arctic O <sub>3</sub> Depletion	13
2.2.3 Mid-latitude Ozone Trends	13
2.2.4 Trends in Temperature, H <sub>2</sub> O and stratospheric aerosol	14
2.2.5 Stratospheric Dynamics	16
2.2.6 Mesospheric Ozone and Clouds	17
2.2.7 Recovery of Stratospheric Ozone	17
2.3 Ozone Depletion	18
2.3.1 Stratospheric Gas-Phase Chemistry	19
2.3.2 Heterogeneous Chemistry	20
2.3.3 Polar Ozone Depletion	21
2.3.4 Middle-Latitude Ozone Trends	23
2.3.5 Consequences of Ozone Depletion	23
2.4 GOMOS Scientific Objectives	24
2.4.1 Primary Scientific Objective: Ozone Trend Observations	25
2.4.2 Secondary Scientific Objectives	26
2.4.3 Long-term, campaign and permanent objectives	27
<b>Chapter 3: Instrument Requirements</b>	
3.1 The Required Measurement Principle	29
3.2 Instrument Requirements: Spectral Coverage and Resolution	30
3.3 The Contribution of GOMOS Measurements	32
3.3.1 Monitoring of O <sub>3</sub> Profile and Trends	33
3.3.2 Other Studies	35

## Chapter 4: Instrument Concept

4.1	Introduction	39
4.1.1	The GOMOS instrument design overview	39
4.1.2	Steering-Front Mechanism Optics (SFM)	42
4.1.3	Telescope	42
4.1.4	UV-visible spectrometer optical design	43
4.1.5	IR spectrometer chain optical design	44
4.1.6	Fast photometers optical design	45
4.1.7	Star tracker optical design	46
4.1.8	UV-visible/IR detector design	46
4.1.9	Photometer detection design	47
4.1.10	Star-acquisition and tracking-unit detection design	48
4.2	Instrument Electronic Design	48
4.3	Mechanical Design	48
4.3.1	GOMOS interface structure (GIFS)	48
4.3.2	Optical bench	49
4.3.3	Opto-mechanical cover (OMC)	50
4.3.4	Telescope Baffle Assembly (TBA)	50
4.4	Thermal Design	50
4.5	Software	51
4.6	Instrument Operation	51
4.7	How to Use GOMOS	53
4.7.1	Modes, Transitions and Commanding Overview	53
4.8	Instrument Performance Summary	55

## Chapter 5: Characterisation and Calibration

5.1	Introduction	61
5.2	Definition of Calibration versus Characterisation	61
5.3	Characterisation and Calibration Database	62
5.4	Ground support equipment	62
5.5	Wavelength Ranges, Assignment and Dispersion	63
5.6	Spectrometer Line Spread Function	65
5.6.1	Contributors to systematic errors	65
5.6.2	Measurement Method	66
5.7	Spectrometer Radiometric Uniformity	67
5.7.1	Definition of radiometric uniformity	68
5.7.2	Measurement of the uniformity map	68
5.8	Spectrometer Linearity	68
5.9	Instrument Radiometric Sensitivity	69
5.10	Instrument Signal-to-Noise Ratio	70
5.11	In-flight Calibration	70
5.11.1	Introduction	70
5.11.2	The GOMOS Calibration database	73

## Chapter 6: Mission Planning

6.1	Introduction	75
6.2	Motivation	75
6.3	Elements of the GOMOS mission planning	76
6.4	Criteria characterising mission objectives	77
6.5	Mission planning tool	78
6.6	Results	81
6.7	Summary	81

## **Chapter 7: Scientific Data Processing and Data Products**

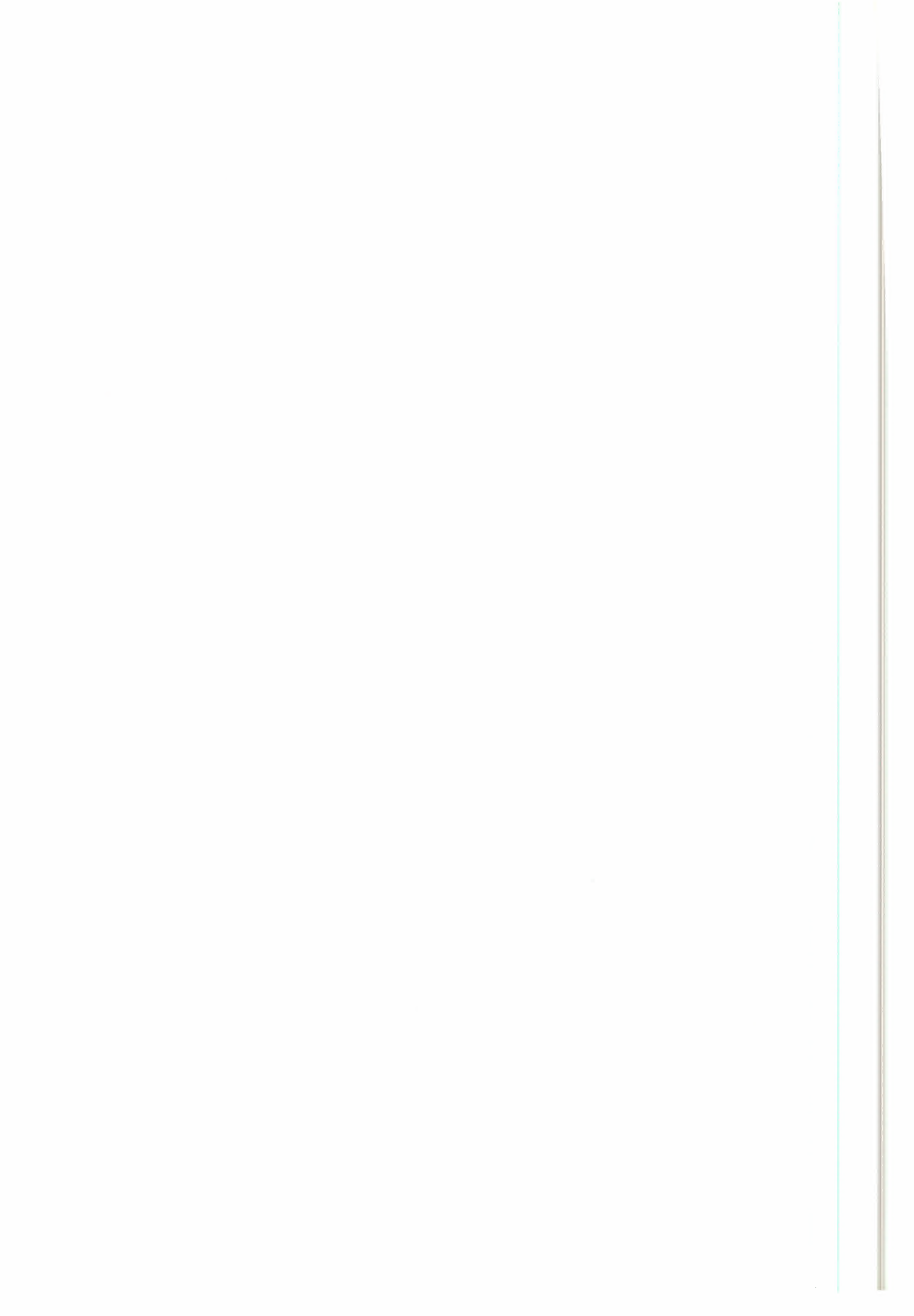
7.1	Introduction	83
7.2	Level 0-1b Processing	83
7.3	Level 1b Data Product	87
7.4	Level 1b-2 Processing	88
7.4.1	Preparation of the inversion process	90
7.4.2	The spectral inversion module	90
7.4.3	The vertical inversion module	92
7.4.4	Level 1b-2 processing loops	92
7.5	Level 2 Data Products	93
7.6	Characteristics of GOMOS products	94

## **Chapter 8: GOMOS Validation**

8.1	Internal Consistency of GOMOS Measurements	97
8.1.1	Measurements at the Same Place	97
8.1.2	Comparison of Temperature Derivations	97
8.1.3	Comparison of Ozone Derivations	98
8.1.4	Self-consistency check of NO <sub>2</sub> , NO <sub>3</sub> , O <sub>3</sub>	98
8.2	Geophysical Validation	99
8.2.1	Introduction	99
8.2.2	Campaign activities	99
8.2.3	Independent Sources of correlative data	99
8.2.4	Analyses using models	102
8.2.5	Activities of the Envisat Validation Team	103
8.3	Discussion and Conclusions	104

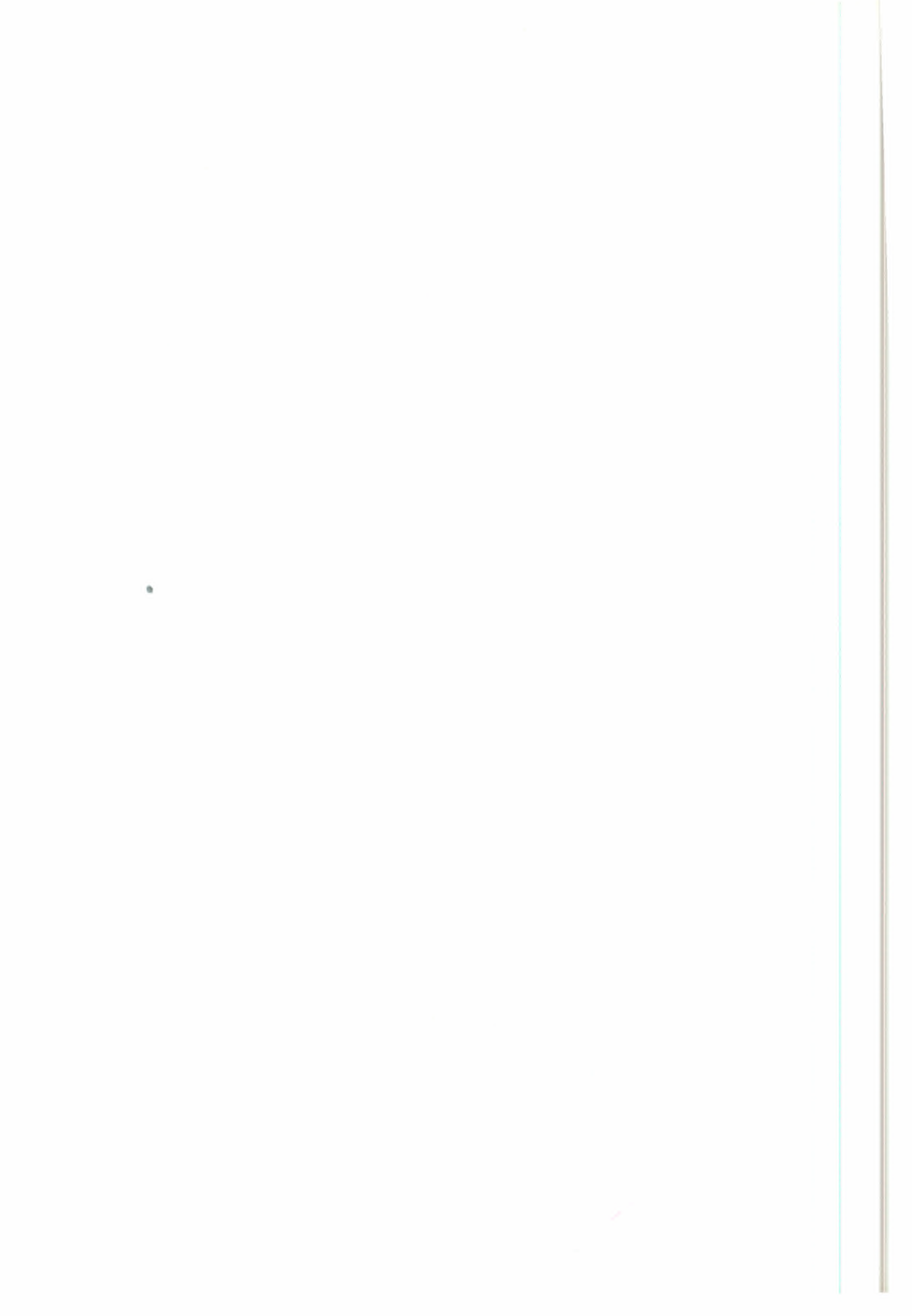
## **Chapter 9: Concluding Remarks** . . . . .105

## **References** . . . . . 107



# List of Acronyms

ACVT	Envisat Atmospheric Chemistry Validation Team
ADEOS	Advanced Earth Observing Satellite
CCD	Charge Couple Device
CFRP	Carbon-fibre reinforced plastic
CNES	Centre National d'Etudes Spatiales
COALA	Calibration for Ozone through Atmospheric Limb Acquisitions
CTM	Chemistry-transport model
ECMWF	European Centre for Medium-Range Weather Forecasts
Envisat	Environmental Satellite
ERS	Earth Remote Sensing Satellite
ESA	European Space Agency
EUMETSAT	European Organisation for the Exploitation of Meteorological Satellites
FM	Flight model
FOV	Field of View
FWHM	Full width half maximum
GCM	General circulation model
GIFS	GOMOS interface structure
GOME	Global Ozone Monitoring Experiment
GOMOS	Global Ozone Monitoring by Occultation of Stars
HIRDLS	High Resolution Dynamics Limb Sounder
ICU	Instrument Control Unit
IPCC	Inter-Governmental Panel on Climate Change
IR	Infrared
LSF	Line spread function
Metop	Meteorological Operational Satellite
MIPAS	Michelson Interferometer for Passive Atmospheric Sounding
MLS	Microwave Limb Sounder
NASA	National Aeronautics and Space Administration
NASDA	National Space Development Agency of Japan
NAT	Nitric acid trihydrate
NDSC	Network for the Detection of Stratospheric Changes
NILU	Norsk Institutt for Luftforskning
NRL	Naval Research Laboratory
NRT	Near real time
NWP	Numerical weather prediction
OMA	Opto-mechanical assembly
OMC	Opto-mechanical cover
OSIRIS	ODIN Spectrometer and IR Imager System
OSS	Optical support struts
PEB	Payload equipment bay
PMC	Polar mesospheric clouds
POAM	Polar Ozone and Aerosol Measurement
PSC	Polar stratospheric cloud
QTH	Quartz-Tungsten-Halogen
RKA	Russian Space Agency
SAGE	Stratospheric Aerosol and Gas Experiment
SAOZ	Systeme d'Analyses par Observations Zenithales
SATU	Star acquisition and tracking unit
SCIAMACHY	Scanning Imaging Absorption Spectrometer for Atmospheric Chartography
SFM	Steering-front mechanism optics
SMR	Sub-Millimeter Radiometer
SNR	Signal-to-Noise ratio
UARS	Upper Atmospheric Research Satellite
UK	United Kingdom
UV	Ultraviolet
VMR	Volume mixing ratio
WMO	World Meteorological Organisation



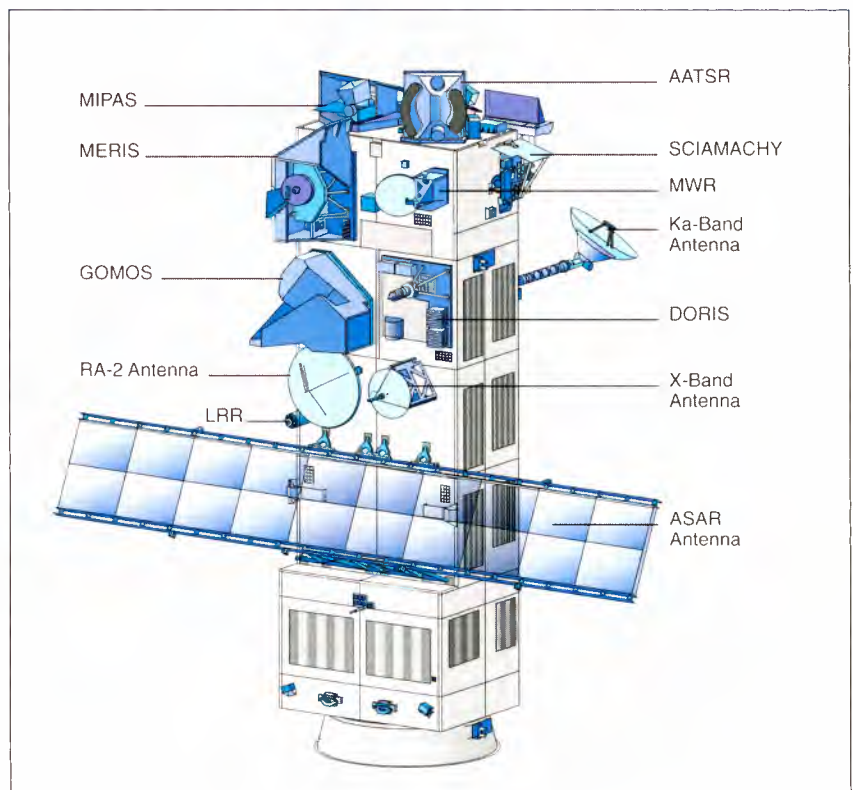
# 1. Introduction

## 1.1 The European Space Agency's Present Atmospheric Chemistry Sounding Missions

The European Space Agency (ESA) is a key-player in global atmospheric chemistry research using spaceborne instruments. Satellite instruments are the ideal tools for process studies and trend observations on a global scale. ESA's activities related to chemistry sounding include ongoing and future GOME activities and the upcoming launch of Envisat, which will carry the GOMOS instrument amongst others. In the future, atmospheric chemistry missions could be realised within the frame of the *Earth Observation Envelope Programme*. Within this programme, the Earth Explorer Missions will provide opportunities for research and technology demonstration missions.

### 1.1.1 Upcoming mission: Envisat

In mid 2001, ESA will launch the environmental satellite, Envisat, an advanced polar-orbiting Earth observation satellite, which will provide measurements of the atmosphere, ocean, land and ice over a five-year period. Envisat will be ESA's largest Earth observation mission so far. In the summer of 2001, an Ariane-5 launcher will place Envisat in a near-polar orbit at 98.5° inclination. Envisat will carry ten scientific instruments including the three instruments dedicated to



atmospheric composition sounding, MIPAS, SCIAMACHY and GOMOS.

**Fig. 1-1 The Envisat Scientific Payload**

The Envisat satellite has an ambitious and innovative payload, as depicted in Figure 1.1, which will ensure the continuity of most of the data measurements of the ESA ERS satellites. The Envisat data will support Earth sciences research and allow monitoring of the evolution of environmental and climatic changes. Furthermore, they will facilitate the development of operational and commercial applications. Besides seven other scientific instruments,

Envisat will carry the following three instruments for measuring the composition of the atmosphere.

### **GOMOS**

GOMOS is the acronym for Global Ozone Monitoring by Occultation of Stars. It is a completely newly developed instrument, exploiting stellar occultation, measuring in the ultraviolet, visible and infrared. The major objective is monitoring of the global vertical ozone distribution from the upper troposphere to the upper mesosphere. This report is concerned with GOMOS.

### **MIPAS**

The Michelson Interferometer for Passive Atmospheric Sounding (MIPAS) is, like GOMOS, a completely new development. It consists of a Fourier transform infrared spectrometer with a contiguous spectral coverage of 685 to 2410  $\text{cm}^{-1}$  and resolution of 0.035  $\text{cm}^{-1}$ . MIPAS scans the limb of the atmosphere in the aft direction or perpendicular to the flight direction, covering the upper troposphere, stratosphere and mesosphere. The measured species are ozone, the source gases  $\text{H}_2\text{O}$ ,  $\text{CH}_4$ ,  $\text{N}_2\text{O}$ ,  $\text{CO}$ ,  $\text{C}_2\text{H}_2$ ,  $\text{C}_2\text{H}_6$ , CFC-11, CFC-12, CFC-22,  $\text{CCl}_4$ ,  $\text{CF}_4$ ,  $\text{SF}_6$ , HDO, the radicals  $\text{NO}$ ,  $\text{NO}_2$ ,  $\text{ClO}$  (if enhanced), reservoir and sink species  $\text{HNO}_3$ ,  $\text{N}_2\text{O}_5$ ,  $\text{ClONO}_2$ ,  $\text{HNO}_4$ ,  $\text{HOCl}$ , and particles (cloud, aerosol, polar stratospheric clouds).

Since thermal emission in the IR is very sensitive to temperature, MIPAS will be able to precisely measure temperature. MIPAS data products will include geolocated calibrated limb emission spectra, vertical profiles of pressure, temperature,  $\text{O}_3$ ,  $\text{H}_2\text{O}$ ,  $\text{CH}_4$ ,  $\text{N}_2\text{O}$  and  $\text{HNO}_3$ . The horizontal resolution will be approximately 300 to 500 km along track. The stratosphere and mesosphere will be covered at all latitudes and

longitudes. MIPAS has been described in *ESA 2000*

### **SCIAMACHY**

The Scanning Imaging Absorption Spectrometer for Atmospheric Chartography (SCIAMACHY) has the following spectral ranges: 240-1750 nm contiguously, 1940-2040 nm, 2265-2380 nm; resolution of 0.2-1.5 nm. It features various operational modes exploiting different measurement principles: (1) Nadir mode: solar radiation (backscattered from the surface), cloud, aerosol or air. Observed species include  $\text{O}_3$ ,  $\text{NO}_2$ ,  $\text{H}_2\text{O}$ ,  $\text{CO}$ ,  $\text{N}_2\text{O}$ ,  $\text{CH}_4$ ,  $\text{BrO}$ ,  $\text{CO}_2$ , under special conditions also  $\text{SO}_2$ ,  $\text{OCIO}$  and  $\text{H}_2\text{CO}$ . (Total columns or in some cases stratospheric profiles with coarse resolution.); (2) Limb mode, backscattered solar radiation: Stratospheric profiles of temperature,  $\text{O}_3$ ,  $\text{NO}_2$ ,  $\text{H}_2\text{O}$ ,  $\text{CO}$ ,  $\text{N}_2\text{O}$ ,  $\text{CH}_4$ ,  $\text{CO}_2$ ,  $\text{BrO}$  (if enhanced) and aerosol extinction. The vertical resolution is 3 km; (3) Once per orbit a solar occultation will be performed to measure atmospheric constituents and produce 1 km resolution profiles of temperature,  $\text{O}_3$ ,  $\text{NO}_2$ ,  $\text{CO}$ ,  $\text{N}_2\text{O}$ ,  $\text{CH}_4$ ,  $\text{BrO}$ ,  $\text{CO}_2$ ; (4) Lunar occultations will be performed when possible.

#### **1.1.2 Ongoing and future mission: the GOME instrument on ERS-2 and Metop**

The Global Ozone Monitoring Experiment (GOME) is currently operating onboard the ERS-2 satellite, which was launched in 1995. GOME activities are being continued in cooperation with EUMETSAT on the future Metop missions (first launch planned in 2005), which will include the improved GOME-2 instrument. The instrument consists of a grating spectrometer operating from 240 nm to 790 nm (UV-visible-near infrared) with 0.2 to 0.4 nm spectral resolution.

Species absorbing in this region include O<sub>3</sub>, O<sub>2</sub>, O<sub>4</sub>, H<sub>2</sub>O, HCHO, SO<sub>2</sub>, NO, NO<sub>2</sub>, ClO, OCIO and BrO. The instrument's main operational mode is nadir view, measuring back-scattered solar radiation. The maximum swath is 960 km and the spatial resolution varies between 40 km × 40 km and 40 km × 320 km.

The GOME-2 instrument on Metop will have a larger swath width (1920 km, but the old swath width will also be possible), a better polarisation measurement and improvements in the optics and the calibration.

The present operational data product contains the calibrated radiances and irradiances and the geophysical products ozone and NO<sub>2</sub> total column measurements.

## 1.2 GOMOS short history

In January 1988, ESA issued a call for proposals for Announcement of Opportunity instruments to be included in the Earth Observation Polar Platform mission, the earlier name of Envisat. Among the responses received was the proposal for Global Ozone Monitoring by Occultation of Stars (GOMOS). The GOMOS proposal came from the European scientists J.L. Bertaux, R. Pellinen, P. Simon, E. Chassefière, F. Dalaudier, S. Godin, F. Goutail, A. Hauchecorne, H. Le Texier, G. Mégie, J.P. Pommereau, G. Brasseur, E. Kyrölä, T. Tuomi, S. Korpela, G. Leppelmeier, G. Visconti, P. Fabian, S.A. Isaksen, S.H. Larsen, F. Stordahl, D. Cariolle, J. Lenoble, J.P. Naudet and N. Scott.

An industrial Phase-A study was conducted for the French Space Agency, CNES, in 1989-1990. Afterwards it was decided at the ESA Member States Ministerial Conference in Madrid in 1992, that GOMOS would fly as an ESA-funded instrument on the Envisat platform. After MIPAS, GOMOS has thus become the second

ESA-developed and ESA-led atmospheric chemistry instrument on Envisat, while SCIAMACHY remains a nationally-funded instrument.

As an ESA facility instrument, GOMOS does not have a principal investigator. Instead, the scientific lead of the instrument lies in the hands of ESA, with support from the GOMOS Science Advisory Group (SAG). The members of the GOMOS SAG are presently, in alphabetic order, J.-L. Bertaux, Service d'Aéronomie du CNRS, France, M. Chipperfield, University of Leeds, United Kingdom, F. Dalaudier, Service d'Aéronomie du CNRS, France, D. Fussen, IASB, Belgium, A. Hauchecorne, Service d'Aéronomie, France, E. Kyrölä, Finnish Meteorological Institute, Finland, G. Leppelmeier, Finnish Meteorological Institute, Finland, G. Mégie, Service d'Aéronomie du CNRS, France, M. Pirre, LPCE/CNRS, France, H. Roscoe, British Antarctic Survey, United Kingdom and P. Simon, Belgian Institute for Space Aeronomy, Belgium.

## 1.3 Scientific rationale

Stratospheric ozone is the main absorber of solar ultraviolet (UV) radiation. Without ozone, life as we know it on the Earth's surface would not exist. Any significant decline in stratospheric ozone is therefore of serious environmental concern. The ozone concentration and distribution of ozone also affects the temperature structure in the stratosphere. Any change in stratospheric ozone can therefore have an effect on the heat budget of the atmosphere and could impact the climate.

Stratospheric ozone production and destruction, plus stratospheric transport and troposphere-stratosphere exchange, control ozone levels. The only source of ozone is the combination of molecular and atomic

oxygen. Atomic oxygen is produced through dissociation of molecular oxygen by solar UV radiation. Ozone is destroyed by the absorption of solar UV radiation, which constitutes the UV filter effect of the ozone layer. Fragments of the destroyed ozone molecule, molecular and atomic oxygen, can re-combine to form ozone molecules again. Besides this natural process of ozone destruction, ozone is depleted by a variety of catalytic cycles involving the oxides of hydrogen, nitrogen, bromine and chlorine. Man-made emissions of ozone depleting substances play a key-role in the drastic reduction in ozone amounts observed in the Arctic and Antarctic regions.

The understanding of those processes involving gas-phase and heterogeneous chemistry has significantly improved in the past years. However, despite the significant improvements in our understanding of stratospheric chemistry and dynamics, the science is still far from being completely resolved. For example, reductions in ozone levels are also observed at mid-latitudes, but the mechanisms responsible are not clear. Thus, stratospheric ozone research still needs further observation of ozone and other parameters relevant to the problem. In order to understand long-term changes of the stratospheric composition, accurate measurements are necessary over decades. GOMOS responds to both this requirement, by ozone monitoring with high accuracy and high vertical resolution.

Stratospheric ozone content has been declining worldwide since the 1970s. The decline is of the order of 4% to 8% per decade. After international agreements regarding the reduction of ozone destroying substances, there is hope that the destruction of ozone will slow down and that eventually recovery will occur. This is, however, a process that will take many decades

and the careful monitoring of ozone and substances related to ozone destruction is therefore necessary.

Besides the necessary ozone monitoring, several scientific questions regarding the ozone depletion processes are still open. Although measurements suggest that most of the ozone decline occurs in the lower stratosphere, in line with current hypotheses, observations of trends in ozone profiles lack sufficient accuracy for definitive statements to be made. Worse, current models of stratospheric chemistry do not predict the magnitude of the observed decline in levels of ozone. The observation of ozone trends is not only important in the lower stratosphere, but in the higher stratosphere and mesosphere as well.

GOMOS, MIPAS and SCIAMACHY on Envisat will explore different observation techniques to address issues related to the ozone problem. The instruments are highly complementary in coverage, resolution and atmospheric parameters observed. GOMOS has the great advantage of a very simple observation technique and comparatively easy algorithms for the retrieval of the atmospheric parameters. It has the potential to become a relatively inexpensive standard ozone-monitoring instrument. As GOMOS measures the attenuation of stellar light through the atmosphere, the atmospheric transmittance can be directly retrieved from the ratio of the stellar light outside the atmosphere to that passing through the atmosphere. The stellar occultation technique enables GOMOS to measure with high vertical resolution and with a global coverage. Since the instrument is in principle self-calibrating, linear ozone trends should be observable with an accuracy in the order of 0.1% per year.

## 1.4 The observation principle

GOMOS is being implemented on Envisat with its overall field of view oriented opposite to the velocity vector, allowing the instrument to observe the successive setting of various stars while the platform moves along its orbit. The principle of stellar occultation is quite simple. When the star is high above the horizon, the light spectrum of the star  $F_o(\lambda)$  is recorded by GOMOS, without any atmospheric absorption. A few seconds later, the light spectrum of the same star, observed while setting through the atmosphere, is recorded. The spectrum  $F(\lambda, z)$  is modified by the absorption of all atmospheric constituents, integrated over the line-of-sight from the satellite to the star, according to the Beer-Lambert law. When only ozone absorption is considered (for simplicity) the spectrum can be written as:

$$F(\lambda, z) = F_o(\lambda) e^{-\sigma_\lambda N(z)} \quad (1.1)$$

where  $\lambda$  is the wavelength,  $z$  is the altitude of the line-of-sight above the horizon,  $N(z)$  (molecules/cm<sup>2</sup>) is the integrated quantity of ozone along the line-of-sight and  $\sigma_\lambda$  the absorption cross section of ozone.

From Equation (1.1) one derives:

$$N(z) = -\frac{1}{\sigma_\lambda} \log \left( \frac{F(\lambda, z)}{F_o(\lambda)} \right) \quad (1.2)$$

During one single occultation, a series of line densities is obtained at various altitudes  $z$ . The vertical distribution of the local ozone density (unit: molecules/cm<sup>3</sup>) can be retrieved from this series, assuming that the atmosphere is locally

spherically symmetric. This vertical retrieval is straightforward, exploiting the so-called 'onion-peeling' technique.

Besides the extreme simplicity of the retrieval algorithm compared to other methods, the occultation technique has one enormous advantage readily expressed from the mathematical form of Equation (1.2): an absolute estimate of  $N(z)$  is obtained from the ratio of two measurements taken with the same instrument within a few seconds interval so very high accuracies are possible. The method is inherently self-calibrated, and even if the spectral sensitivity of the instrument is changing with time, the ratio and the column density  $N(z)$  will be measured correctly during the relatively short time of a single occultation. This protection against long-term drift is of course ideal for the study of trends of ozone and other constituents.

This self-calibration characteristic is shared with the solar occultation technique, used very successfully in the past by the US instruments SAGE and SAGE II, whose results are often taken as a reference for vertical ozone distributions. However, one should note that, by definition, solar occultations occur during a transient photochemical situation, which is more complex than the plain night-time situation. Furthermore, stellar occultation measurements can be performed both during night and day over a wide geographic region, providing a much denser global coverage.

### 1.4.1 Vertical distribution, resolution and accuracy

Instruments like TOMS and SBUV, observing solar back-scattered UV radiation, have successfully mapped total ozone (integrated vertical column) and monitored its trends over the past.

In principle, it is sufficient to know the total ozone to predict how much harmful ultraviolet radiation reaches the ground. However, the ozone-destruction processes depend heavily on the altitude and simulations and available trend data confirm that the ozone decrease also depends strongly on the altitude.

**Fig. 1-2 A set of synthetic weighting functions representative of a vertical occultation. The limits of the acquisition are 20 to 21.5 km, 50 to 51.5 km, respectively, from bottom to top. The second plot is a zoom of the lowermost weighting function emphasising its shape around the maximum.**

Therefore, in order to validate the understanding of the ozone evolution, one must obtain ozone measurements from the whole stratosphere, with a good altitude resolution and to high accuracy.

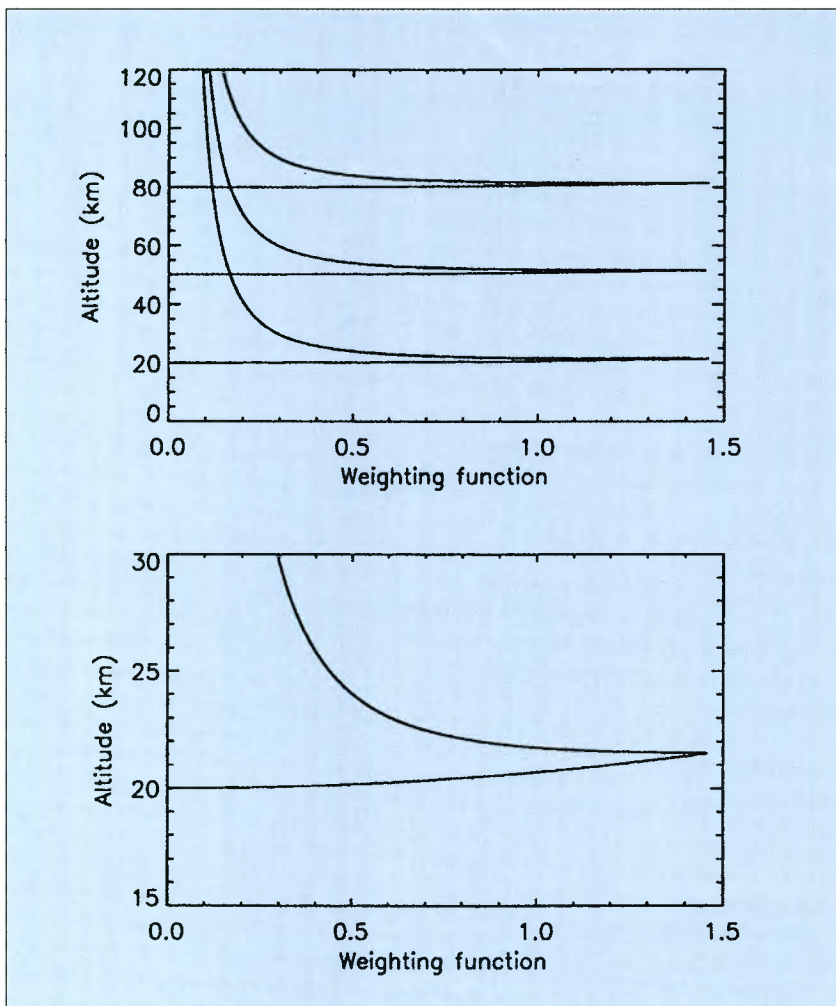
As shown in Figure 1.2, the weighting functions of the vertical

distribution, sampled by the occultation geometry, are strongly peaked, with no contribution from the regions lying below the altitude  $z$  of the line-of-sight, and a rapidly decreasing contribution from upper layers. This ensures a well-behaved solution for vertical profile retrieval.

The altitude of the measurement is entirely defined by the direction of the star and by the position of the spacecraft. The position of Envisat will be known to an accuracy of 30 m or better, ensuring accurate knowledge of  $z$ . Therefore, the location of the observed air mass, and the tangent altitude of the line of sight can be determined without considering the attitude of the spacecraft. Altitude accuracy is important, because an error of 100 m in the tangent altitude would result in a 1% error in the ozone density estimate in the altitude region above the ozone peak.

During one occultation GOMOS will measure stellar light in 0.5 sec integration time intervals. This corresponds in the worst case (occultation in the orbital plane) to an interval of  $\Delta z = 1.7$  km of altitude projected at the limb, which is equal to a quarter of a scale height. The weighting functions are accordingly modified as in Figure 1.2. The vertical resolution is therefore 1.7 km in the case of an occultation in the orbital plane and better than 1.7 km for oblique occultations.

The accuracy of the retrieved geophysical parameters depends on the temperature and brightness of the respective star. Up to about 30 km, where the Chappuis band is used to determine ozone, the accuracy does not depend on the star temperature. The accuracy at 25 km altitude is about 2% (for a star with magnitude 0) to 10% (magnitude 2) and degrades



rapidly above and below that height for a cold star (temperature up to about 6000 K). Above 30 km, where UV absorption is used, the ozone profile retrieval accuracy strongly depends on the star temperature. A star around 10000 K provides about the same accuracy for the altitude range 25 to 60 km. A star hotter than 10000 K provides an improved accuracy for the upper stratosphere and lower mesosphere. The best accuracy can be achieved around 60 km. For example, at 60 km altitude a 30000 K star provides a retrieval accuracy around 0.5% (magnitude 0) or 3% (magnitude 2).

#### 1.4.2 Geographical coverage

Inherent self-calibration and algorithm simplicity are two characteristics shared by both solar and stellar occultation. However, the stellar occultation method has superior geographical and local time coverage for two reasons:

- from a Sun-synchronous polar orbit like the Envisat orbit, solar occultations occur only in a limited range of high latitudes (North and South), preventing ozone monitoring in the mid latitudes.
- there is only one Sun, but there are many stars.

Simulations have shown that the occultation of 25 to 45 stars can be observed in a single orbit, distributed over all latitudes. It can be noted that when a star is observed on one orbit, it can also be observed during the following orbit at almost the same latitude. As the star is fixed in an inertial system, the orbital plane has moved by only a small fraction ( $\approx 1/15$ ) of a degree and the Earth has rotated by  $25^\circ$ . Therefore, the succession of points of occultation of

the same star are aligned along a constant latitude circle, regularly spaced in longitude. (An example of the distribution of occultations will be shown in Chapter 6: Mission Planning, Figure 6.8.) In addition, because there are  $14+11/35$  orbits per 24 hours, nearly the same longitude sampling applies three days later, and sampling on day two and day three are interlaced with those of day one. Since the correlation time of ozone is more than three days [Frederick 1984], it will be of great interest to regroup three days of orbit to provide a more complete global coverage. GOMOS mission planning will be discussed in a separate chapter when an example of the global coverage will be given.

#### 1.4.3 A short history of the stellar occultation technique

The stellar occultation technique has been reviewed by *Smith & Hunten, 1989*. It has been used several times to probe the vertical structure of planets (and Titan), exploiting refraction. GOMOS will exploit the *absorptive* properties of the occulted atmosphere, as described on detail by e.g. *Hays and Roble, 1968*. The technique has only been used to observe the Earth's atmosphere a few times in the past from orbit: for the detection of  $H_2$  with the Copernicus satellite [Atreya et al., 1976] and for the vertical profile of ozone with OAO-3 [Riegler et al., 1976,1977]. This observation yielded the first direct observation of the secondary maximum of ozone at 90 km.

However, the quantity of ozone, which was derived from the measurements around 50 km was larger (by a factor of three) than predicted by models for reasons which were never elucidated. It might have been a combination of imperfect orbit knowledge (10 km) and the presence of some other

absorber besides ozone. The problem is that with only one wavelength monitored during the occultation, one can never be sure of the identification of the absorber, and indeed in most cases there is more than one absorber at any wavelength, modifying Equations (1.1) and (1.2).

The advent of multi-element detectors has allowed enormous progress to be made in exploitation of the technique of stellar occultation by using instruments capable of making 'multi-spectral' occultations: the absorption of the atmosphere is measured simultaneously at many wavelengths, ensuring the proper identification of the various absorbers and discriminating their individual contribution for each line-of-sight. This is because the cross sections,  $\sigma_\lambda$ , of gaseous absorbers vary as a function of wavelength, their *spectral signature*.

#### **1.4.4 Difficulties associated with stellar occultation**

The most obvious difficulty is the weakness of the stellar fluxes compared to the levels of solar radiation. This calls for a relatively large optical collecting area compared to the optics requirements of a solar occultation instrument. Another important difference to solar occultation is the significant variation in temperature and brightness between the stars. This results in a corresponding variability of measurement precision and accuracy.

Atmospheric refraction causes loss of light, by dilution, when lower parts of the atmosphere are probed (below 30 km). Here, the light path is not a straight line. In addition to that, the short-term variability of the density and temperature of the air along the light path results in scintillations in the light intensity detected by

GOMOS. These fast variations of light intensity do not occur simultaneously at all wavelengths so the spectrum of a star seen through the atmosphere is not only affected by absorption, but is also deformed by scintillations. This problem is resolved by the use of two fast photometers, which allow the measurement of scintillations and reconstruct the actual deformation of individual spectra. Furthermore, the analysis of the scintillation signal can be used to retrieve the vertical fine structure of the atmosphere that causes the scintillation.

On the day-side, the bright limb is an extended source competing with the stellar signal, calling for a small instrument field-of-view, which in turns requires an accurate pointing. Clearly, day-side occultations will achieve less accurate results than night-side occultations, but they are considered necessary, to avoid a possible bias linked to photo-chemistry.

#### **1.4.5 This report**

This report discusses the GOMOS instrument on Envisat. The aim is to present the scientific rationale, instrument concept, data processing and products in sufficient detail for the scientific reader.

Chapter 2 presents the scientific rationale and derived mission objectives, followed by the instruments requirements in Chapter 3. The instrument concept is presented in Chapter 4, with an emphasis on the technical details necessary to understand of the technical concept and modes of operation. Instrument characterisation and calibration are described in Chapter 5.

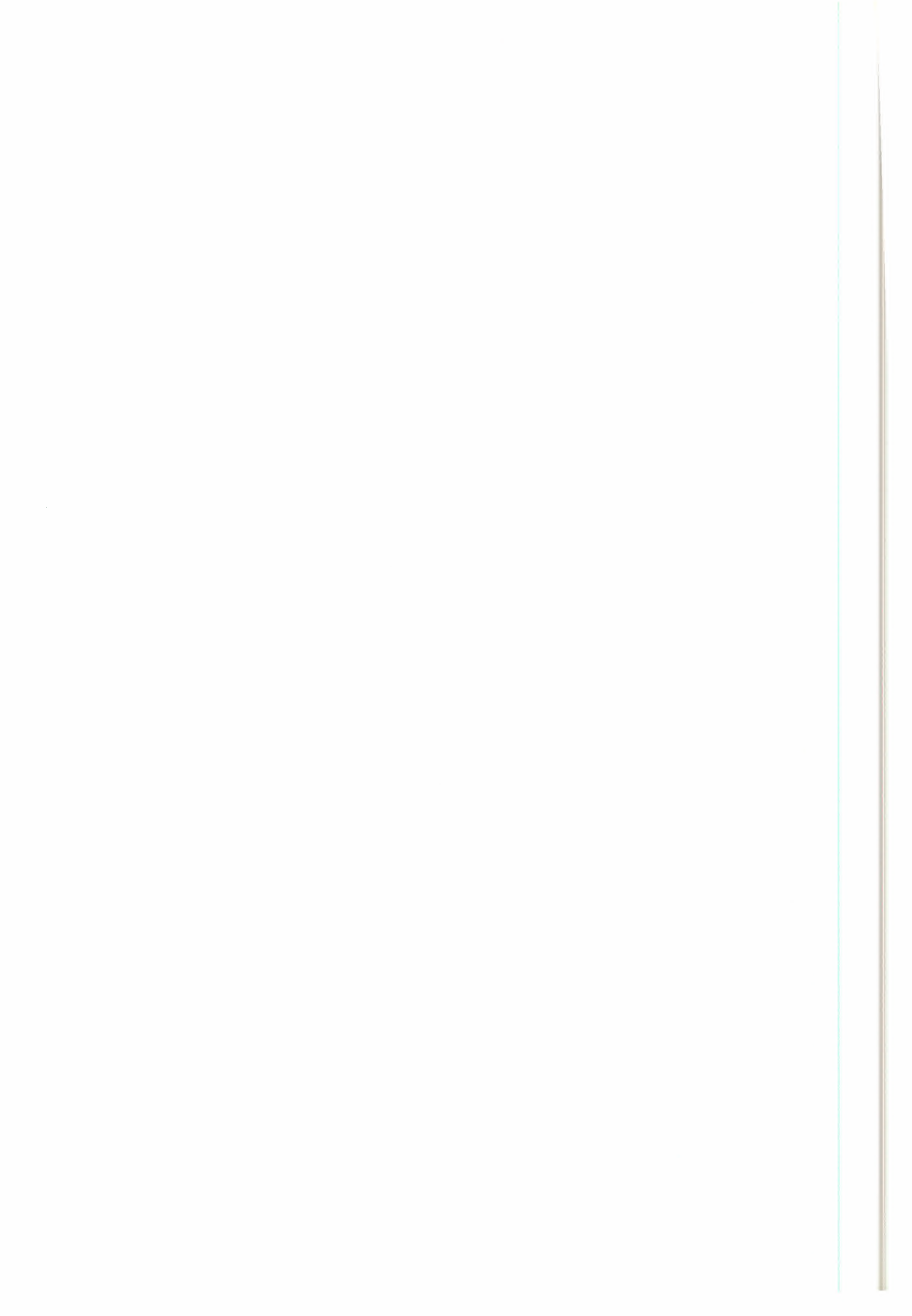
The fact that GOMOS uses stars as light sources means that, most of the time, choices have to be made as to

which star to use amongst several alternatives lying in the instrument's field-of-view.

A selection procedure has been developed to optimise the star selection in order to fulfil the mission objectives, as described in Chapter 2, in the best way. This mission planning strategy is described in Chapter 6.

The GOMOS data products are discussed in Chapter 7. This includes the scientific data processing and a discussion of the retrieval approach. Chapter 8 outlines the planned data validation activities.

The overall conclusion is that GOMOS, an instrument for stratospheric and mesospheric ozone monitoring, as its primary objective, particularly well suited for trend observation because it exploits the self-calibrating principle of stellar occultation. The occultation principle make the data analysis relatively simple and the use of stars instead of the Moon or Sun as the light source results in a very good global coverage, including tropical regions, mid-latitudes and polar regions.



## 2. Scientific Objectives

### 2.1 Motivation

The stratospheric ozone layer protects the Earth's surface from ultraviolet (UV) radiation. It extends from the tropopause, at a height of around 8 km (in polar regions) or 15 km (in the tropics), to the stratopause at around 50 km. The stratosphere is characterised by an increase in temperature with height, caused by the absorption of solar UV radiation by ozone. The highest concentration of ozone is typically at an altitude of around 25 km, as shown in Fig. 2-1. The stratosphere contains about 90% of the total atmospheric ozone.

Normally the stratospheric ozone layer absorbs UV-B radiation almost completely, preventing it from reaching the Earth's surface. Ultraviolet radiation (UV-B at 290-320 nm and UV-C at 200-290 nm) is strongly absorbed by the DNA molecules of living cells and can alter or stop the reproductive processes of these cells. Therefore, a substantial reduction of stratospheric ozone can increase the risk of skin cancer and other genetic disorders caused by UV-B radiation in flora and fauna.

The absorption of UV by ozone is the most important heat source in the stratosphere. A decrease in stratospheric ozone concentrations would therefore have an impact on stratospheric temperatures, which would lead to a disturbance in the

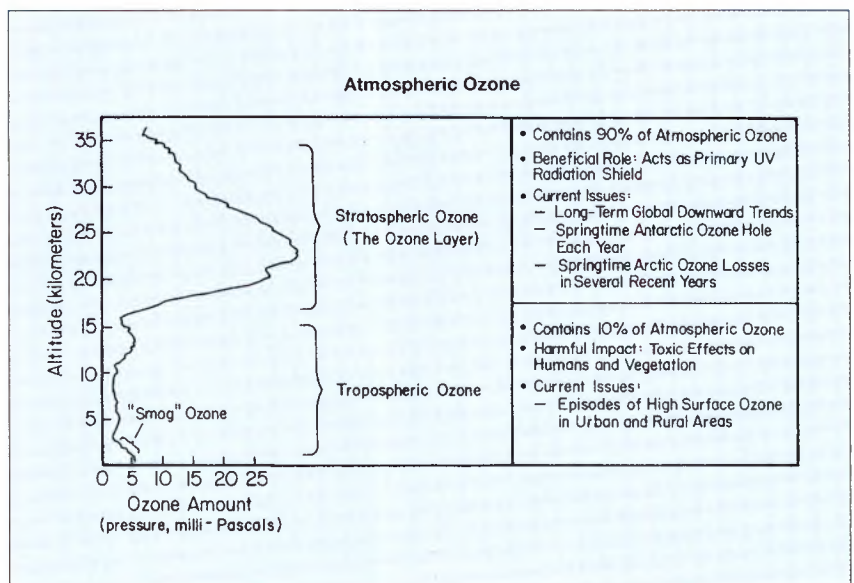


**Fig. 2-1 Typical distribution of ozone. (WMO, 1998)**

dynamics, with a possible impact on the climate system. Furthermore, a cooling of the stratosphere favours ozone depletion in the polar regions of the globe via heterogeneous chemical processes acting on solid or liquid cloud particles.

Stratospheric ozone has decreased globally since the 1970s. The most spectacular ozone loss occurs in the Antarctic region, where the ozone loss every year is now large. Each October, the total ozone now falls below half its former value and at some altitudes the ozone concentration already falls below detection limits. As well as in the Antarctic, the ozone concentration is declining elsewhere. Since 1991, significant ozone reduction has also

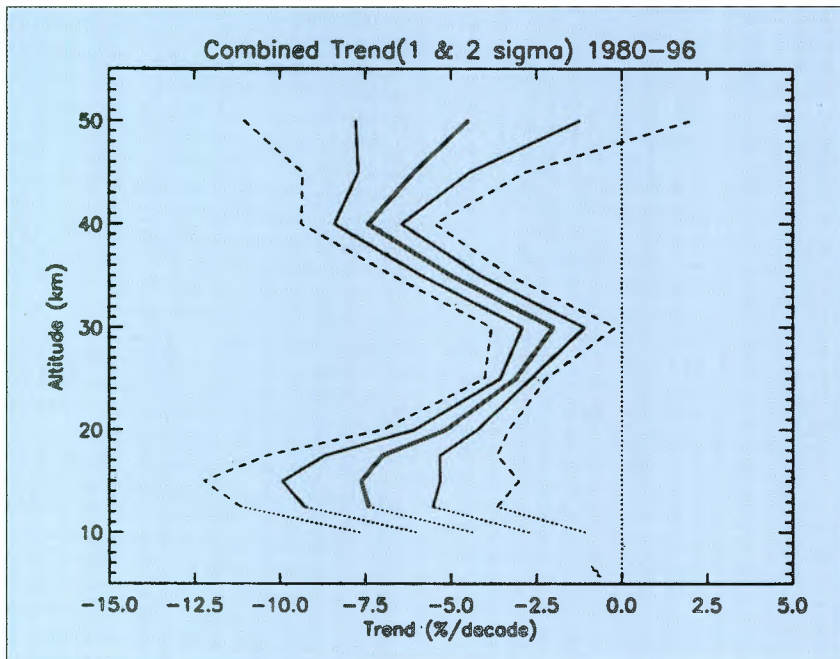


**Fig. 2-2** The mean, annually averaged trend in the vertical distribution of ozone that has occurred over northern mid-latitudes from 1980-1996 (heavy solid line) is calculated using the trends derived from SAGE I/II, ozonesondes, Umkehr and SBUV measurements. The combined uncertainties are shown for 67% confidence limits (light solid lines) and 95% confidence limits (dashed lines). The results below 15 km are a mixture of stratospheric and tropospheric trends and the exact numbers should be viewed with caution. (SPARC/IOC/GAW 1998)

been observed at northern mid- and high-latitudes. Fig. 2-2 shows ozone trends for latitudes between 30°N and 50°N during the 1980s, as a function of altitude, derived from different observation systems. In the mid-latitudes, the largest ozone loss occurs in the chemically most active altitude region around 40 km. Also in the 25 km region with the highest ozone concentration the decrease in ozone is significant. In polar regions the ozone loss is at its highest in the lower stratosphere, where heterogeneous ozone depletion occurs.

The main cause for the observed ozone destruction since 1980 is anthropogenic pollution, namely the release of chlorofluorocarbons (CFCs), which produce free chlorine in the lower stratosphere, and halons, which release bromine radicals. Regulations, such as those in the Montreal Protocol and its amendments, have reduced the release of CFCs and other source gases so that a decline in ozone destruction can be expected and eventually a slow recovery of the

ozone layer (over the next few decades). Today global ozone destruction is still continuing. However, in 1998, the trend of increasing global chlorine loading appeared to be stagnating, possibly as a result of the Montreal Protocol. In a best-case analysis [Engel and Schmidt, 1999], chlorine loading in the stratosphere was found to decrease after 2000, but not reach pre-ozone-hole values for at least six decades.

Current stratospheric chemistry models do not quantitatively reproduce the observed decline in ozone. Hence it is essential to further improve atmospheric composition observations and to continue to monitor trends in ozone, and in its profile, but with improved accuracy. Only in this way can it be confirmed that the hypotheses about the details of ozone depletion are accurate and whether the provisions of the Montreal Protocol are having the desired effect.

## 2.2 Current Science Issues

Despite the significant advances in the understanding of polar ozone depletion over the last few years, there are still significant uncertainties in the understanding of stratospheric chemistry which must be addressed. In particular, further work is needed to help attribute the observed mid-latitude O<sub>3</sub> trend to different proposed causes, and to investigate the interaction of other trends (e.g. in temperature and H<sub>2</sub>O) with that of stratospheric O<sub>3</sub>. In addition to the efforts towards advancing understanding of the chemical and dynamical processes, continued monitoring of ozone and its profile is essential to confirm the observed trends, and their changes, especially as the stratospheric halogen loading

becomes stabilised, and starts to reduce, following implementation of the Montreal Protocol and its amendments.

### **2.2.1 Monitoring profiles of O<sub>3</sub> and trends**

Statistical studies show that significant reductions in ozone have occurred at northern mid-latitudes and, although details of the mechanism are not clearly understood, a consensus has emerged that these reductions are at least partly due to the presence of reactive chlorine derived from man-made halocarbons. Measurements strongly suggest that most of this decline in ozone amounts occurs in the lower stratosphere, in agreement with current hypotheses about the actual mechanism.

However, measurements of trends in ozone profiles lack the accuracy of measurements of trends in the ozone column and current models of stratospheric chemistry do not reproduce the observed decline in ozone amounts. To resolve this conundrum it is essential to continue to monitor trends in total ozone to current accuracies and trends in its profile with improved accuracy.

The total ozone (60°N to 60°S) declined by 2.9% per decade in the period from 1979 to 1994. Consequently, the ozone changes in the stratosphere (where about 90% of the total ozone resides) must be monitored globally with an accuracy of 0.3% per year.

### **2.2.2 Increasing Arctic O<sub>3</sub> depletion**

It is now clear that conditions favourable to ozone loss are found most years within the Arctic vortex, leading to ozone depletion. Unlike its

southern counterpart, the Arctic vortex is highly variable and mobile, often moving above middle latitudes under the influence of forcing by planetary waves and by tropospheric weather systems. In recent years (1994/95 to 1996/97 and 1999/2000) significant O<sub>3</sub> loss has been observed in the Arctic, due to favourable meteorological conditions (i.e. lower temperatures). Further study of the Arctic is necessary to investigate whether this variation is a consequence of natural variability or a consequence of lower stratospheric temperatures in the Arctic spring related to stratospheric radiative cooling caused by the increase of greenhouse gases. In this case the Arctic ozone depletion will become more severe.

### **2.2.3 Mid-latitude ozone trends**

Despite the observations of the downward O<sub>3</sub> trend at mid-latitudes, the causes have not yet been firmly established. Mid-latitude ozone depletion in the lower stratosphere is probably dominated by heterogeneous chemistry on the surface of sulphate aerosols. Whereas ozone depletion cycles involving the HO<sub>x</sub> radicals, are most important at altitudes below about 20 km, cycles involving the halogen radicals (BrO and ClO) also play a significant role. Important insights into the relative roles of different catalytic cycles, in controlling the ozone abundance in the mid-latitude lower stratosphere, have come from *in-situ* measurements made on the NASA ER-2 aircraft, suggesting that the understanding of the fast gas phase chemistry is satisfactory.

In May, for an assumed ClO concentration of about 25 pptv, the ozone loss rate would be more than 1% per month. Analysis of data from the MLS instrument on the UARS satellite reveals ClO concentrations

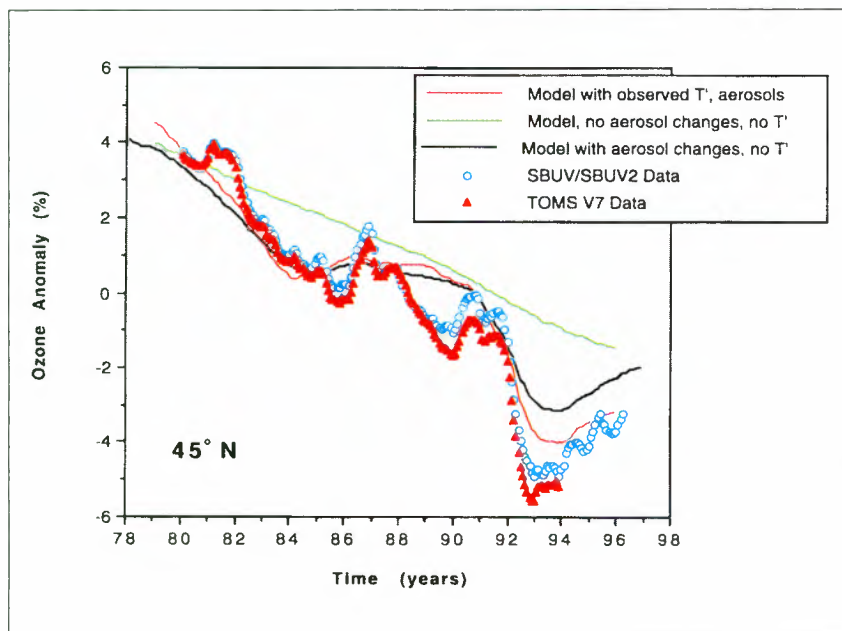


Fig. 2-3 Observed and calculated total ozone anomalies from 1979 to 1997 at 45°N. All cases shown are smoothed by a 25-month running mean to average over both the annual cycle and the QBO. Red triangles show the zonally averaged TOMS V7 data and the blue circles show the combined SBUV/SBUV2 data. All model results shown include chlorine and bromine increases. In addition, the red line shows the model results including observed aerosol variations and zonal mean temperature and planetary wave temperature amplitudes ( $T'$ ) estimated from National Centers for Environmental Prediction (NCEP) observations. The black line is similar to the red line except the planetary wave temperature amplitudes are not used in the model. The green line shows model results with constant 1979 aerosol observation used throughout the calculation. (WMO, 1998)

exceeding 100 pptv at middle latitudes in the lower stratosphere in winter, implying a significant year-round contribution of reactive chlorine to mid-latitude ozone loss in this region. It is now clear that BrO is present in significant amounts outside the polar vortex. Observations of BrO in the lower stratosphere demonstrate that reactions involving bromine account for more than 50% of the catalytic destruction of ozone by halogens at 20 km altitude.

A recent model study showed that, in the presence of the contemporary chlorine and bromine stratospheric loadings, the changes in aerosol loading during the 1980s and 1990s, following major volcanic eruptions, correlate with variations in modelled and observed mid-latitude levels of ozone. Although, it is clear that mid-latitude aerosol is also playing a role in determining ozone amounts, the magnitude of the effect is larger than can be reproduced in the model (Fig. 2-3). Thus it appears that the knowledge of the chemistry and/or dynamics is incomplete; further quantification is required.

Emissions of  $\text{NO}_x$  and other gases from aircraft exhausts are expected to affect stratospheric ozone. However, the incomplete knowledge of the details of the chemical and meteorological processes in the very low stratosphere and upper troposphere, where long-distance aircraft fly, limits the ability to predict the impact of aircraft emissions in this region.

#### 2.2.4 Trends in temperature, $\text{H}_2\text{O}$ and stratospheric aerosol

Observations indicate that stratospheric water vapour is increasing. Measurements obtained at a single station at northern mid-latitudes indicate that water vapour concentrations in the lower stratosphere increased between 1981 and 1994 [Oltman and Hofmann, 1995]. Furthermore, HALOE satellite data from 1991 onwards indicate that these positive trends extend throughout the stratosphere [Evans et al., 1998; Nedoluha et al., 1998]. These increases are larger than can be explained by the increase in the chemical production of water resulting from the observed changes in atmospheric methane, and they may be indicative of other longer term changes in the stratosphere or at the tropical tropopause. A general increase in water vapour concentrations would increase  $\text{HO}_x$  radicals and would also enhance ozone loss through an increased incidence of PSCs. However, it is important to note that reliable long-term measurements of water (i.e. greater than 15 years) have only been made at this one site, with shorter records from satellites and other stations. The cause of these trends is not clear and more measurements are needed.

If the increase in stratospheric water vapour is related to a warming of the tropopause this will be important as the processes involved in

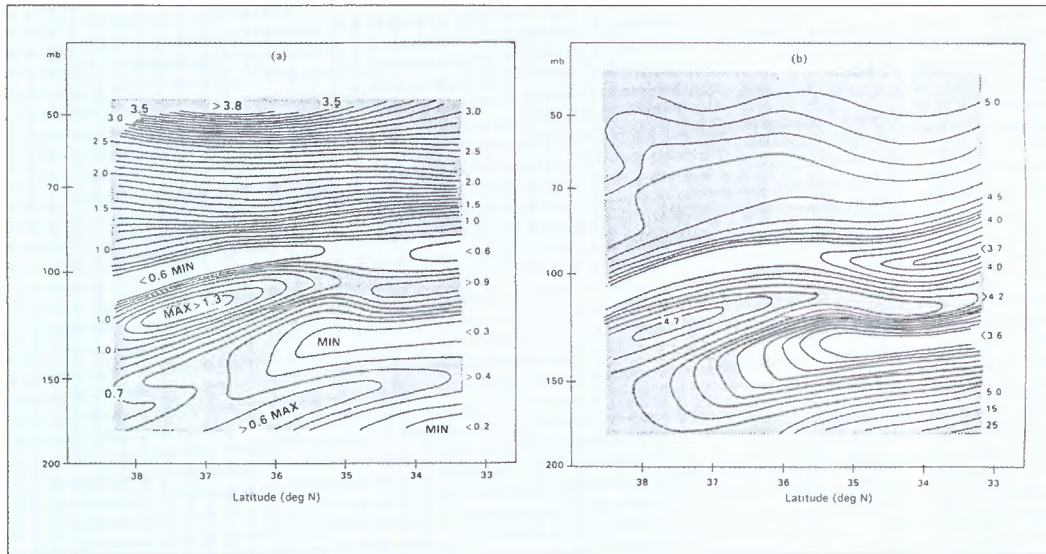


**Fig. 2-4 Observations from a high-altitude aircraft of mixing ratios of (a) ozone and (b) water vapour (ppmv), in April 1984 at Northern mid-latitudes during a tropopause fold. Note the fine resolution of the features, with tongues of air of thickness 20 mbar at 100 mbar - about 1 km. (WMO, 1985)**

stratospheric/tropospheric exchange are poorly understood. This transport determines the amount of water vapour present in the stratosphere and it is crucial for predictions of:

- a) stratospheric concentrations of the shorter-lived substitutes for CFCs (transport from the troposphere to the stratosphere, mostly in the tropics);
- b) the amounts of tropospheric ozone observed away from polluted areas (transport from the stratosphere to the troposphere, mostly in tropopause folds at mid-latitudes).

Because its concentration is much greater in the stratosphere than in the troposphere, ozone is a particularly useful tracer for observing stratosphere-troposphere exchange, as illustrated in Fig. 2-4. The exchange of water vapour is still poorly understood, despite being studied for many years.

Water vapour is a potent greenhouse gas. The amount present in the upper troposphere is therefore important for the radiation budget. Global warming

will increase the upper tropospheric humidity as long as the water vapour concentration is below saturation. If the air is near saturation, the cloudiness increases. The effect of increased cloudiness is not a clear forcing signal, as the effect of clouds depends strongly on altitude (e.g. fog acts to cool the Earth's surface). Hence a high-resolution global climatology of humidity in the upper troposphere is an important climatic variable.

The amount of sulphate aerosol in the stratosphere is also important because the heterogeneous reactions involved in ozone loss occur on aerosols both at mid-latitudes and in polar regions. The amounts of sulphate aerosol in the stratosphere increased significantly in 1991 and 1992 as a result of the eruption of Mount Pinatubo in June 1991. Because of the lack of significant volcanic eruptions since 1992, the amount of aerosol in the stratosphere is now less than at any time since satellite measurements started in 1979. Measuring the stratospheric aerosol requires a high vertical resolution because of the strong vertical and horizontal gradients of aerosol concentration.

### 2.2.5 Stratospheric dynamics

Stratospheric circulation is characterised by general ascent in the equatorial region, poleward transport and a descent at high latitudes. This global circulation is controlled by extra-tropical pumping [Holton *et al.* 1995]. Extratropical planetary waves propagate from the troposphere to the upper stratosphere where they dissipate and decelerate the mean zonal wind, induce the mean poleward transport and so redistribute ozone. When looking at the trends in stratospheric ozone at middle and high latitudes, one has to consider a possible evolution of the poleward transport, due to changes in this planetary wave activity, as a contributory factor.

Extratropical pumping also imposes upward equatorial motion hence the global injection of tropospheric air into the stratosphere. However, the detailed mechanisms involved in this process still need to be clarified. The main mechanism is deep convection in cumulo-nimbus clouds reaching the tropopause and inducing very cold temperatures. This leads to the condensation of water vapour and strong dehydration of air injected into the stratosphere (i.e. the so-called 'cold trap'). However, the lowest water vapour mixing ratio (hygropause) is not encountered at the tropopause but a few kilometres above. Some additional dehydration may occur in the very low stratosphere to explain this feature. It is possible that local cooling occurs, leading to the condensation of a fraction of the water vapour into equatorial stratospheric clouds. One of the hypotheses put forward to explain this is the transient cooling associated with the propagation of Kelvin waves and gravity waves.

Another important mechanism to be considered in interpreting the

concentration of ozone in the lower stratosphere at middle latitudes is the meridional transport of air, eventually depleted in ozone, from high latitudes in polar filaments formed at the edge of the polar vortex. The contribution of this mechanism to the trend of ozone observed at middle latitudes has yet to be quantified. The rate of mixing of air out of the polar vortex is expected to vary with altitude; it is probably most efficient in the very low stratosphere.

The transport of air which is poor in ozone, from the tropical upper troposphere to the mid-latitude lower stratosphere in subtropical intrusions, should also be considered as a potential contributor to the mid-latitude ozone budget. This mechanism is responsible for the dynamically induced mini-holes visible on global satellite maps of total ozone.

The irreversible mixing of air coming from different latitudes and altitudes occurs in turbulent layers generated by the breaking of gravity waves. They are generated in the troposphere above mountains, above convective clouds, and in the jet stream. They propagate upwards in the middle stratosphere, with an amplitude increasing as the inverse of the square root of the density, until they reach a condition of instability and break, inducing turbulent layers and the acceleration of the mean wind in the direction of the phase propagation. They are the main contributor to the mesospheric circulation and may also play a role in the stratospheric circulation. Small-scale motions induced by the breaking of gravity waves, coupled with molecular diffusion, transport the various chemical species through the atmosphere. Many local studies of gravity waves and turbulent layers have been performed using *in-situ*

balloon measurements and ground-based radars and lidars, but nothing is known concerning the global climatology of these phenomena in the stratosphere.

### **2.2.6 Mesospheric ozone and clouds**

Ozone in the mesosphere is produced by the photo-dissociation of  $O_2$  and the subsequent reaction of O with  $O_2$ . It is destroyed by reactive hydrogen radicals, i.e. H, OH and  $HO_2$ . The photochemical lifetimes of the oxygen and hydrogen radicals are only hours in the mesosphere so only the distributions of the long-lived molecules that produce hydrogen radicals (i.e.  $H_2O$  and  $H_2$ ), are likely to be affected by atmospheric transport. However, despite the apparent simplicity of this situation, there exist significant disagreements, which need to be resolved, between the predictions of current models and observations.

These centre on the variations in mesospheric ozone: diurnal and semi-diurnal variations and those associated with variations in solar activity. The amplitude of the diurnal variation increases from a few percent at an altitude of 50 km to 80% at 70 km. This mainly reflects variations in the equilibrium between  $O_3$  and O. The equilibrium value of the ratio  $[O]/[O_3]$  increases rapidly with altitude and exceeds unity above 65 km while below this altitude almost all the O is converted to  $O_3$  after dusk.

Polar mesospheric clouds (PMC) are cirrus-like clouds of small particles, confined to a small altitude range (82-85 km) where the atmospheric temperature is at a minimum (i.e. the mesopause). They were first observed from the ground and called 'noctilucent clouds' as they could only be observed under specific twilight

conditions i.e. when the observer is in the dark and the clouds are still illuminated by 'Earth grazing' sunlight.

PMCs appear only at high latitudes during summer. This feature is explained easily by the fact that mesospheric air descends during summer conditions at high latitudes and the temperature reaches its minimum value (below 150 K; the coldest region of the entire atmosphere). Then the amounts of water vapour exceed the local saturation vapour pressure and ice particles form around condensation nuclei, which could be either meteoritic dust particles or large clusters of ionised water.

In his review of the subject, *Thomas, 1991*, advocated that the appearance of PMCs is a strong indicator of global change. He argued that the first reported observation was made in 1885, though there were a large number of talented observers before. The explanation would be that methane has been increasing steadily since around 1850 (growing population and associated development of agriculture and livestock), with a present growth rate of 1% per year. Indeed, oxidation of  $CH_4$  is an important source of  $H_2O$  above about 50 km, and therefore an increase of  $CH_4$  at ground level will be reflected some years later by an increase of  $H_2O$  at mesopause level. The saturation vapour pressure decreases by a factor of 5 for a decrease of 4 K for summer mesopause conditions, so that even a moderate climatic temperature change (induced by increased  $CO_2$ ) could cause an increase in global PMC cover.

### **2.2.7 Recovery of stratospheric ozone**

The peak in bromine loading is expected to occur between the years

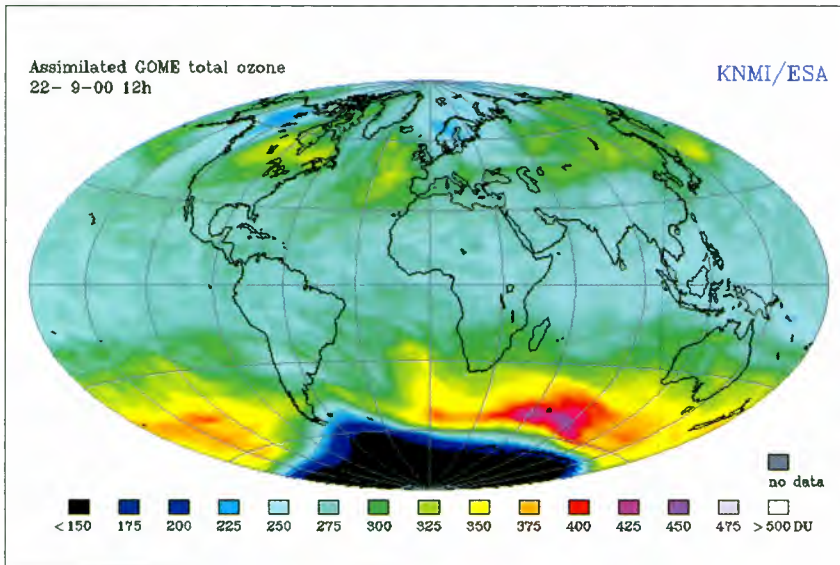


**Fig. 2-5 Antarctic ozone hole September 2000 observed by GOME on ERS-2, assimilated by KNMI. (Courtesy KNMI, The Netherlands)**

2000 and 2010 and, when coupled with the expected decline in chlorine loading, would result in only a small decrease in total effective halogen loading between now and then, with a much sharper fall thereafter. Stratospheric ozone is expected to recover as the loading of stratospheric chlorine and bromine decreases. Large ozone loss in the Arctic, similar to that seen in the winters of 1995/96, 1996/97 and 1999/2000, can be expected to continue for at least the next decade in cold winters. This picture may change if stratospheric temperatures continue to decrease, in which case recovery would take longer, or if there are further changes in atmospheric composition.

During the winter of 1999-2000 large ozone losses were observed inside the Arctic stratospheric polar vortex. These ozone losses were observed from ground-based and ozone-sonde measurements. At altitudes around 18 km cumulative losses of over 60% occurred between January and March. These are among the largest chemical losses at this altitude observed during the 1990s. Satellite observations (e.g. by the ESA Global Ozone Monitoring Experiment GOME) showed a clear ozone minimum over the polar region during February and March. The average polar column

amount of ozone for the first two weeks of March was 16% lower than observed in the 1980s.

In September 2000, the Antarctic ozone hole developed with extremely low ozone values, which occurred earlier in the season than ever observed before.

Fig. 2-5 shows assimilated GOME observations

These recent observations have reinforced the concern that even if halogen loading decreases eventually, changing dynamical conditions causing a colder stratosphere would support ozone-depleting conditions during the polar winter. This would lead to a delay in the recovery of the ozone layer.

Therefore, it is presently far too early to assume that the ozone layer would automatically recover if international agreements on reduction of halogen emissions (Montreal Protocol) were effective. A continued monitoring of ozone, species involved in ozone depletion, and of dynamical conditions, is therefore required with high accuracy, vertical resolution and global coverage.

Further study of the  $O_3$  depletion at 40 km is also important. In this photo-chemically controlled regime, the influence of changes in chlorine and temperature should be discernible in the local  $O_3$  abundance. The ability of GOMOS to produce accurate ozone density profiles in this critical region will make it possible to study closely the coupling of ozone to chlorine density and temperature.

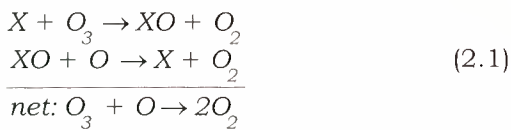
### 2.3 Ozone Depletion

While stratospheric ozone is formed by one principal set of reactions, the photodissociation of  $O_2$  followed by combination of molecular and atomic

oxygen, there are numerous reactions, which destroy ozone in gas phase. There are also heterogeneous reactions, on or at the surface of particles, which affect ozone-depleting species.

### 2.3.1 Stratospheric gas-phase chemistry

In the stratosphere, ozone is in balance between production and destruction, with a time constant of a few days to many years. In the mid-upper stratosphere ozone is formed by the dissociation, by ultraviolet sunlight, of molecular oxygen ( $O_2$ ) to atomic oxygen (O), followed by a reaction between the atomic oxygen and molecular oxygen to give ozone ( $O_3$ ). It is removed by a variety of catalytic cycles, which can be of the form:



Globally, one of the important ozone depleting cycles is that containing  $NO_2$ , which will be measured by GOMOS. See also Fig. 2-6, the odd nitrogen cycle.

As well as these (and other) short-lived radicals there are a number of important reservoir gases, so-called because they store Cl, Br, OH and NO in less reactive forms, such as HCl, ClONO<sub>2</sub> (from the reaction of  $NO_2$  and ClO) and  $HNO_3$ . Fig. 2-6 summarises some of the known interactions that occur between these families of radicals and reservoirs.

The cycles involving the oxides of hydrogen and nitrogen arise naturally though there is concern that the anthropogenic production of  $NO_2$  (from current commercial aircraft and future high-altitude aircraft) might increase stratospheric  $NO_2$ , thereby changing the amount of stratospheric

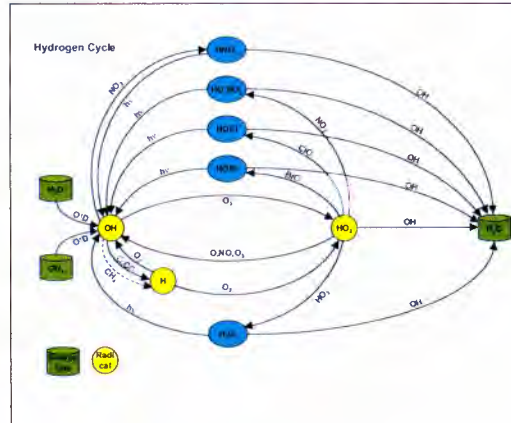
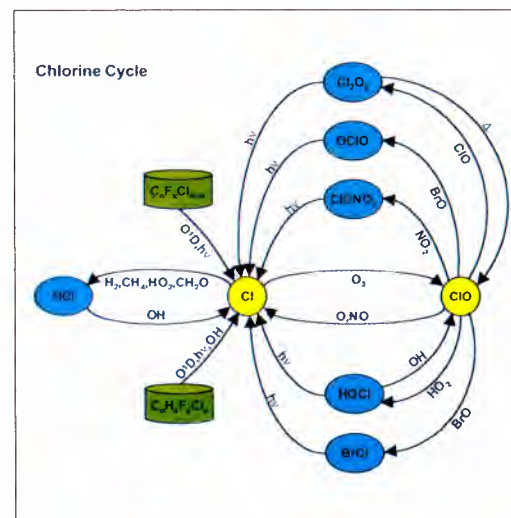
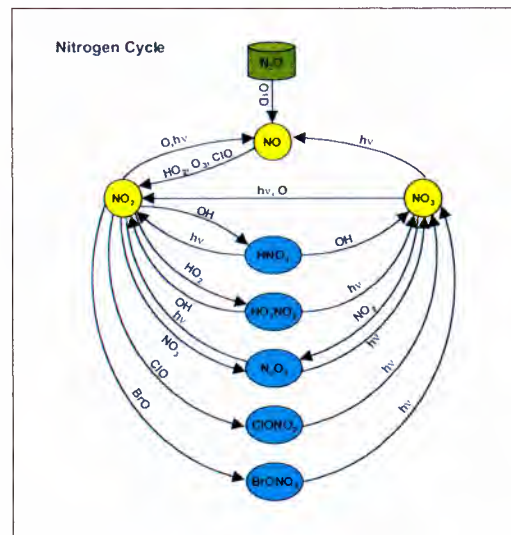


Fig. 2-6 Cycles of the reactive gases that control loss of ozone by gas-phase chemistry



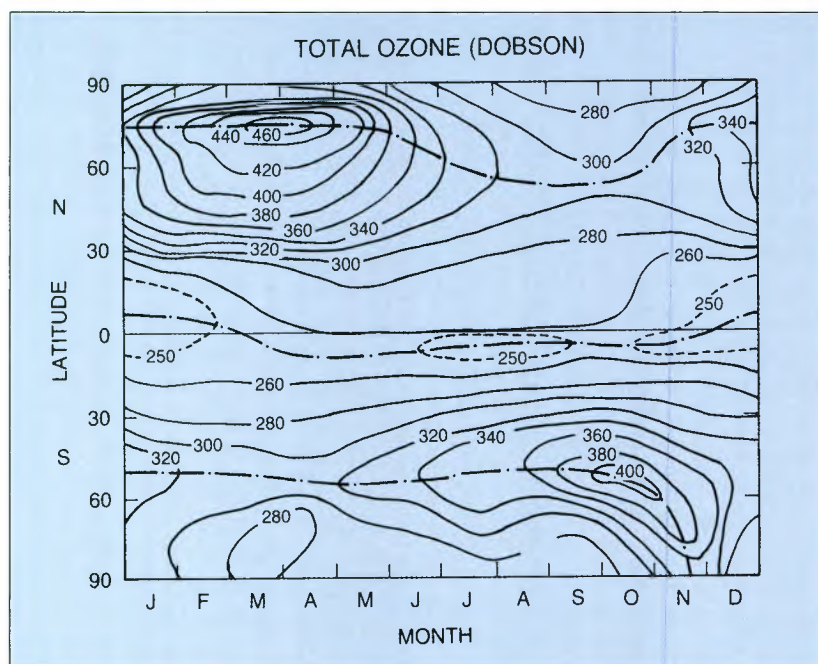


Fig. 2-7 Variation of total ozone with latitude and season (WMO, 1990)

ozone, although this effect is now believed to be small in the stratosphere. This may be contrasted with the situation for stratospheric chlorine where only 15-20% arises from natural sources – most originates from man-made halocarbons, e.g. chlorofluorocarbon (CFCs). Anthropogenic sources also contribute significantly to the stratospheric bromine loading.

Until recently CFCs were widely used in domestic spray-cans and foam products, and are still used in refrigerators. CFCs are very inert, therefore non-toxic, but have very long life-times (70 to 150 years) in the lower atmosphere. Therefore, they survive long enough to reach the stratosphere through convection and dynamical troposphere-stratosphere exchange processes. Only in the stratosphere can UV radiation eventually break up the molecules and release the chlorine atoms, which can then enter into ozone-depleting cycles. Bromine-containing halocarbons were used in many fire extinguishers, and methyl bromide is still widely used as

an agricultural fumigant and soil steriliser. Reactive bromine is many times more effective at removing ozone than reactive chlorine.

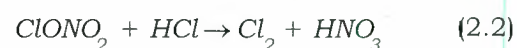
Because of the varied lifetime of ozone in the stratosphere, its distribution is determined by a combination of transport and chemistry. As mentioned in Section 2.2.5, transport is particularly important in the lower stratosphere, where the photochemical lifetime of ozone becomes long and it is transported poleward and downward from the photochemical source region. Fig. 2-7 shows clear evidence of this transport – the ozone column maximum does not occur in the tropics, the region of maximum production, but at high latitudes.

### 2.3.2 Heterogeneous chemistry

In addition to the gas-phase chemistry outlined above it is now known that heterogeneous chemistry on aerosols and particles plays an important role in stratospheric ozone depletion.

Liquid sulphate aerosols are present throughout the lower stratosphere. Their abundance can be enhanced significantly following major volcanic eruptions, as happened after the eruption of Mt. Pinatubo in June 1991. Under cold polar conditions (temperatures less than 200 K), these liquid aerosols take up water and grow. This yields polar stratospheric clouds (PSCs) which can be either liquid, supercooled solutions, or solid particles.

When PSCs form, heterogeneous reactions convert the chlorine reservoirs HCl and ClONO<sub>2</sub> into active chlorine via reactions such as:



This heterogeneous reaction occurs rapidly on ice and solid nitric acid trihydrate (NAT) as well as on liquid aerosols composed of super-cooled ternary solutions of  $\text{H}_2\text{SO}_4$ ,  $\text{HNO}_3$  and water.

It appears that liquid droplets must be supercooled to at least a few degrees below 195 K before solid particles can form. However, once formed, the solid particles may survive at temperatures above 195 K although their surface area will decrease at the higher temperatures. The rate of chlorine activation on these particles is a function of their physical condition (solid or liquid, water content). Because of the current incomplete understanding of the physical properties of PSCs, the ability to predict the future evolution of Arctic ozone depletion is limited. This is particularly important in winters in which the conditions for the formation of PSCs are marginal. This is also true of ozone depletion in locations where PSCs are marginal, such as the edge of Antarctica.

### 2.3.3 Polar ozone depletion

It has been demonstrated unequivocally that the presence of reactive chlorine and bromine from anthropogenic halocarbons leads to the destruction of stratospheric ozone and that their presence accounts quantitatively for the formation of the Antarctic ozone hole. Reactive chlorine compounds have also been observed in the Arctic in the lower stratosphere in winter, indicating chlorine-catalysed ozone destruction, by the same mechanisms as occur over Antarctica. Indeed, in cold winters, large ozone depletion has now also been observed over the Arctic.

In the Antarctic, ozone depletion in the spring is now so severe that

between each August and October, over half of the total ozone is destroyed. This did not happen before the 1970s when the stratospheric halocarbon loading was much smaller. The depletion occurs in the lower stratosphere, where the catalytic cycles described in Section 2.3.1 cannot operate as the abundance of atomic oxygen is too small.

The catalytic cycles which operate in the polar lower stratosphere involve ClO and BrO while competing non-depleting pathways involve OClO, whose presence is therefore indicative of significant amounts of ClO and so of the potential for ozone depletion. Large amounts of ClO are possible via the heterogeneous reactions occurring on or in PSCs. The heterogeneous reactions also suppress the amounts of  $\text{NO}_2$ , which would otherwise react with the ClO to form  $\text{ClONO}_2$  and prevent ozone depletion.

The mechanism for  $\text{NO}_2$  removal is via the reaction of  $\text{NO}_2$  with  $\text{NO}_3$  (at night) to produce  $\text{N}_2\text{O}_5$ , followed by heterogeneous reaction of  $\text{N}_2\text{O}_5$  to form  $\text{HNO}_3$ , which in turn can be incorporated into the aerosols. If it is cold enough for ice to condense around the nitric acid trihydrate (NAT) core of a PSC, natural deposition occurs and the particles eventually fall out of the stratosphere, a process known as denitrification.

In the Arctic in winter the conditions when significant ozone depletion could arise are quite commonly observed. There is now clear evidence of significant and widespread ozone loss in the Arctic in winter, with features similar to the early years of the Antarctic ozone hole being seen in the winters 1995/96, 1996/97 and 1999/2000. Maximum loss rates of up to 2% per day have been observed in the Arctic at altitudes around 18 km.

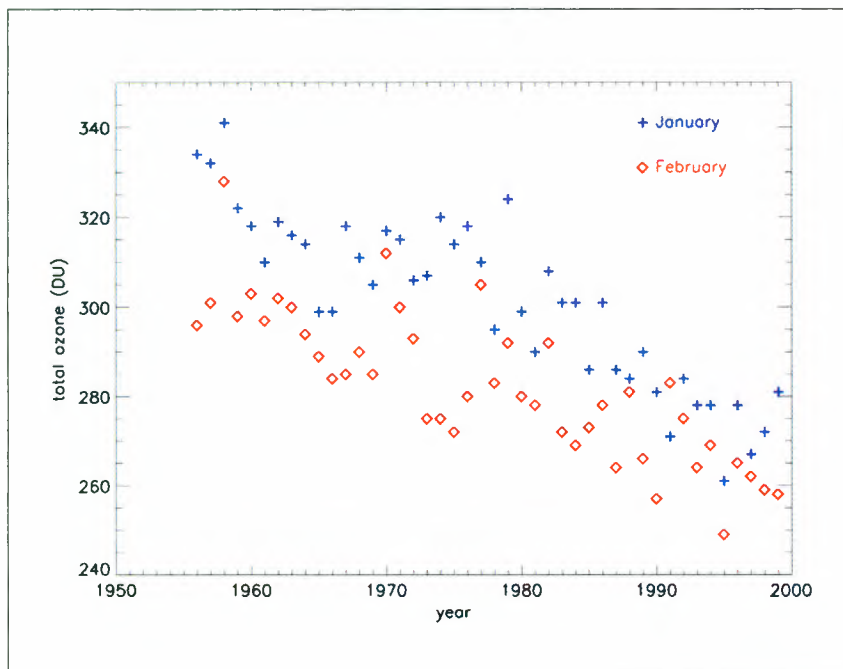
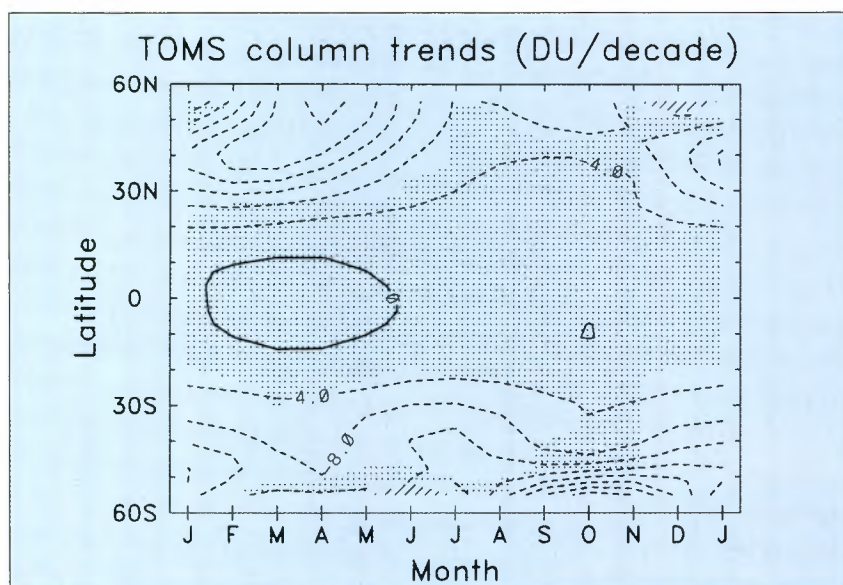


**Fig. 2-8 Trends in total ozone in summer in Antarctica, measured by the Dobson spectrophotometer at Halley at 76°S (Courtesy of J.D. Shanklin, British Antarctic Survey, UK).**

**Fig. 2-9 Seasonal and latitudinal variation of trends in column ozone from TOMS. (WMO, 1998)**



At these altitudes the local losses, integrated through the winter and spring, were as large as 50-60%. These ozone losses occur during periods of chlorine activation. Stratospheric temperatures during the 1995/96 winter were the lowest in the previous 30-year record, leading to conditions that were particularly conducive to ozone loss. In early

March 1996, Arctic air in the stratosphere, which had earlier been depleted in ozone, was displaced as far as the southern UK, where total ozone was the lowest in the data record. Temperatures in 1996/7 were lower still and ozone losses exceeding 20% were identified by March 1997.

However, the largest ozone losses continue to be observed over Antarctica each spring. In recent years, there have been increased ozone losses at higher and lower altitudes leading to larger overall declines in total ozone amounts in this region. The inter-annual variability in the ozone depletion means that the depth and the areal extent of this depletion have not increased monotonically each year. Total ozone in January and February (Antarctic summer) has decreased by over 20% since the 1960s, as shown in Fig. 2-8. There has also been a marked decline in the maximum ozone values that occur during the final warming, suggesting that dynamical effects are involved.

When temperatures rise at the end of the polar spring, the recovery of reactive chlorine compounds into the chlorine reservoirs takes place. This recovery usually occurs later in Antarctica than elsewhere because of the lower temperatures and the widespread denitrification. Analysis of recent northern hemisphere winters has shown the substantial chlorine activation that occurs there each winter. For any particular year the duration of this activation is determined by the evolution of temperatures during the winter. Measurements, made since 1991/92 from NASA's Upper Atmosphere Research Satellite (UARS), have shown that, when activation occurs, it usually occurs throughout the polar vortex and that the maximum concentrations of ClO in the northern

and southern hemispheres are comparable.

### 2.3.4 Middle-latitude ozone trends

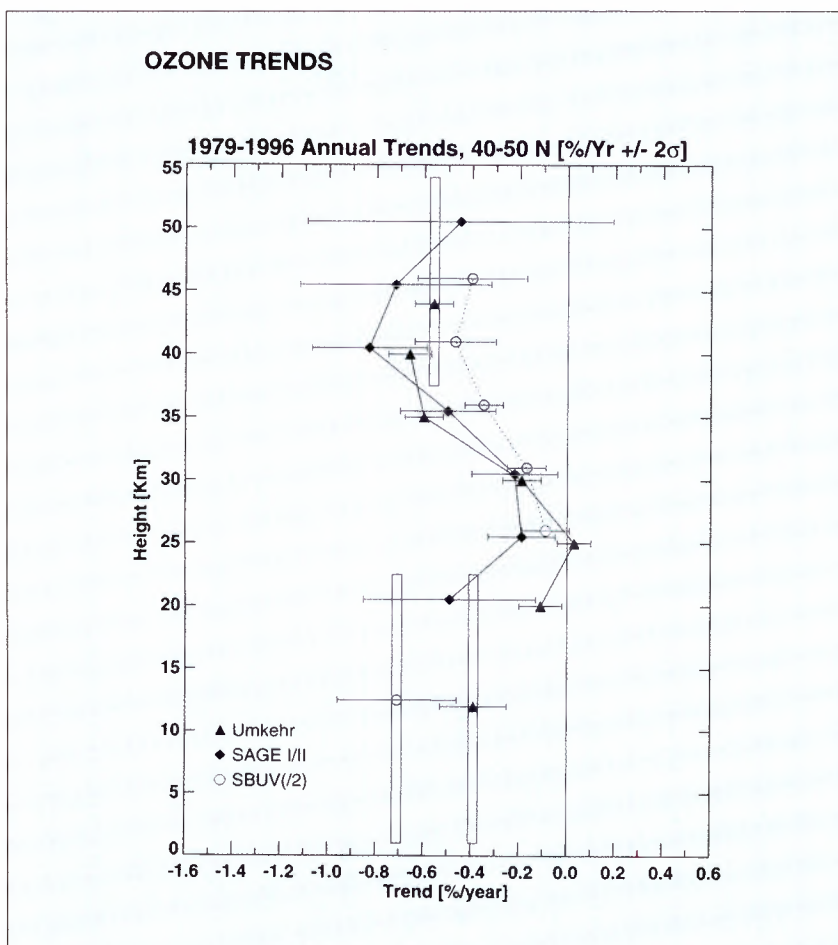
At northern mid-latitudes, total ozone is declining by between 4% and 8% per decade depending on the season. This rate excludes variations in ozone due to solar cycles and other known natural atmospheric phenomena. Fig. 2-9 illustrates this trend from satellite data.

The observed decreases in ozone arise primarily as a result of ozone destruction in the lower stratosphere, between altitudes of 15 and 25 km. Since 1979 there is good quantitative agreement between the trends derived from the measurements made by ozone sondes and those by the Stratospheric Aerosol and Gas Experiment (SAGE) satellite instruments. However, below 20 km the uncertainties in the trends derived from SAGE data are too large to be useful. Other ozone losses occur near 40 km where gas-phase destruction was first predicted, but there is too little ozone present at this altitude for this to have a significant effect on trends in the ozone column. Figs. 2-2 and 2-10 show the magnitude of these trends.

The cause of the trend at mid-latitudes has not been unequivocally determined. It is likely to be at least partly related to increases in stratospheric halogens, but changes in transport may also have had a significant effect.

### 2.3.5 Consequences of ozone depletion

Because ozone absorbs ultraviolet light, without compensating mechanisms ozone depletion must lead to an increase in ultraviolet at the surface. This would increase the incidence of human skin cancer and



probably reduce crop yields, as well as having an uncertain effect on other biota because of the ability of UVB to destroy DNA.

Fig. 2-10 Ozone trends (% per year) from 40-50°N over the period 1979-1996. (WMO, 1998)

Because the absorption of sunlight by ozone warms the stratosphere, without compensating mechanisms ozone depletion must lead to a cooling of the stratosphere. This would have an uncertain effect on climate, as well as changing the rates of many chemical reactions in the stratosphere because they are temperature-dependent.

Ultraviolet radiation at the Earth's surface has been observed to increase under the Antarctic ozone hole. Ozone depletion in Antarctica has also been at least partly

responsible for the observed seasonal decreases in stratospheric temperatures.

Observations under clear skies have confirmed that periods of reduced amounts of ozone outside Antarctica are associated with increases in the amount of ultraviolet radiation at the Earth's surface. However, records of ground-level ultraviolet radiation are not yet of good enough quality, or length, to allow the separation of the smaller increases associated with cloudy conditions from the large natural variability. Not only is this increase in ultraviolet radiation of concern in its own right, due to the potential biological effects of the change, but ultraviolet radiation also plays an important role in the chemistry of the troposphere.

Recent calculations have supported the suggestion that stratospheric ozone loss outside Antarctica leads to a cooling of the Earth's surface. Models indicate that since 1979 the observed ozone loss has offset at least 30% of the warming effect of increases due to increases in other greenhouse gases over the same period. The offset may be even larger than this as the decline in stratospheric ozone could have affected climate indirectly through chemical reactions driven by enhanced ultraviolet radiation reaching the troposphere.

The increased penetration of ultraviolet associated with ozone depletion increases the amounts of hydroxyl radicals in the troposphere (if all other controlling variables are unchanged). Any increase in hydroxyl radical concentrations will reduce the lifetime of methane (an important greenhouse gas) and may, via the oxidation of sulphur compounds, lead to an increase in the reflectivity of clouds. Both of these effects will act

to enhance the tendency to cool the surface associated with stratospheric ozone depletion.

## 2.4 GOMOS Scientific Objectives

The foregoing part of this chapter gives an overview of the ozone problem and the present state of knowledge. There is still a considerable need for further and improved measurements regarding the chemical processes involved in the ozone chemistry and of long-term changes of the ozone layer. The scientific issues described in this chapter are numerous and will require the data from a large number of spaceborne, airborne and ground-based instruments in order to measure the large number of relevant atmospheric parameters with the required temporal and spatial coverage and resolution.

Atmospheric chemistry is therefore one of the key mission targets for the Envisat satellite. Three instruments, namely GOMOS, MIPAS (see *ESA 2000*) and SCIAMCHY, are dedicated to atmospheric composition sounding. They will provide unique and highly synergistic data sets with respect to measured atmospheric parameters and spatial coverage and resolution.

GOMOS is an excellent space instrument for ozone monitoring. Since there are very many stars to use as light sources, the stellar occultation technique has the potential to provide much more complete spatial coverage than is available from solar occultations. Therefore, measurements at nearly all latitudes are possible even though Envisat will be in a polar Sun-synchronous orbit. Within the Envisat mission it is even more valuable as the

higher-level data analysis can benefit from the atmospheric parameters measured (more or less) simultaneously with MIPAS and SCIAMACHY.

The key objective of GOMOS is the long-term monitoring of ozone, with global coverage, high vertical resolution and long-term stable accuracy. This objective can be achieved with stellar occultation, making GOMOS an ideal instrument for the requirement.

Operational stellar occultation instruments should follow the Envisat mission to continue GOMOS-type measurements in order to get the required coverage for long-term trends. A derivative of GOMOS, COALA, is presently being studied as a possible operational stellar occultation instrument for ozone profile trend observation. COALA is somewhat smaller than GOMOS and focuses only on GOMOS' primary mission objective: ozone monitoring with high vertical resolution, high accuracy and global coverage.

Because of the significantly better global coverage compared to the solar occultation technique, GOMOS and COALA could prove to be the preferred solution for ozone profile monitoring.

#### **2.4.1 Primary scientific objective: ozone trend observations**

The primary scientific objective of GOMOS is the global monitoring of the stratospheric and mesospheric vertical ozone distribution with high accuracy, high vertical resolution and full global coverage. The expected high accuracy of the ozone profile measurements should allow ozone trends to be studied over the lifetime of Envisat in the stratosphere and mesosphere.

GOMOS ozone trend observations will address:

- the degree of Arctic (polar) ozone loss under different meteorological conditions (Section 2.2.2).
- increased data for determining height-resolved trend analysis (Section 2.2.3).
- monitoring, which will indicate the beginning of expected 'recovery' in ozone (Section 2.2.7).

The primary scientific mission objective points to the use of an instrument applying the occultation technique, as this is self-calibrating, protecting the measurements from long-term instrument drifts. Stars have been chosen as light sources in order to provide sufficient global coverage.

The occultation technique has one significant advantage, which is that an absolute estimate of the molecule density is obtained from the ratio of two measurements taken with the same instrument within a few seconds. This makes the method inherently self-calibrating, since even if the spectral sensitivity of the instrument is changing with time, the ratio will be measured correctly. This protection against long-term drift is ideal for the study of atmospheric trends.

GOMOS measures in the UV and visible wavelength regions where ozone shows strong absorption. The measured wavelength range is 250 nm to 675 nm, covering the ozone Huggins and Chappuis band. The UV wavelength range is particularly well suited for mesospheric and upper stratospheric measurements. The visible band is well suited for probing the stratosphere, including the lower stratosphere, where the UV signal is no longer strong enough because of

the UV absorption by ozone. Roughly, the UV yields the best results for the mesosphere and stratosphere above 35 km and the visible band for the stratosphere below 35 km.

A highly desirable follow-on programme with GOMOS or COALA-type instruments could provide long-term trend observation.

#### **2.4.2 Secondary scientific objectives**

As pointed out in earlier sections,  $\text{NO}_2$  and  $\text{NO}_3$  play important roles in the nitrogen chemistry relevant to ozone.

Observations of  $\text{NO}_2$  and  $\text{NO}_3$  will help to address:

- the degree of denoxification/denitrification in the Arctic winter and the availability of  $\text{NO}_2$  to deactivate ClO.
- the abundance of lower stratosphere  $\text{NO}_2$ , which varies with the aerosol loading.
- future  $\text{NO}_x$  observations relevant to the ozone recovery. As  $\text{NO}_x$  dominates ozone loss on a global scale,  $\text{NO}_x$  observations are important to interpret ozone changes as halogens decrease.

GOMOS will therefore observe  $\text{NO}_2$  and  $\text{NO}_3$  (if enhanced) in the UV-visible band.

OCIO and BrO are key species in the polar ozone depletion processes. They can possibly be detected with GOMOS if their concentration is enhanced. Measuring the aerosol extinction is an additional secondary objective. Aerosols are important for a number of reasons, including the provision of surfaces for heterogeneous reactions,

which can strongly affect the partitioning of chlorine and nitrogen compounds.

Stratospheric water vapour is fundamental to the budget of many trace gases in the stratosphere. It is therefore important to determine its three-dimensional distribution and long-term trends. Water vapour is measured in a near-infrared channel at 926-952 nm.

A further secondary objective is to study stratospheric dynamics. This requires measuring atmospheric temperature and density profiles. Temperature and air density will be derived from a near-infrared channel (756-773 nm). Complementary to this, a high-resolution temperature profile can be retrieved from observations of atmospheric scintillation, which will be measured using two fast photometers, one sensitive to blue and the other to red.

The measurement of temperature is also needed to support the primary mission objective, ozone monitoring. The ozone cross-sections in the Huggins band (310-350 nm) are strongly dependent on the atmospheric temperature. Therefore, a long-term variation of UV absorption might be due to a temperature variation and could be wrongly attributed to an ozone variation. Temperature measurements are possible with the A-band of  $\text{O}_2$  at 760 nm.  $\text{O}_2$  is a perfectly mixed gas and the air can be assumed to be in hydrostatic equilibrium. Therefore, its scale height is directly connected to the atmospheric temperature. The  $\text{O}_2$  measurements make it possible to relate measurements of ozone density (and other species) to the air density to yield the mixing ratio  $[\text{O}_3]/[\text{air}]$ , which is a quantity most readily used in models. Furthermore, temperature and air density are essential parameters for studying

atmospheric dynamics, including mixing of gases.

The mission objectives have also been described by *Bertaux, 1999*.

### 2.4.3 Long-term, campaign and permanent objectives

The scientific objectives can be divided into three groups. The first consists of long-term objectives. These objectives will be satisfied according to the overall GOMOS mission plan during the whole mission lifetime, in a more or less regular manner. The most important of these objectives is the monitoring of stratospheric ozone.

The second group consists of campaign type objectives. These have more limited scope than those of the long-term objectives. The activation of a campaign objective is based on an agreement among the partners in the GOMOS mission planning.

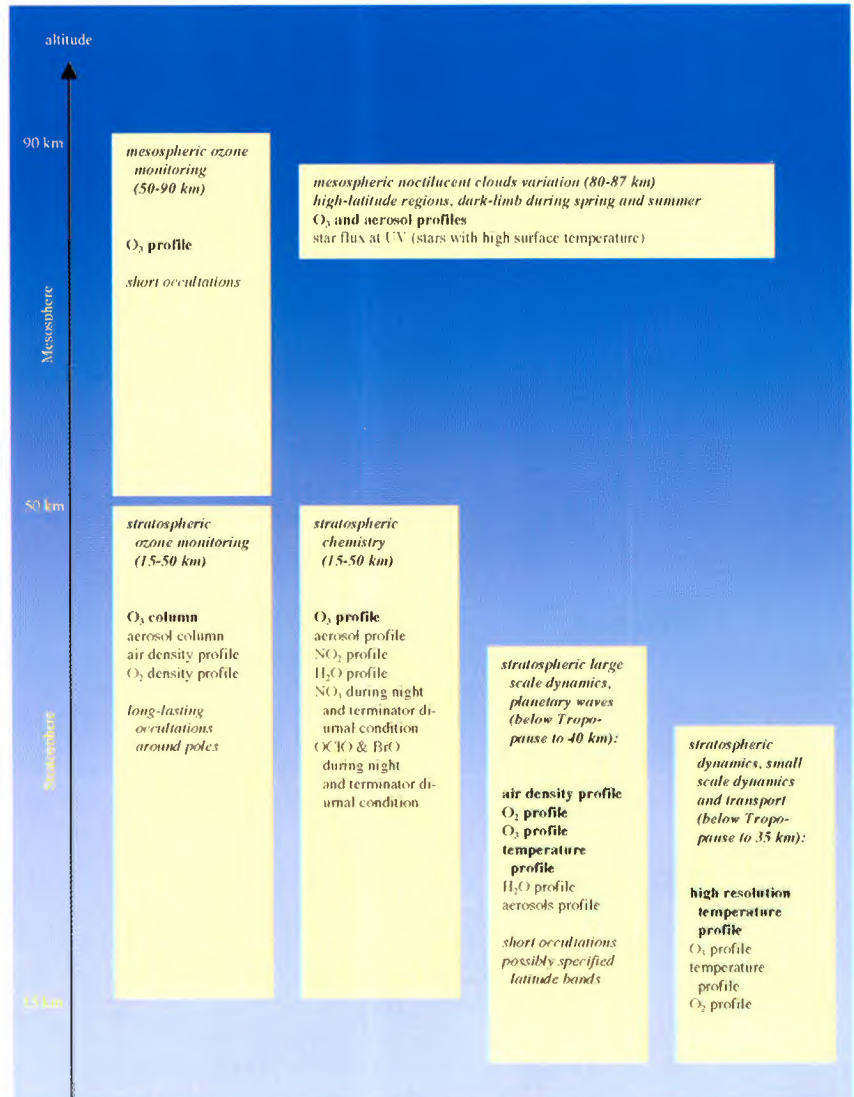
The third group consists of a few permanent objectives. For example, whenever possible, certain stars (e.g. Sirius) should always be occulted and predefined locations (e.g. selected validation sites) should be prioritised. Therefore, these objectives have an overriding priority.

In more detail, the three groups include:

#### Long-term objectives

The following different objectives have been identified:

- stratospheric ozone monitoring (15-50 km),
- mesospheric ozone monitoring,
- stratospheric chemistry: upper stratosphere (35-50 km),



- stratospheric chemistry: lower and middle stratosphere (15-35 km),
- stratospheric dynamics: large scale dynamics, polar vortex, planetary waves,
- stratospheric dynamics: small scale processes,
- mesospheric noctilucent clouds variation (80-87 km).

**Fig. 2-11 GOMOS long-term mission objectives according to the altitude regions involved**

The objectives are summarised in Fig. 2-11.

### **Campaign type objectives**

- geophysical validation of GOMOS products:
  - validation of gas concentration retrieval for particular species,
  - collocated measurements e.g. overpass flights over validating ground based instrument or coincident regions with validating satellite instrument,
  - validation of diurnal condition. (Depending on the validating instrument).
- comparisons with MIPAS and SCIAMACHY:
  - at specified times,
  - comparison of ozone and aerosols profiles,
  - comparison of NO<sub>2</sub>, air, O<sub>2</sub> and temperature profiles,
  - comparison of H<sub>2</sub>O, OClO and BrO profiles.
  - interesting diurnal condition: depending on the validating instrument (MIPAS day and night, SCIAMACHY nadir and limb modes day, SCIAMACHY occultation mode twilight),

- collocated simultaneous measurements with uniform global coverage.

- campaigns: Campaign-specified latitude regions and priorities for gases,
- special events, for example, volcanic eruption: ozone and aerosol profiles (with highest accuracy) around the eruption,
- stellar spectra, with increased occultation starting altitude.

### **Permanent objectives**

- fixed region measurements,
- fixed star measurements,

The permanent objectives have overriding priority over the other mission objectives. But it must be noted that the permanent and other mission objectives can be fulfilled – or nearly so – at the same time, because of the large number of occultations per orbit. More generally, almost all mission objectives are to some extent fulfilled in any mission plan. The degree of fulfilment, of course, varies. The best results are obtained for mission objectives for which observations are optimised.

# 3. Instrument Requirements

The primary objective of GOMOS is the high accuracy monitoring of the three-dimensional global distribution of ozone. Additional objectives are measurements of aerosols, air density, temperature,  $\text{NO}_2$ ,  $\text{NO}_3$  (if enhanced),  $\text{H}_2\text{O}$  and possibly  $\text{BrO}$ . The coverage is global for the altitude range of the tropopause up to 100 km using day and night observations. The vertical resolution is 1.7 km or better, depending on the obliqueness of the occultation.

To fulfil the scientific objectives, GOMOS will observe stars as they set behind the Earth's atmosphere, and measure spectral changes in the observed starlight intensity through atmospheric absorption. From the absorption at different wavelengths and altitudes the concentration of the various gases and aerosols will be retrieved.

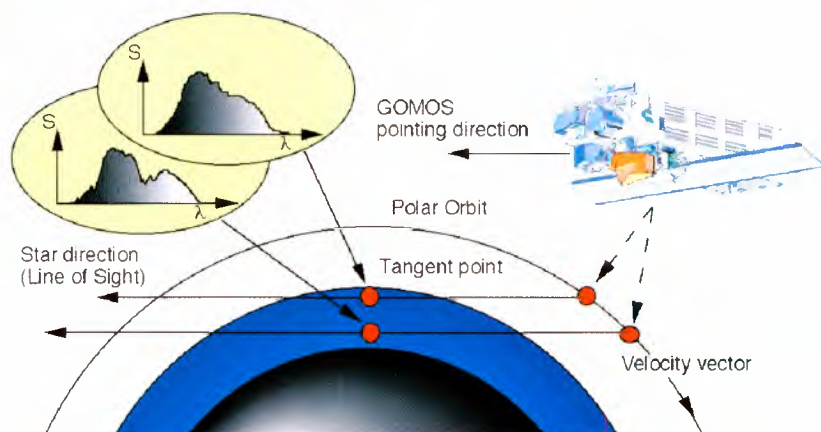
## 3.1 The Required Measurement Principle

GOMOS uses the stellar occultation technique. A sketch of the GOMOS measurement principle is shown in Fig. 3-1. It is located on the nadir-facing side of Envisat with its overall field-of-view opposite to the orbital velocity vector. The instrument's line-of-sight can be successively oriented towards stars and maintained while the star sets behind the Earth's

atmosphere. The orientation of the field of view is opposite to the orbital velocity vector. During the star's occultation, the ultraviolet, visible and near-infrared spectra of the star are continuously observed.

As the star sets through the atmosphere, its spectrum becomes more and more attenuated by the absorption of various trace-gases in the atmosphere. Each trace gas is characterised by a known, well-defined, spectral signature. On the ground, these attenuated spectra will be divided by the unattenuated stellar spectrum measured a few tens of seconds earlier above the atmosphere, so allowing the absorption spectra to be derived very accurately. This radiometric self-calibrating method is insensitive to longer-term sensitivity drifts of the instrument's hardware and is therefore capable of fulfilling

**Fig. 3-1 Principle and Geometry of the GOMOS stellar occultation measurements**



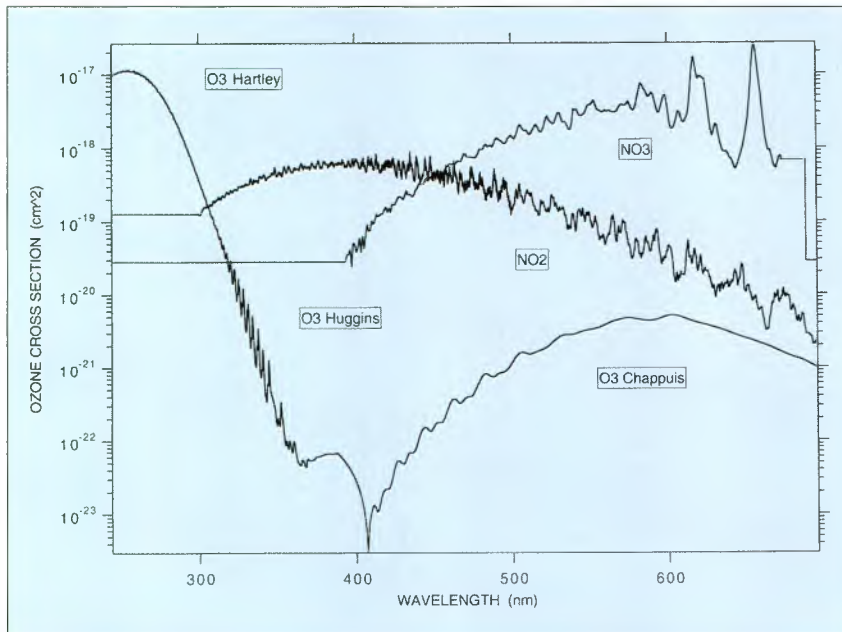
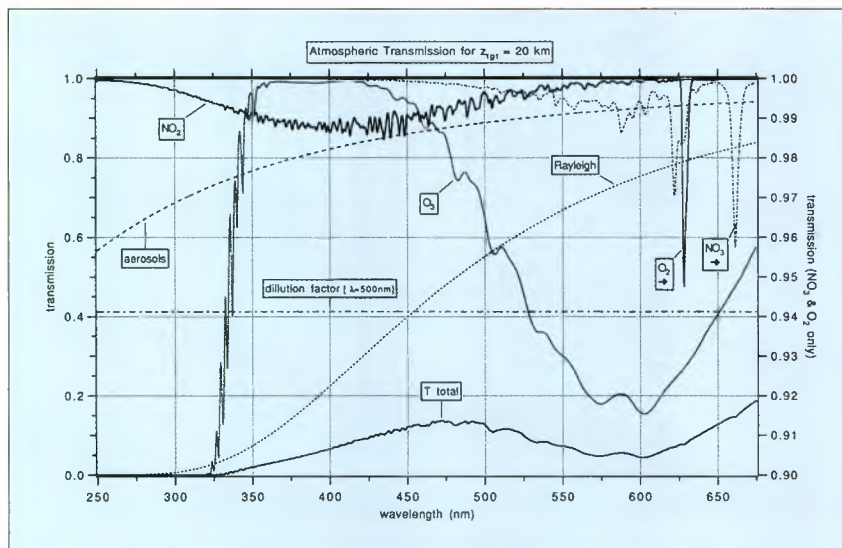


**Fig. 3-2 Cross sections of O<sub>3</sub>, NO<sub>2</sub>, and NO<sub>3</sub>**

the challenging requirement of reliably detecting very small changes and long term trends in the three-dimensional distribution of ozone concentrations.

During daytime observations, the sunlight scattered by the atmosphere is superimposed on the star's signal. In order to retrieve the star's signal without this component, the imaging spectrometers also record the

**Fig. 3-3 Simulation of atmospheric transmission at 250-675 nm**



spectrum of the sky just above and below the star. These spectra are used for removal of the signal due to the scattered sunlight.

### 3.2 Instrument Requirements: Spectral Coverage and Resolution

The cross sections of ozone, NO<sub>2</sub> and NO<sub>3</sub> in the 250-700 nm band are shown in Fig. 3-2. Ozone absorbs strongly in the ultraviolet, which allows it to be measured at high altitudes. This can be seen by performing simulations of the atmospheric transmission  $T(l, z)$  as a function of tangent altitude  $z$  and wavelength  $l$ , by multiplying the transmissions of various gases and aerosols (Fig. 3-3). At lower altitudes where the ultraviolet light is highly attenuated, ozone can be measured by observing the Chappuis band in the visible. Measurements in both bands may consequently be used to retrieve tangential column densities of ozone over a wide range of altitudes. Model calculations for transmissions in the infrared of O<sub>2</sub> and H<sub>2</sub>O, respectively, are shown in Figs. 3-4 and 3-5.

Suitable multi-element detectors are charge coupled devices (CCDs), semiconductor devices composed of intrinsic Si and a matrix of charge confirming electrodes, which define pixels. By coincidence, there is an almost ideal match between the quantum efficiency curve  $q(l)$  of silicon as a function of wavelength and the domain over which ozone absorbs radiation. At short wavelengths there are technical limitations which still allow the GOMOS spectral range to extend down to 250 nm, where  $s(O_3)$  is at its maximum value. At long wavelengths ozone absorbs significantly up to 800 nm (the CCD sensitivity limit is at 1000 nm).

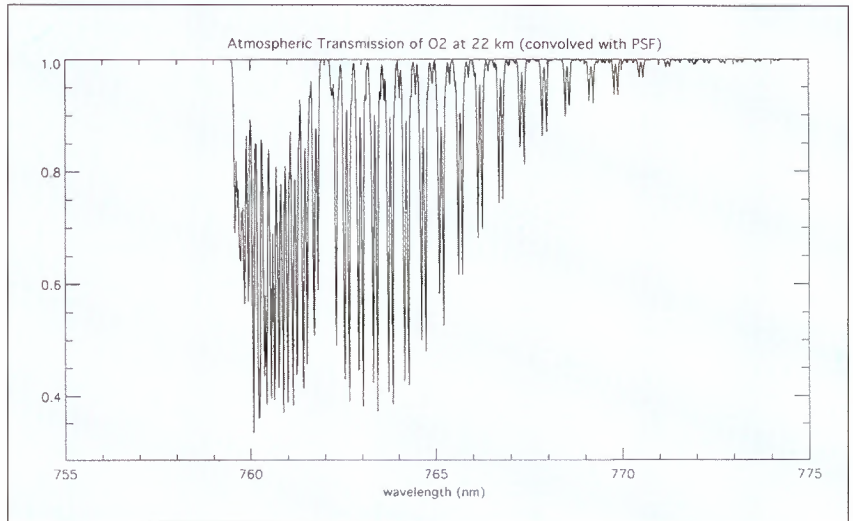
In the Huggins bands (310-350 nm),  $O_3$  cross-sections are strongly dependent on the atmospheric temperature. Therefore, a long-term variation of absorption of the ultraviolet as measured by GOMOS might be due to a temperature, as opposed to an ozone, variation. To avoid this, GOMOS measures temperature via the A band of  $O_2$  at 760 nm. Since  $O_2$  is a perfectly mixed gas and the air is in hydrostatic equilibrium,  $O_2$  density is directly connected to atmospheric temperature:

$$\frac{l}{T} \frac{dT}{dz} + \frac{l}{[O_2]} \frac{d[O_2]}{dz} = - \frac{mg}{kT} \quad (3.1)$$

This measurement of  $O_2$  also makes it possible to relate all observed densities of ozone and other trace gases to the air density, to compute the mixing ratio  $[O_3]/[\text{air}]$  directly, without reference to other data which might bring additional error sources. This is important because mixing ratio rather than density is the quantity more often used in models and comparison of GOMOS measurements with models is therefore easier.

Stratospheric water vapour  $H_2O$  is fundamental to the budget of many trace gases in the stratosphere. It is therefore important to determine its three-dimensional distribution and long-term trends. The strongest  $H_2O$  absorption band in the CCD silicon domain is at 936 nm, therefore GOMOS also covers this wavelength range. The chemistry of ozone is also very much connected to reactive nitrogen gases.  $NO_2$  absorbs in the whole visible domain and  $NO_3$  (existing only at night) can be observed at 662 nm.

In view of these considerations from the scientific objectives, GOMOS will

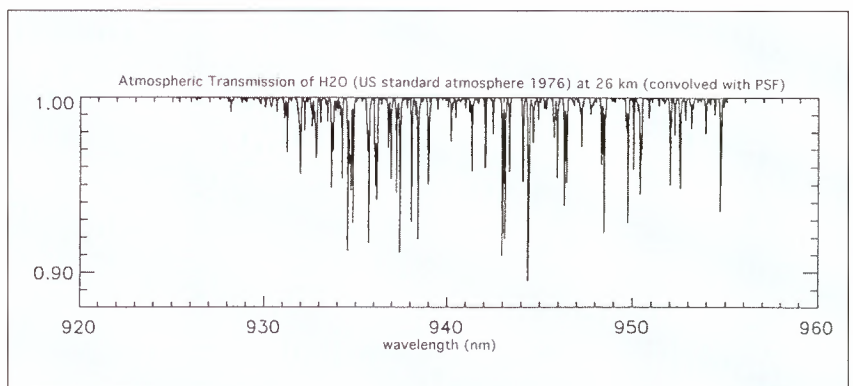


observe in the spectral bands given in Table 3-1.

**Fig. 3-4 Atmospheric transmission of  $O_2$  at 755-775 nm**

Several aspects were taken into consideration in deciding on the spectral resolution. One important aspect is that, if there is an unknown atmospheric absorber, which is not taken into account in the ozone retrieval process, it can bias the  $O_3$  retrieval. If, in addition, this absorber has a trend during the lifetime of GOMOS, one might confuse this with an ozone trend. Therefore, the observed spectra must be compared with model spectra in order to identify systematic discrepancies. This consideration called for a complete monitoring of the spectrum with a resolution of about 1 nm.

**Fig. 3-5 Transmission of  $H_2O$  around 950 nm**



Band	Wavelengths	Resolution	Main Usage
UV-visible	250 nm - 675 nm,	1.2 nm	O <sub>3</sub> , NO <sub>2</sub> , NO <sub>3</sub> , Aerosol, (OCIO, BrO)
Near IR (1)	756 nm - 773 nm,	0.2 nm	O <sub>2</sub> (density and temperature)
Near IR (2)	926 nm - 952 nm,	0.2 nm	H <sub>2</sub> O
'Blue' photometer	470 nm - 520 nm,	50 nm	scintillations, turbulence
'Red' photometer	620 nm - 700 nm,	50 nm	scintillations, turbulence

**Table 3-1 GOMOS wavelength ranges and their usage**

Several atmospheric trace gases have spectral features with structure on a wavelength scale in the range of 1 nm: in particular there are the NO<sub>2</sub> features around 410 nm, the ozone Huggins bands, SO<sub>2</sub> (of volcanic origin) around 300 nm and OCIO (SO<sub>2</sub> and OCIO might be detectable under certain conditions, but are not an objective or design driver for GOMOS). In such cases, differential absorption in limited portions of the spectrum may be used to determine the quantity of gas, by measuring the structure in the spectrum of the transmission (DOAS method).

For O<sub>2</sub> and H<sub>2</sub>O in the near IR, the spectral signature has variations on a scale smaller than 1 nm, calling for a resolution of about 0.2 nm.

The signal-to-noise (S/N) ratio has to be specified for a given integration time, which is connected to vertical resolution. With the Envisat orbit at 800 km, the tangent height of the line-of-sight to a star changes by 3.4 km/s for the fastest occultation, one that occurs in the orbital plane. Therefore, an integration time of 0.5 s will give a vertical sampling better than 1.7 km or one quarter of an atmospheric scale height (as small as 1 km for many occultations). Vertical sampling provides a limit to vertical resolution when the signal-to-noise ratio is large. An important advantage of the stellar occultation technique is that it provides a very accurate

definition of the tangent heights encompassed by each measurement, better than 30 m, independent of the spacecraft attitude.

Simulations have shown that, in order to retrieve ozone density with an accuracy of better than 1% in a significant range of altitude, a signal to noise ratio of 100 was required for each spectral pixel (of width 0.3 nm). Given the brightness of the brightest stars, this determined the size of the optical collecting area for GOMOS.

Small-scale structures in the temperature/density profile (and therefore refraction index) induce fast variations of the stellar intensity during occultation, as observed from the Salyout space station [Gretchko et al., 1981]. Because the index of refraction of air depends on the wavelength, scintillations are not collocated at all wavelengths, and the star's image will be distorted by chromatic refraction. However, measuring the scintillations at high frequency (1 kHz) with two fast photometers at different wavelengths allows the reconstruction of the scintillations at all wavelengths, so that each spectrum can be corrected for the scintillation effect.

In dayside, in order to account for contributions from scattered light, the instrument has to simultaneously observe the spectrum of the target star, of the sky above the star and of the sky below the star. The plane of dispersion must always be parallel to the limb of the atmosphere.

### 3.3 The Contribution of GOMOS Measurements

The mission objectives of GOMOS are discussed in Chapter 2. This section describes how GOMOS data can be used to achieve the scientific objectives

### 3.3.1 Monitoring of O<sub>3</sub> profile and trends

Because GOMOS measurements of ozone only rely on two measurements of the same star closely spaced in time, there are no calibrating devices in GOMOS that can drift with time. All drifts in GOMOS spectral parameters cancel when the ratio is taken. This immunity to drift applies not just to total ozone but to the measurements of the profile of ozone. Furthermore, in the lower stratosphere, GOMOS will measure ozone using its visible absorption bands, which are not temperature sensitive. Hence not even errors in atmospheric temperature combined with drifts in atmospheric temperature will give rise to drifts in GOMOS ozone in this crucial altitude region.

#### a) Night-side and day-side occultations

Because of the presence of scattered sunlight on the day-side, stellar occultations are much more difficult to achieve than on the night-side. However, day-side occultations are necessary as there is diurnal variation in NO<sub>2</sub> above 20 km and in ozone above 50 km (from photochemical models). The relatively narrow entrance slit of the spectrometer (200 μm, or the size of 10 spectral pixels) will limit the day-side limb contribution entering the spectrometer. It should be noted that the spectral resolution of the stellar spectrum is not affected by the slit width, but rather by the blur circle of the telescope, the pointing stability and the grating performance.

#### b) Number of stars that can be observed

The brightest stars give the best ozone retrievals. Also the colour of the

Limiting magnitude	Numbers of stars
$m_V \leq 0$	4
$0 < m_V \leq 1$	11
$1 < m_V \leq 2$	34
$2 < m_V \leq 3$	120
$3 < m_V \leq 4$	340

star is important; hot stars being favoured for the ultraviolet (ozone at high altitudes), while cool stars are preferred for the infrared (H<sub>2</sub>O at 936 nm).

**Table 3-2 Observable stars**

With the capabilities of GOMOS as presently defined, it will be possible to perform useful occultations with about 500 stars; they are distributed as shown in Table 3-2.

Among the 500 stars, only about 200 are occulted for a particular orbit and time of year. Not all of them can be observed in each orbit due to a lack of time. A natural criterion for the selection of a star is its brightness and temperature. A scientific strategy has been established, taking into account the actual star distribution and desired geographical coverage and scientific objectives (see Chapter 6 on mission planning).

#### c) Ozone trend

An estimate of the trend capabilities is made in analogy with an earlier computation made by **Frederick, 1984**. He addressed the problem of the detection of an ozone trend from one single ground station, performing a total of  $n$  measurements  $x$  at regular intervals  $\Delta t$ , over a duration  $D = n\Delta t$ . Annual, semi-annual and quasi-biennial variations are assumed to be regressed. The calculation made by Frederick is valid for measurements fully decorrelated spatially and in time. GOMOS measurements, however, are not fully decorrelated, which leads to a slightly

modified calculation of the minimum detectable trend.

The minimum trend  $\delta$  that can be detected with a confidence interval of 95% is:

$$\delta = 1.96 \frac{\sigma(x)}{\Delta t} \sqrt{\frac{12}{N_{ind}^3}} \quad (3.2)$$

$N_{ind}$  is the number of independent measurements. If  $N_{cor}$  is the number of correlated occultations and  $N_{tot}$  the total number of occultations during GOMOS' lifetime, the number of independent measurements is  $N_{ind} = N_{tot}/N_{cor}$ , with  $N_{cor}$  being approximately 8 (3 to 4 in space and 2 to 3 in time) for the lower stratosphere. In the middle stratosphere  $N_{cor}$  is approximately 4 and in the upper stratosphere 1.  $N_a$  is the number of independent measurements per year with  $D$  being the total lifetime of GOMOS (nominal 4 years) and  $N_a = 25 \times 14.33 \times 365 / N_{cor}$ . The mean time between two independent measurements is

$$\Delta t = 1/N_a.$$

The total variance of each independent measurement is given by:

$$\sigma^2(x) = \sigma_{stv}^2 + \frac{\sigma_{inst}^2}{N_{cor}} \quad (3.3)$$

If the globe is divided into  $K$  geographical regions (for each altitude), the minimum trend can be calculated for each region as:

$$\delta = \frac{6.8}{D^{3/2}} \sigma(x) \sqrt{\frac{K}{N_a}} \quad (3.4)$$

A 4% variance of ozone at 40 km ( $s_{stv} = 4\%$ ) and a worst precision of 5% on stars of magnitude 3 ( $s_{inst} = 5\%$ ) is assumed, leading to  $s = 4.4\%$  (for  $N_{cor} = 8$ ). When the  $K$  regions are 9 latitude bands of  $20^\circ$  each, the minimum trend that can be detected by GOMOS is shown in equation (3.5).

When the world is divided into 100 geographical regions where the ozone trend must be studied, as suggested from Dobson-network analyses [WMO, 1990], the minimum detectable ozone trend is shown in equation (3.6).

Note that these are the extra limits to linear trends imposed by noise on GOMOS measurements. They do not include limits imposed by non-periodic variations in ozone (e.g. by volcanic eruptions) nor do they apply to nonlinear trends.

It can be noted that a higher precision is obtained for tangential column densities than for local concentrations. These primary data

$$\delta_{GOMOS}(lat, K = 9) = \begin{cases} 0.09\%/year & \text{in the lower stratosphere} \\ 0.07\%/year & \text{in the middle stratosphere} \\ 0.05\%/year & \text{in the upper stratosphere} \end{cases} \quad (3.5)$$

$$\delta_{GOMOS}(lat, K = 100) = \begin{cases} 0.3\%/year & \text{in the lower stratosphere} \\ 0.2\%/year & \text{in the middle and upper stratosphere} \end{cases} \quad (3.6)$$

will also be archived for trend studies as a function of altitude.

In summary, GOMOS will be able to respond to the accuracy requirement for ozone trend observations as noted in Section 2.2.1. On the other hand, GOMOS will obviously not be able to monitor over the required periods (decades) because of the limited lifetime of Envisat, but a successful operation of GOMOS would prove that this observation technique could provide a highly desirable option, possibly a key-instrument, for future ozone monitoring space programmes.

### 3.3.2 Other studies

#### *Other gases, SO<sub>2</sub> and volcanic aerosols*

GOMOS measurements of NO<sub>3</sub> and OClO are particularly important as they are potentially superior to measurements of these gases by other instruments, which observe sunlight rather than starlight: NO<sub>3</sub> only exists at night; and OClO is only present in small amounts until sunset, building up rapidly during the early part of the night. The profile of NO<sub>3</sub> is difficult to deduce with any accuracy from ground-based measurements, and total NO<sub>3</sub> has only been measured from a few sites. The rate of build-up of OClO is only known to limited accuracy; its geographic variability is not known at all. Hence GOMOS is in a position to make uniquely valuable measurements of NO<sub>3</sub> and OClO.

In addition to ozone, the trends in other constituents (NO<sub>2</sub>, NO<sub>3</sub>, H<sub>2</sub>O, T, aerosols...) will also be measured, and correlated with ozone trends for possible explanations of ozone depletion mechanisms, by comparison with models.

In conditions of polar ozone depletion, OClO might be measured with bright stars. In conditions of volcanic

activity, SO<sub>2</sub> might be also detected in the lower stratosphere with its strong spectral signature around 310 nm. Aerosols of volcanic origin may also be characterised from their spectral signature, different from aerosol between eruptions.

Improvements to models often require simultaneous measurements of many gases. Other instruments on Envisat are complementary to GOMOS in this respect. However, modern model assimilation techniques, if applied to chemical as well as dynamical measurements, should mean that simultaneity of measurements is not essential. By means of such assimilation, measurements on other satellites or from the ground can be integrated into a meaningful whole and can thereby allow useful tests of model predictions.

#### *Atmospheric turbulence and high-resolution temperature profile*

Scintillations of the stellar intensity are recorded with the photometers at two different wavelengths in order to correct each spectrum for the effect of scintillation. Scintillations result from the fine structure of the atmospheric vertical temperature profile. The spatial vertical frequency spectrum, obtained by Fourier transform of the photometer signals, is representative of the vertical fluctuations of the temperature, which in turn are representative of motions in the atmosphere (waves, turbulence, advection, convection).

Single-wavelength scintillations during a stellar occultation were obtained from the Salyut space station [*Gretchko et al., 1981, 1997*] and interpreted in terms of vertical structure of temperature. GOMOS should yield for the first time a climatology of small scale dynamics

parameters important for studying the mixing of species.

Furthermore, since there are two photometers, one can determine the actual high-resolution vertical profile of the temperature [Théodore, 1998] from a careful analysis of the time correlation of the two signals at two different wavelengths. This will allow the determination of the climatology of temperature perturbations induced by gravity waves and will give very valuable information for processes sensitive to temperature as for instance the formation of PSCs.

### ***Tangential occultations***

Stars in the orbital plane stay in the orbital plane during an occultation, and the line-of-sight of GOMOS tracks the star at the same azimuth ( $0^\circ$ ). This is the definition of a *vertical occultation*.

Stars outside the orbital plane are observed to move in azimuth at the horizon while they are setting behind the atmosphere. In a frame coordinate system related to GOMOS, during one orbit, a given star describes a cone around the pole of the Envisat orbital plane, of half-angle  $\alpha$ . When a star lies between an angle of  $\alpha = 62^\circ$  and  $\alpha = 66^\circ$  the cone is tangent to the Earth's limb, at the point where it reaches its minimum altitude. This is the definition of a tangential occultation, in which the horizontal displacement of the tangent point to the star is much larger than the vertical displacement.

For a given star, the angle  $\alpha$  varies by  $1^\circ$  per day at most. Therefore, tangential occultations of one star are seen at each successive orbit at an increasing altitude by steps of 4 km (or less). For a given bright star, tangential occultations cluster around a particular day of the year.

The horizontal structures of both scintillations and line densities are of great scientific interest, and GOMOS offers a unique observation opportunity. The slant column densities obtained from tangential observation are fully valid, but the vertical profiles have to be used with great caution because of the large horizontal extension – possibly over several hours local time, in particular in high latitudes and polar regions – of the observation.

### ***Polar stratospheric clouds (PSCs)***

In some cases, the horizontal optical thickness of PSCs is so large that the star tracker will lose the stellar signal. The fact that the star tracker loses the star could possibly be used as an indicator for the presence of PSCs. This could at least make the detection of the cloud possible, allowing the production of statistics of PSC occurrence and their cloud top altitudes.

### ***Noctilucent clouds***

Noctilucent clouds are seen from the ground during twilight. They are the 'visible' part of polar mesospheric clouds (PMC), most of which can only be observed from space. These are patchy thin layers (2 km) of small ice particles ( $r < 0.1 \mu\text{m}$ ) at 83-85 km of altitude, with vertical optical thicknesses of  $10^{-4}$  and tangential optical thicknesses of about  $10^{-2}$  (wavelength dependent). They are connected to the condensation of water vapour during the cold conditions of the summer mesosphere.

In emission, PMCs would be detected by the GOMOS spectrometers, mainly in the two background bands (the bands on the CCD above and below the star image). The actual brightness is about the same as

Rayleigh scattering at 50 km altitude and should give a significant signal, which could be interpreted in terms of Mie theory and particle size and nature. In absorption, the 1% absorption over 2 km altitude would be measurable with the fast photometers, which would give the exact height, vertical extent and vertical distribution. Because the absorption is so small, the effect might be detectable only in absorption spectra of the brightest stars. The emission spectrum would always be observable.

With its capability to detect the presence of PMCs at each occultation, GOMOS should establish an unprecedented corpus of data on these phenomena over the whole globe. Of particular interest will be its ability to document the north-south asymmetry and to monitor the evolution of PMC cover and the location of its equatorial boundary. Validation observations would be made with high-latitude lidar stations.

### ***Water vapour in the lower stratosphere***

GOMOS measurements of water vapour will have an uniquely good vertical resolution for remote sensors, and can cover locations where balloon-borne sondes cannot be launched. This good vertical resolution is particularly important in the lower stratosphere and upper troposphere. It is this altitude where the signal-to-noise ratio of GOMOS measurements of water vapour will be at a maximum.

GOMOS will be particularly well suited for the study of air dehydration near the tropical tropopause, as it has the capability to retrieve simultaneously high-resolution temperature profiles, water vapour

and aerosols. Furthermore, it can make measurements just above thick convective clouds without being perturbed.

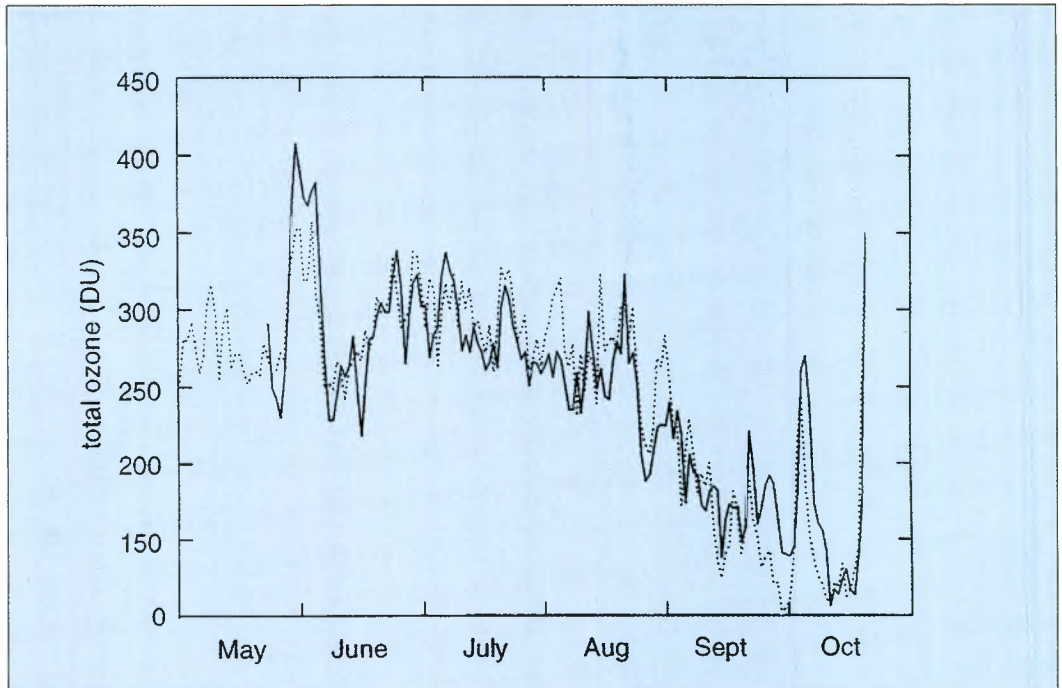
### ***Limb radiance and O<sub>3</sub> retrieval***

On the dayside, the limb radiance is due to Rayleigh and aerosol scattering of solar light. The spectrum of the recorded light contains absorption by ozone and other gases and may be analysed in terms of their vertical profile. Though the retrieval algorithm is much more complex than that for occultation, it will be useful to compare values of ozone retrieved by the two techniques. GOMOS has the capability to perform a 'fictitious star mode' occultation, in which the tracking mirror is no longer piloted by the image of a star in the star tracker, but rather programmed to perform a motion as if there were a star to be occulted, sweeping the whole range of altitudes across the bright limb. The limb radiance as a function of altitude can be measured and a SCIAMACHY-type algorithm applied. This type of data analysis for GOMOS would be experimental.

### ***Atmospheric transport***

As a result of extensive recent efforts by the scientific community, the dynamics of ozone in the lower stratosphere near the poles are now represented fairly well in numerical models (see Figure 3.6). However, poleward transport and descent are less well understood. GOMOS observations of temperature (from density) as well as of ozone, with good vertical resolution, should help to greatly enhance the understanding of this transport and the processes involved.

**Fig. 3-6 Ozone measured by the ground based UV-visible spectrometer SAOZ at Faraday in Antarctica during winter and spring 1994, compared to predictions by the Cambridge SLIMCAT 3-D model (Courtesy of A.M. Lee, Cambridge Centre for Atmospheric Science)**



# 4. Instrument Concept

## 4.1 The GOMOS instrument design overview

### 4.1.1 Introduction

GOMOS contains two different spectrometers, A and B, to meet both the spectral coverage and the spectral resolution requirements.

Spectrometer A covers the whole UV-visible range 250-675 nm.

Spectrometer B is used to cover the O<sub>2</sub> band at 760 nm and the H<sub>2</sub>O band at 936 nm, with the spectral sampling defined by the dispersion and pixel size (20 μm in the spectral direction, 27 μm in the vertical direction). The plane of dispersion is always parallel to the limb.

Two fast photometers, with bandwidths in the blue and the red, are also fed by the same telescope and measure fast variations of the stellar flux (scintillations) with a 1 kHz sampling rate all along the occultation. The star acquisition and tracking unit (SATU), with a 100 Hz sampling rate provides the necessary information for the acquisition of the star, the tracking and guidance. The image of the star must be kept within the entrance slit of the spectrometer, in spite of the motion of the star on the horizon, scintillations and micro-vibrations induced by the Envisat subsystem and other instruments. The optical bench of GOMOS, including the telescope, is fixed to the body of Envisat, and a flat mirror,

feeding the telescope, is piloted by the SATU and moved to keep the star in the slit during the whole occultation.

The star acquisition probability will be better than 91% (obviously a function of the star magnitude) and is specified for both day and night-side operation. Because of the signal attenuation through the atmosphere, a star cannot be acquired close to the limb. Therefore, GOMOS always acquires setting stars outside the atmosphere. In average, GOMOS will observe 40 stars per orbit.

GOMOS is located on the nadir-facing side of Envisat with its overall field-of-view opposite to the orbital velocity vector. The limitations on the overall motion of the mirror motion allow measurements only from -10° to +90° in azimuth (where 0° is the orbital plane), and in the range of +62° to +68° (with respect to nadir direction) in elevation. The elevation range corresponds to a tangential altitude range of -30 km to +280 km. Early simulations with the actual star field showed that this 100° azimuth angle restriction still allowed to perform a large number of occultations per orbit (30 to 50, depending on the season).

In order to cover the whole spectral range, there are four CCDs. Each of them has a band of 5 to 10 lines devoted to the measurement of the star spectrum, which are binned together electronically. In order to

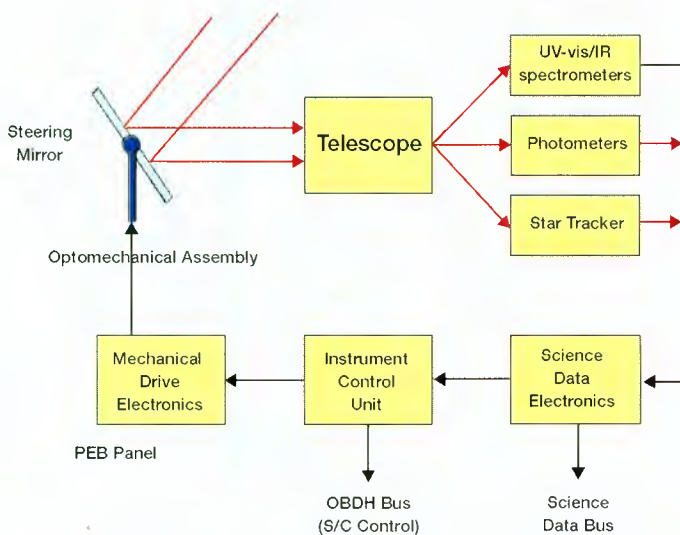


Fig. 4-1 Instrument block diagram

Fig. 4-2 GOMOS 3-D drawing



remove the background signal (scattered sunlight) from the star signal, two bands of 7-10 lines are devoted to the measurement of the background above and below the altitude of the star.

All blocks of lines (their separation and height are programmable by ground commands) are binned electronically so that all pixels of a column in a band are added together in the output shift register to form one spectral sample. Three spectra are transmitted to the ground for each CCD: one for the star, the two others for the sky background. The electronic on-chip binning is preferred over numerical addition to reduce the read-out noise, since there is only one readout per spectral sample. The readout noise is a limiting factor when dim stars are observed, and also in the case of strong absorption. The integration time is 0.5 sec.

An occultation will begin when the star is seen at an altitude of around 120 km (to avoid any atmospheric absorption). The occultation will end when the stellar sensor loses the star signal in the lowest atmospheric layers (cloud top, for instance). Then the mirror is sent to a new position to track the next star to be occulted, according to a mission scenario which will be computed in advance on ground.

The GOMOS instrument design fulfils two basic functions. The first is an *optical measurement function* to acquire spectral data. The second is the *pointing function*, which enables the instrument to maintain the star image within the field-of-view as the star sets through the atmosphere. The orientation of the field of view of the instrument will be in the direction of setting stars, i.e. opposite to the direction of the instrument's velocity vector. The block diagram of the

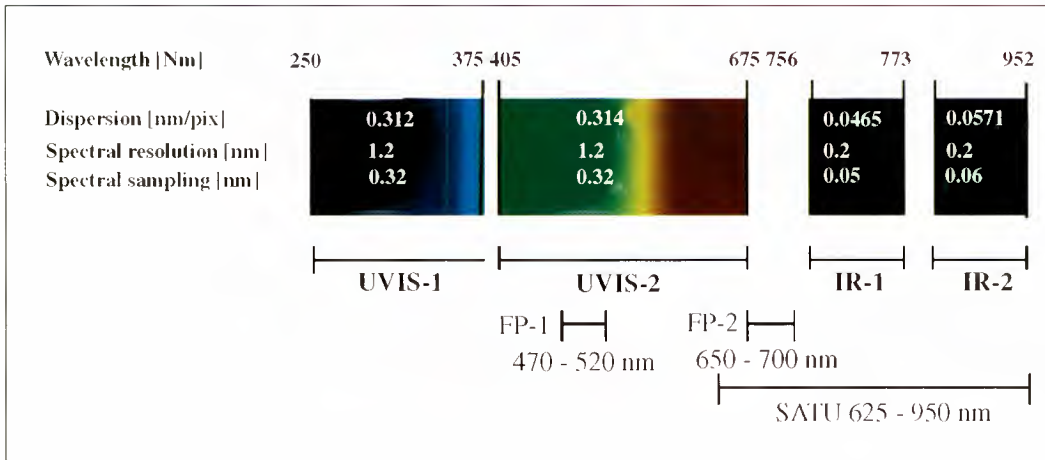


**Fig. 4-3 Spectral coverage of the GOMOS detection units**

instrument is shown in Fig. 4-1 and a 3-D drawing is shown in Fig. 4-2.

The instrument's optical design is based on a single telescope. Via a beam splitter in its focal plane this feeds simultaneously a medium resolution UV-visible spectrometer, a two-channel high-resolution near-IR spectrometer, a two-channel fast photometer, and two star trackers. The spectral coverage of the detection units is shown in Fig. 4.3. The detailed optical bench layout is shown in Fig. 4-4.

An important feature of GOMOS is the fact that for stellar observations, it functions as a slitless spectrometer, i.e. the star image itself is fed to the spectrometers and to the photometer. The main reason for the choice of this concept is that it allows the use of the entire stellar signal, very important in view of the poor signal provided by stars of magnitudes as weak as 4. The price paid for this optically efficient design is that a high performance pointing system has to be used to keep the star image fixed at the input of the spectrometers (in order not to degrade the spectral resolution and the spectral stability).

All the detection units are implemented on a thermally-

controlled optical bench. The optical bench and the telescope are mounted together and fixed on the instrument interface structure via carbon-fibre struts.

The steering front mechanism is a two-stage mechanism for line-of-sight pointing. The first stage, the orientator, is used to move the instrument's line-of-sight from one star direction to another. The orientator does not move during the

**Fig. 4-4 GOMOS detailed optical bench layout (OBD = optical beam dispatcher)**

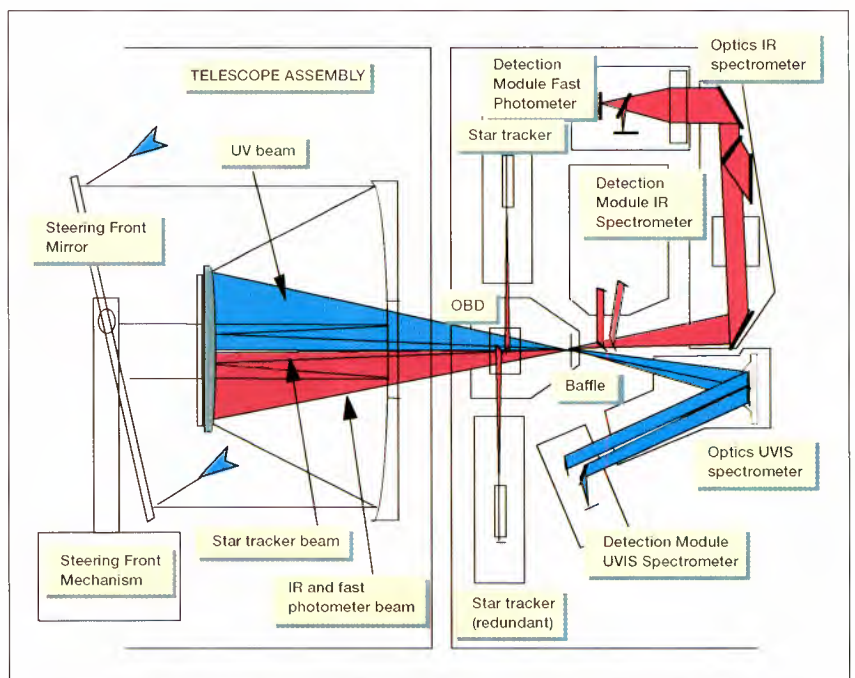




**Fig. 4-5 Steering Front Mechanism and input mirror**

tracking of the stars. The tracking phase is performed by the fine pointing system mounted on top of the orientator. The quick and accurate tracking function (100 Hz, better than 20 microradian tracking accuracy) is controlled in closed loop (i.e. feedback-loop via the star tracking unit back to the mechanism control unit) using the star-tracker correction information as calculated within the instrument control unit.

An opto-mechanical cover is mounted around both the optical and the steering front mechanism to provide the adequate straylight baffling and thermal insulation.

#### **4.1.2 Steering-front mechanism optics (SFM)**

The basic objectives of the SFM are to:

- acquire the image of a star in a large angular range ( $\pm 26^\circ$ ). The SFM rotates and maintains the mirror in a commanded position.
- track this star in a narrow angular field ( $\pm 2^\circ$  in both azimuth and elevation) with a 5 Hz control bandwidth.
- steer light from the star into the telescope via a plane mirror.

The first two objectives were realised through a two stage mechanism composed of a coarse stage ensuring a mirror rotation over a large azimuth angular range, and a fine stage ensuring a mirror rotation over a reduced azimuth and elevation angular range. Both stages are used in order to achieve an accurate initial rallying positioning, while the fine stage carries out the tracking function used during the actual occultation.

*Pointing performance* : as a constituent of the GOMOS instrument tracking loop, the SFM has been submitted to very stringent performance requirements which impose strict design constraints. The SFM design has also taken into account various constraints like spacecraft perturbing torques and forces, spacecraft microvibrations, larger perturbations induced by mechanism on the spacecraft, mechanism lifetime, mass and power. A torque control concept has been chosen for the fine stage mechanism due to the fact that it allows a low-pass rejection of microvibrations and the minimisation of perturbations induced into the platform.

Fig. 4-5 shows a photograph of the steering front mechanism and the input mirror.

#### **4.1.3 Telescope**

The Cassegrain telescope focuses light from the star and the nearby sky on

to the entrance plane of the imaging spectrometer. It uses a parabolic primary and a hyperbolic secondary mirror, which minimises astigmatism and coma.

The main design drivers were:

- low mass
- high stiffness
- long term stability of the inter mirror distance

The main optical requirement for the telescope is expressed in terms of a knife-edge distribution (KED) along the spectral and the spatial axes. Table 4-1 summarises the requirements.

The relative location of the pupils is shown in Fig. 4-6. The entrance pupil is located on the primary mirror. It provides adequate collecting areas according to photometric requirements for the back-optics. The rectangular entrance pupil is split into four sub-pupils dedicated to UV-visible spectrometer, IR spectrometer/fast photometers and to the optical chain of each star-tracker.

Table 4-2 summarises the telescope dimensions. The minimisation of the straylight has been a driver of the telescope design and is ensured by:

- stringent mirror reflectance requirements.
- baffle design, which prevents any focal plane direct illumination and minimises indirect illumination.
- use of additional fins on the structure and black painting of surfaces which can be illuminated by starlight or by scattered sunlight.

Pupil	Knife-edge distribution at 85 %	
	Spectral direction	Spatial direction
UVIS sub-pupil	20 $\mu\text{m}$	25 $\mu\text{m}$
IR and Photometer sub-pupil	25 $\mu\text{m}$	30 $\mu\text{m}$
SATU (tracking)	40 $\mu\text{m}$	45 $\mu\text{m}$
SATU (acquisition)	45 $\mu\text{m}$	50 $\mu\text{m}$

The primary and secondary mirrors are made of Zerodur and are isostatically mounted on a rigid structure. Each mirror is optically divided in two areas with silicon-oxide protected aluminium used for the IR-spectrometer/photometer and SATU channels. Yttrium/oxide-coated silver has been chosen for the UV-visible spectrometer channel to ensure a good UV reflectivity.

**Table 4-1 Telescope knife-edge distribution including the diffraction at end of life (4 years operation)**

Focal length	1050 mm
Mirror separation	250 mm
Primary mirror size	323 $\times$ 197 mm <sup>2</sup>
Secondary mirror size	176 $\times$ 111 mm <sup>2</sup>

**Table 4-2. Telescope dimensions**

#### 4.1.4 UV-visible spectrometer optical design

The UV-visible spectrometer provides a medium spectral resolution (1.2 nm) over a wide spectral bandwidth (from 250 nm to 675 nm).

The spectrometer design and its accommodation on the optical bench have been optimised to avoid important flux losses, mainly in the UV part of the spectrum. The UV-visible beam is folded only once, in

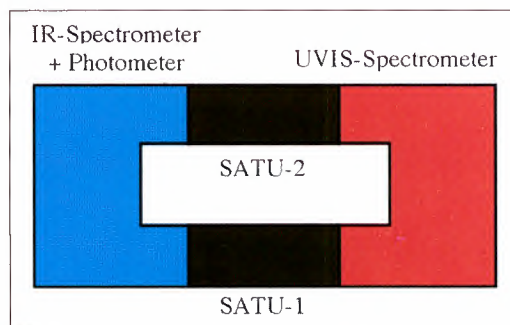


**Fig. 4-6 Telescope mirror pupil**

the optical beam dispatcher. Dispersion and imaging are performed by the same component, a concave reflective grating. The design is based on a Rowland configuration.

The major design constraints are the transmission, mainly in the UV band (250-350 nm), and the imaging quality. Consequently an aberration-corrected ion-etched holographic grating was chosen as the main element, with the blaze wavelength of 305 nm and with the UV band efficiency at its maximum at this wavelength.

Since the UV-visible spectrum length is 27.4 mm and the useful length of the CCD is 27 mm, the spectrum is imaged on two CCDs via a folding mirror located close to the image plane. A minor drawback is that the spectrum corresponding to the gap is lost (375-405 nm). On the other hand, an advantage of this design is that the use of two CCDs enables partial compensation for the grating's residual spectrum curvature and therefore improves the spectrometer image quality and removes a single-point failure.

In the UV-visible spectrometer the main straylight sources are the intrinsic grating straylight and the unused orders of diffraction, which are superposed on the useful spectrum or reflected toward the detectors by the mechanical parts surrounding the spectrometer. This straylight is minimised by filters located in front of each detector and by a dedicated baffle surrounding the grating. The grating 0 order is eliminated by a light-trap.

#### **4.1.5 IR spectrometer chain optical design**

The IR spectrometer provides a high spectral resolution (0.14 nm) over two narrow spectral bands:

- IR1 : 756 - 773 nm (O<sub>2</sub> band)
- IR2 : 926 - 952 nm (H<sub>2</sub>O band)

The spectrometer is based on a Littrow configuration. The main design drivers are the imaging quality and the transmission, and the fact that the IR spectrometer collimating optics are also used for the photometers' input beam collimation.

The use of a Littrow configuration in high orders of diffraction (order 16 for IR2 and order 13 for IR1) enables both spectra to be diffracted in the same direction, so the grating blaze angle is optimised for the middle of both IR1 and IR2 spectral bands. The flux diffracted in both useful bands is therefore at maximum.

The separation between the IR and the photometer channels is performed in the focused beam which optimises the dichroic splitter performances in terms of wavefront distortion and of transmission and reflection coefficients. The IR beam is reflected (its associated spectral band is narrower than that of the photometers) and the incidence angle on the dichroic splitter is minimised.

The diffracted IR1 and IR2 spectra are folded by the dichroic splitter and then focused toward the detection plane. The collimator is slightly off-centred and tilted with respect to the spectrometer input beam, so that the output beam is spatially separated from the input beam.

A dichroic splitter located close to the IR spectrometer image plane separates the IR1 and IR2 spectra, which are imaged on two CCD detectors, similar to the UV-visible spectrometer ones. The main straylight sources of the IR spectrometer are the unused orders of diffraction, which are superimposed on the IR1 and IR2 spectra. They are

rejected by narrow band-pass filters, which are located before the detectors.

Fig. 4-7 shows a sketch of the IR spectrometer optical layout. A photograph of the IR optical spectrometer unit is shown in Fig. 4-8.

#### 4.1.6 Fast photometers optical design

The fast photometers' optical channel provides images of the observed star in two spectral bands:

- photometer band 1: 650 - 700 nm
- photometer band 2: 470 - 520 nm

The main constraint concerning the photometers channel is the spot size because the detectors are small (14 x 14 pixels CCD). The photometer beam shares the same telescope sub-pupil as the IR input beam and is

collimated and separated from the IR beam in the IR optical spectrometer unit, refocused by dedicated optics (see Fig. 3-8). A dichroic splitter located after the focusing optics separates the red and blue

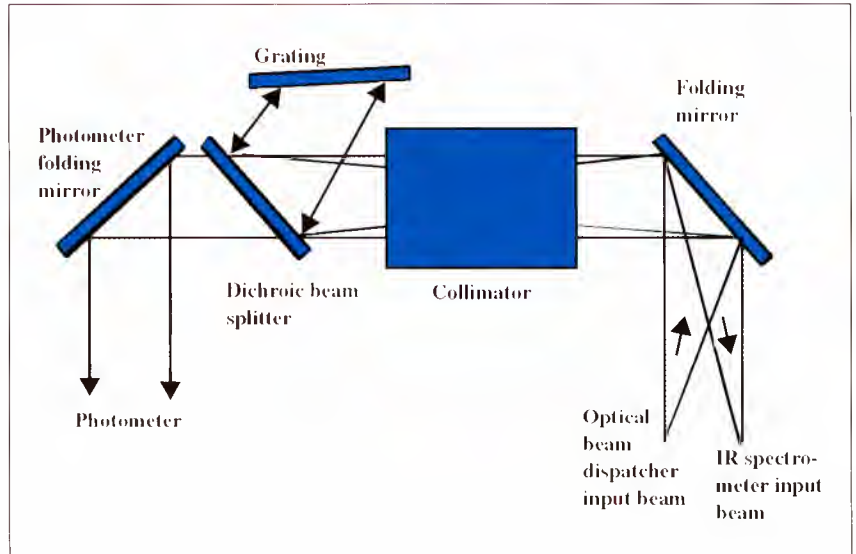


Fig. 4-7 IR-spectrometer and photometer optical layout

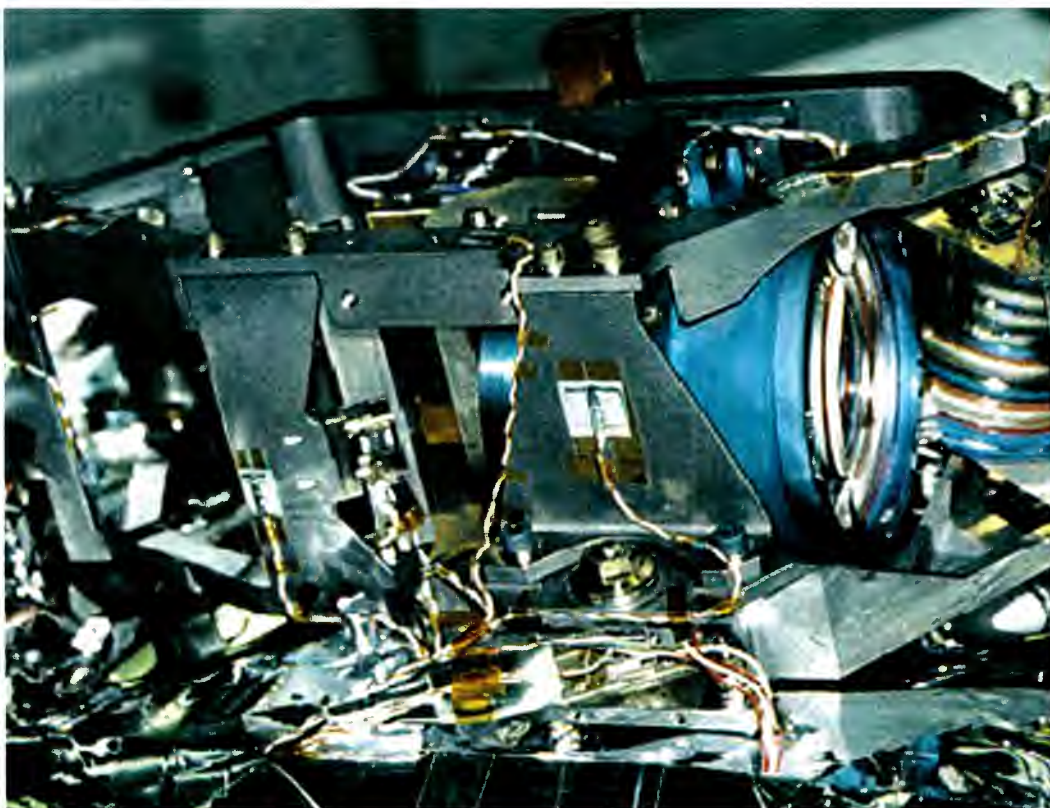
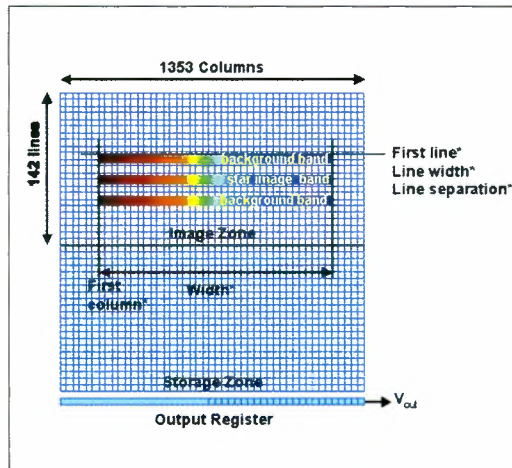


Fig. 4-8 IR Optical Spectrometer Unit

**Fig. 4-9 CCD Readout structure**  
(\*= programmable)



photometer channel bands. Each spectral band is imaged on a dedicated detector.

The focusing optics only perform a good chromatic correction over the red photometer band, so an additional optical correction element is located between the dichroic splitter and the blue photometer detector. A band-pass filter is located in front of each detector to select each spectral band.

The overall photometer channel is composed of the following elements:

- the telescope
- the optical beam splitter
- the IR optical spectrometer
- the detection module, which includes the focusing optics and the additional optics for chromatism correction, the phot 1/phot 2 dichroic splitter, the filters and the detectors.

#### 4.1.7 Star tracker optical design

The nominal and redundant star tracker channel provides, on each Star Acquisition and Tracking Unit (SATU) detector, an image of the observed star, with an equivalent

focal length of 630 mm. The main constraint affecting the star tracker channel is the star spot size, which must be  $30\ \mu\text{m}$  (85 % encircled energy) in the tracking field of view (FOV), and  $40\ \mu\text{m}$  in the acquisition FOV in order to meet the acquisition and tracking accuracy requirements. This optical quality is achieved using the Cassegrain telescope and a focal reducer with a 0.6 magnification. The star tracker's spectral band is 625-1050 nm, determined by a high-pass filter located close to the detector plane, which filters it. The upper limit of the SATU spectral band corresponds to the limit of sensitivity of the detector.

#### 4.1.8 UV-visible/IR detector design

For the UV-visible/IR detector, GOMOS uses CCDs with 143 lines of 1353 pixels. Two of these are used in the UV-visible spectrometer and two in the IR spectrometer.

The CCD operation is optimised for GOMOS such that only the part of the image containing information on the star spectrum and the adjacent background will be read out and processed. For each CCD, three bands are read out. Each of these bands consists of a programmable number of lines summed on-chip in the output shift register (see Fig. 4-9). The devices are thinned, back illuminated and treated with an antireflective layer, which is optimised in the UV band. During the integration period the devices work in inverted mode (multipinned mode) and thus exhibit extremely low dark current. Even though the inverted mode is inhibited during readout (resulting in a somewhat larger dark current), the additional dark charge generated is kept small due to the relative short readout time (with respect to the integration time) and contributes only about 1.5% of the overall dark charge.

The UV quantum efficiency (Fig. 4-10) is achieved using a complex backside treatment process, which consists of an ion (Boron) implant, laser annealing, anodisation, stripping and anodisation. The ion implant and laser annealing process creates an electrical field that allows UV photo electrons to reach the potential well. If this electrical field is not provided, UV photo-electrons would be recombined quite close to the air/silicon interface and would not reach the associated potential well. The anodisation and stripping process allows the minimisation of the ion implant thickness (which increases the UV sensitivity) and creates a SiO<sub>2</sub> layer which acts as an anti-reflective layer. The thinning of the substrate is performed by chemical etching after having sealed the CCD substrate on a thick substrate, which allows to maintaining flatness and rigidity.

The main characteristics are:

- pixels : 20 μm × 27 μm
- image zone : 143 × 1353 pixels
- memory zone : 142 × 1353 pixels
- dark signal : < 25 pA/cm<sup>2</sup> at begin of life at 20°C
- image zone charge capacity : 5.9 × 10<sup>5</sup> e<sup>-</sup>
- register zone charge capacity : 1.2 × 10<sup>6</sup> e<sup>-</sup>
- CCD linearity : < 0.6 %

Due to the optics line-spread-function (LSF) the star image (point source) will be spread out in the spatial direction and will cover several CCD lines. The instrument's static LSF width is close to the CCD line width, but adding also the

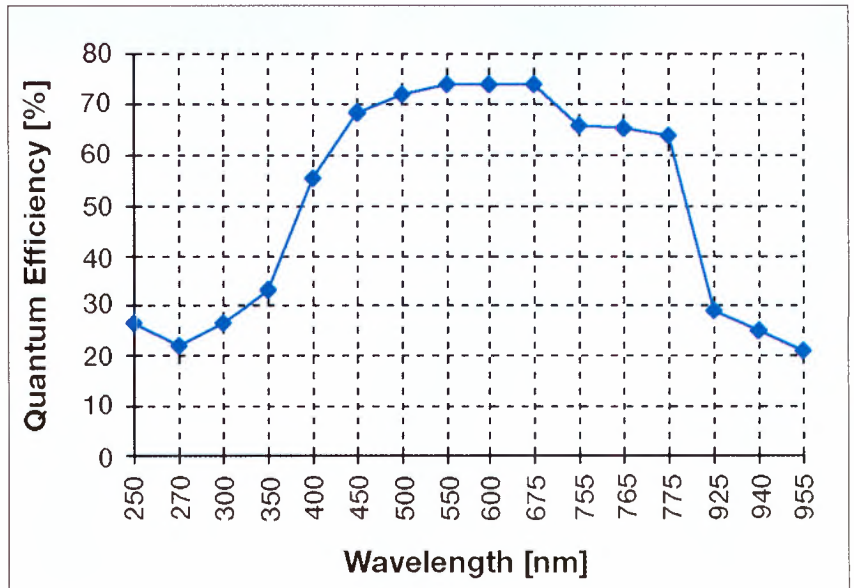


**Fig. 4-10 UVIS/IR CCD Quantum Efficiency**

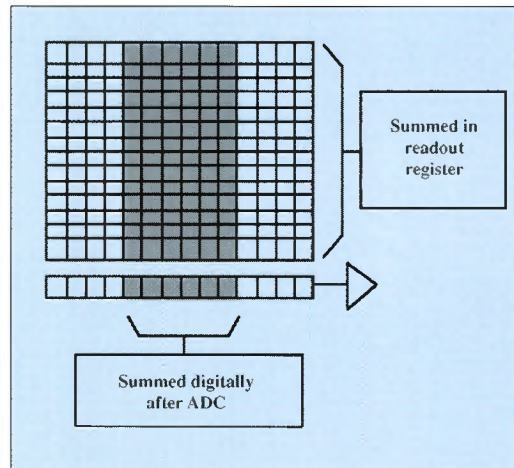
dynamic LSF (and scintillation in the lower atmosphere) insures that the spatial information will in fact cover several lines. In view of this, 7 lines of binning have been chosen for both star and sky band as the optimum width (selectable during in-orbit operation).

#### 4.1.9 Photometer detection design

The photometer uses a CCD with the following main characteristics:

- frame Transfer mode
- useful image zone : 14 x 14 pixels
- pixel size : 23 μm × 23 μm (100% aperture)
- quantum efficiency (average) :
  - in PHOT1 band (470-520 nm) : 0.2
  - in PHOT2 band (650-700 nm) : 0.4
- technology : photomos, buried channel

Fig. 4-11 Photometer readout scheme



- dark current (beginning of life) :  
1 nA/cm<sup>2</sup>

Since there are no imaging requirements for the photometer, all 14 rows will be summed in the readout register. Furthermore, five columns centred around the star position will be summed digitally after the analogue-digital converter.

Using the 'uniformity' mode (instrument mode) it is possible to access all pixels. A sketch of the photometer readout scheme is shown in Fig. 4-11.

#### 4.1.10 Star-acquisition and tracking-unit detection design

The main characteristics of the CCD device used for the SATU detection chain are:

- frame transfer mode
- image area : 288 × 384 pixels
- quantum efficiency:
  - 600 nm: 0.4
  - 800 nm: 0.4
  - 900 nm: 0.2
- dark current (begin of life)  
<1 nA/cm<sup>2</sup>

## 4.2 Instrument Electronic Design

The architecture consists of three parts:

- an instrument control unit (ICU), in charge of the instrument management, sequencing, TM/TC, housekeeping, active thermal control, pointing loop management, auxiliary data generation. It interfaces on the instrument side with the science data electronics and mechanism drive electronics and on the platform side with the on-board data handling bus (through the data bus unit) and the power buses.
- a science data electronics, in charge of all detector powering, sequencing and control, spectrometer and photometer data acquisition, processing, formatting and transfer to the platform low bit-rate interface, star tracker data acquisition, pre-processing and transfer to the ICU.
- a mechanism drive electronics. This equipment drives the steering front mechanism under ICU control.

A block diagram of the instrument electronic design is shown in Fig. 4-12.

## 4.3 Mechanical Design

The GOMOS instrument's structural hardware, split into five functionally independent structural parts as shown in Fig. 4-13.

### 4.3.1 GOMOS interface structure (GIFS)

The main function of the GIFS is to hold all GOMOS units (except

electronic units) together and to provide the mechanical interface with the Envisat platform. The GIFS interfaces on one side with the satellite (through a set of fixation points) and on the other side with the following instrument units:

- steering front mechanism and its connector bracket
- optical supporting structure struts and optical bench central machining (ball joint)
- telescope baffle
- optomechanical cover (OMC)
- optomechanical assembly (OMA) electrical harness and the associated connectors brackets
- purging pipe bracket and a set of purging covers
- thermal blankets

In addition the GIFS provides handling points for ground operation and optical cubes for instrument alignment.

The GIFS main panel is a sandwich structure (carbon-fibre reinforced plastic (CFRP) skins, aluminium honeycomb core). The thickness of the skins (1 mm) and of the core (70 mm) complies with the stiffness and stability specification.

#### 4.3.2 Optical bench

The optical bench is mounted on the GIFS by means of the optical-bench support struts and provides a highly stable mechanical interface with all the optical bench units on one side and with the telescope on the other side.

The optical bench includes the following hardware:

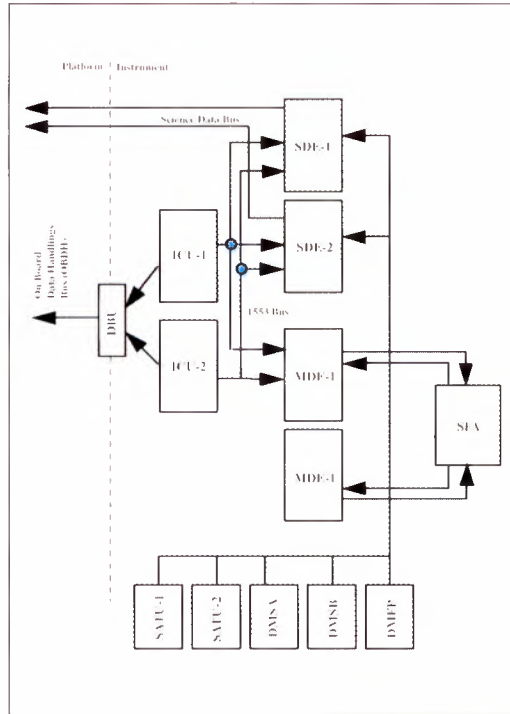


Fig. 4-12 Electronic Design

- optical bench main panel
- inserts for telescope and optical bench units
- harness fixation device and connectors bracket fixation devices

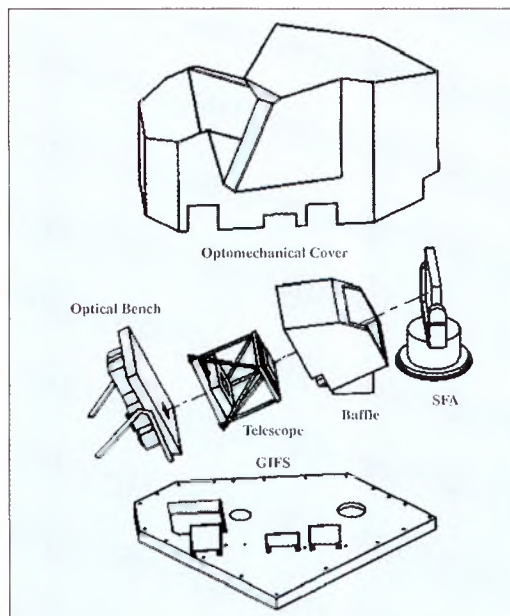


Fig. 4-13 Structural Elements

- grounding hardware
- heater mat carrier which provide support for the heaters
- active thermal control hardware
- alignment devices (optical cube)

The optical bench has to meet stringent dynamic and thermoelastic requirements in order to satisfy instrument pointing and stability performance requirements. Therefore, the optical bench main panel comprises a sandwich plate with CFRP skins (2.5 mm) and an aluminium core. Thick skins are necessary to ensure adequate stiffness as well as to provide a high thermal conduction (minimisation of thermal gradients). The optical bench is isostatically mounted on the GIFS in order to minimise the interface loads and induced distortions.

The optical support struts (OSS) are a set of four struts and one ball joint on a diaphragm supporting the optical bench in a defined and fixed position with respect to the GIFS and the steering-front mechanism optics (SFM). The struts consist of CFRP with an orientation of the fibres optimised to obtain a quasi-zero coefficient of thermal expansion for a strut after glueing of the titanium end-fittings.

#### **4.3.3 Opto-mechanical cover (OMC)**

The OMC is a secondary structure mounted on the GIFS, which aims to:

- protect the instrument core from Sun inputs, albedo and Earth thermal radiation
- insulate the instrument from space and provide a 'smooth' thermal environment

- support thermal hardware

The OMC is light proof in order to prevent any straylight arising near the focal plane. In addition the OMC provides an interface for fixing the hardcover used during on ground purging phase. Each part of the OMC is made of several flat CFRP sandwich facings with an aluminium core. Flat panels are linked together with bonded CFRP corner profiles.

#### **4.3.4 Telescope baffle assembly (TBA)**

The telescope baffle surrounds the telescope in order to protect it from straylight inputs, and to provide the telescope with a smooth and controlled thermal environment. The telescope baffle supports thermal hardware for the thermal control of the telescope environment and is made of CFRP skin sandwiches with aluminium cores, isostatically mounted on the GIFS, and including straylight fins. All internal surfaces of the telescope baffle are painted black. The whole telescope baffle is wrapped in a multilayer insulation.

### **4.4 Thermal Design**

Thermal regulation of the GOMOS opto-mechanical assembly (OMA) is performed independently from that of the spacecraft, while the electronics panel depends partly on the internal thermal environment of the payload equipment bay (PEB).

The OMA is thermally insulated from the PEB panel and ejects heat via three thermal panels integrated in the opto-mechanical cover (OMC) on the front of the instrument. These thermal panels guarantee an overall temperature below the maximum permitted operating temperature. The correct temperature is achieved using

a distributed network of heating elements and thermistors, controlled by the instrument control unit. The electronics unit, located in the PEB, releases its heat energy by radiation into the regulated interior of the spacecraft.

## 4.5 Software

The GOMOS ICU Software runs on a 1750 microprocessor located in the ICU.

Its main functions are the following:

- the management of the interface with the ground,
- the handling of the instrument modes. This involves handling the mode transitions requested by the ground macro commands,
- the on-board monitoring and anomaly management,
- the pointing control. This is the main function of the software and the most complex. It is a 100 Hz process, with very tight deadlines within each 10 millisecond cycle. This function manages all the 15 different pointing sub-modes and the transition between them. The most constraining sub-modes are centring and tracking, where the computations to be performed by the software are important compared to the allocated deadlines,
- the management of the star observation programme. In order to observe stars, the pointing function is commanded by some macro-commands that contain the sequences of stars to be observed,
- thermal control.

## 4.6 Instrument Operation

The Envisat platform is four-axis stabilised and permanently nadir-oriented. GOMOS is located on the nadir-facing side of Envisat with its overall field-of-view opposite to the orbital velocity vector.

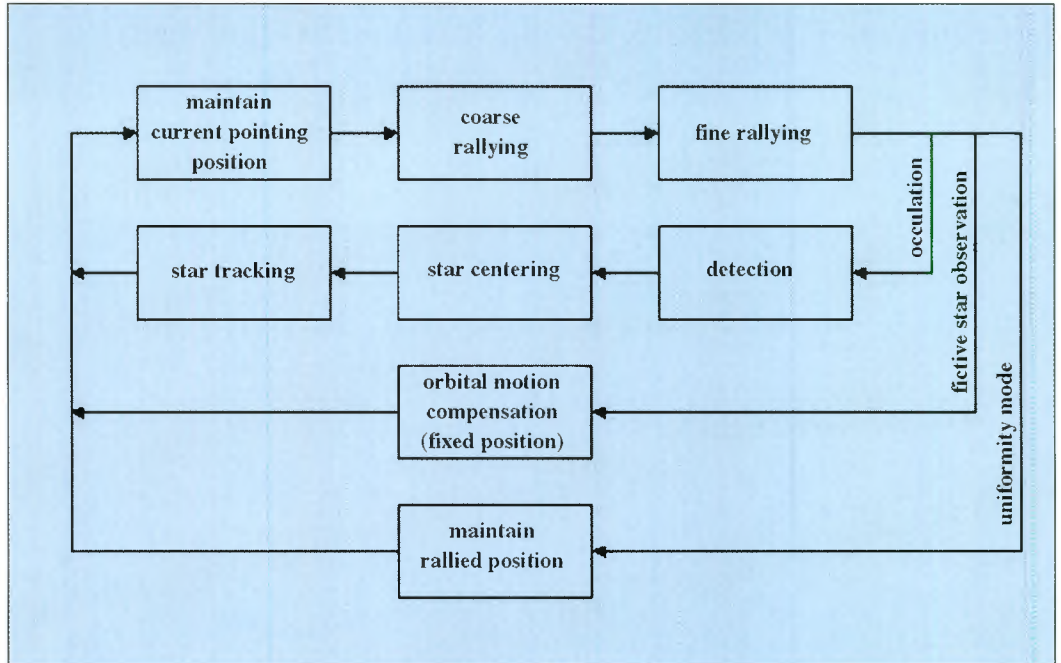
The GOMOS operation scenario is composed of three major activities, starting with uploading of all command, operation and star selection parameters. Each star acquisition will be time-tagged and executed sequentially. Prior to the expected arrival of each star, the instrument will direct the line-of-sight (i.e. the steering front mirror) in the direction where the star is expected to appear at the programmed rendezvous time. Once the rendezvous time is triggered, the instrument will start searching a  $\pm 0.3^\circ$  cone for the brightest stellar object. Once this is found, the instrument will lock on to it and direct the line-of-sight, using the fine steering mechanism, centring the image of the star on the tracking detector.

In order to perform the acquisition and tracking of targets, several pointing sub-modes are implemented, as sketched in Fig. 4-14. The transitions between these pointing sub-modes are performed automatically and do not need any user interaction. However the sub-mode status is monitored in telemetry.

All GOMOS operations use these pointing sub-modes in different sequential orders.

The typical sequence of a *star occultation measurement* will be:

Fig. 4-14 Instrument pointing loop



1. The steering-front mechanism optics (SFM) will be controlled to maintain its current position, i.e. it is not moving.
2. After receiving an observation command the SFM will be rallied to the commanded position by:
  - coarse rallying of the SFM coarse stage (azimuth only). During this sub-mode the fine stage will be controlled to maintain its current position. At the end of this phase the coarse stage actuator will be switched off.
  - fine rallying of the SFM upper stage (azimuth and elevation) in order to point the mirror to a fixed position with respect to the platform. The orientation is such that the instrument's line-of-sight will be close to the predicted star direction. If the commanded position has been successfully rallied, the pointing function will switch to the 'detection pointing' sub-mode at the rendezvous time.
3. At the commanded rendezvous time the 'detection pointing sub-mode' will be started. This acquires the star image within a specific detection window of the SATU CCD. The satellite's orbital motion will be compensated by a mirror counter-rotation in order to allow a successful star detection. When the star has been successfully detected, the pointing will automatically switch to the 'centring' sub-mode.
4. The 'centring pointing sub-mode' will perform a centring and stabilising of the star image on the SATU CCD in order to move it inside the tracking field-of-view.
5. If the star image is successfully centred in the SATU CCD, the tracking phase will be started. The SFM fine stage will be moved to maintain the target star within the tracking field-of-view located in the centre of the SATU CCD matrix. The pointing control must be performed precisely; a line-of-sight stability of typically 20  $\mu$ rad over a 0.5 sec period can be reached.

6. At the end of the tracking duration the current SFM position will be maintained (i.e., the mechanism stops).

In case of a *fictitious star observation*, the pointing switches to the 'orbital motion compensation' sub-mode at the end of the 'fine rallying pointing' sub-mode. In this sub-mode Envisat's orbital motion is compensated and no star detection is attempted. At the end of a defined duration, the pointing goes to 'maintain current position' sub-mode.

In case of the '*uniformity monitoring*' mode, the pointing switches to the 'keep rallied position' sub-mode after termination of the 'fine rallying' sub-mode. In this sub-mode (like in the 'maintain current position' sub-mode) the SFM fine stage is controlled to a fixed given orientation, with respect to the instrument reference frame. The SFM orientation at the end of the 'fine rallying' sub-mode is kept. The star tracker is in its 'centring' mode. At the end of a defined duration, corresponding to the 'uniformity monitoring' mode duration, the pointing function goes to the 'maintain current position' sub-mode.

- *Occultation mode*: performs acquisition and tracking of a star or, alternatively, performs the observation of a fictitious star, i.e. the orbital motion is compensated so that the instrument points in the direction of a fictitious star.
- *Linearity monitoring mode*: performs periodic monitoring of the instrument's radiometric response linearity by the observation of stars with variable integration times.
- *Uniformity monitoring mode*: performs periodic monitoring of the instrument pixel to pixel response uniformity by the observation of an extended uniform target (i.e. Earth limb).
- *Spatial spread monitoring mode*: performs periodical monitoring of the star spectrum and star image location by the observation of the instrument pixel to pixel response.
- *Pause mode*: intermediate operation mode performing preparation activities for observation sequences.

## 4.7 How to Use GOMOS

### 4.7.1 Modes, Transitions and Commanding Overview

The GOMOS instrument implements two categories of operational mode (see Fig. 4-15):

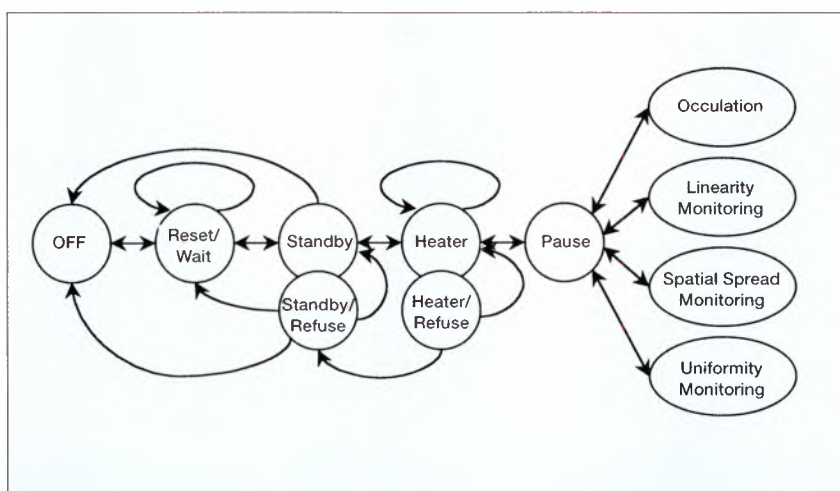
a) Support modes

The support modes are used to achieve or maintain full instrument operational conditions.

b) Operation modes

There are five operation modes:

Fig. 4-15 GOMOS Operational Modes



Type of measurement data	Occultation	Linearity	Uniformity	Spatial spread	Fictitious star
Spectrometer A/B binned spectra	yes	yes			yes
Spectrometer A/B 33 unbinned spectra			yes	yes	
Photometer summed image	yes				yes
Photometer pixel map		yes	yes		
SATU tracking window coordinate	yes	yes		yes	

Table 4-3. The various types of science data produced by GOMOS during the different operation modes

operation mode \ sub-mode sequence	maintain current position	rallying (coarse and fine)	keep rallied position	orbital motion compensation	detection	centring	tracking	(mechanism in zero position)	Objectives
Occultation Mode <sup>(1)</sup> (real star)	✓	✓			✓	✓	✓		perform spectral measurement during star occultation
Occultation Mode (fictive star)	✓	✓		✓					perform spectral measurements from bright limb scattered light
Linearity Monitoring	✓	✓			✓	✓	✓		monitoring of radiometric response linearity by observation of a stable target
Uniformity Monitoring	✓	✓	✓						monitoring of pixel-to-pixel response uniformity by observation of an extended, uniform target, e.g. Earth limb
Spatial Spread Monitoring <sup>(2)</sup>	✓	✓			✓	✓	✓		monitoring of pixel-to-pixel response by observation of a stable target
Pause								✓	preparation of observation sequence; ability to switch immediately to any of the measurement models

<sup>(1)</sup> Two types of occultation mode are available:

- *synchronous occultation mode*, repeating a list of star observations over several orbits (evolving star rendezvous parameters are interpolated between first and last orbits).
- *asynchronous occultation mode*, executing a list of star observations once.

Synchronous and asynchronous observations cannot be mixed within one orbit.

<sup>(2)</sup> The result of the spatial spread monitoring mode will be the information on which pixel of the CCDs the star image will be displayed. With this information specific macro-commands will be generated for the proper setting of the CCD columns and rows used for the star occultation.

Table 4-4 Sub-mode sequences used by the operation modes

The types of science data of the different operation modes are summarised in Table 4.3.

Table 4.4 summarises the sequences of sub-modes used by the operation modes. Table 4.5 summarises the parameters specifying the observation entry in an observation sequence.

### 4.8 Instrument Performance Summary

The instrument performance is summarised in Table 4.6.

operation mode \ specification parameters	star identifier	apparent magnitude	dark/bright limb flag	azimuth and elevation	azimuth and elevation rates	rendezvous time	tracking duration	integration time	mode duration
Occultation Mode (real or fictive star)	✓	✓	✓	(1)	(1)	✓	✓		
Linearity Monitoring	✓	✓	✓	✓	✓	✓	✓	✓	
Uniformity Monitoring				✓		✓		✓	✓
Spatial Spread Monitoring	✓	✓	✓	✓	✓	✓	✓	✓	

<sup>(1)</sup> for the first orbit and the last orbit (if synchronous observation)

**Table 4-5 Summary of parameters specifying the observation entry in an observation sequence**

*Acknowledgements:* MATRA MARCONI SPACE GOMOS Team and K.-D. Mau from DORNIER supplied part of this text.

## Requirement description

## Requirement

### SPECTROMETERS

Star characteristics

Defined by the 95% probability of the tracking system to detect the star

Visual magnitude range: max. -1.6 to min. 2.4 to 4 for stars with 30000 K and 3000 K temperature respectively

The spectral bands

Defined by the full-width half-maximum (FWHM) of the spectral response function

UV: 250 - 375 nm

VIS: 405 - 675 nm

IR1: 756 - 773 nm

IR2: 926 - 952 nm

Spectral resolution

Defined by the FWHM of the spectral rejection function

1.2 nm in UVVIS

0.2 nm in NIR

Spectral sampling

Spectral distance in nm between the centre of two adjacent pixels

0.3 nm in UVVIS

0.05 nm in NIR

Spectral rejection

Defined by the minimum spectral width containing 85% of the signal

UVIS: 85% within 4 samples monochromatic

NIR: 85% within 4.5 samples

Spectral stability knowledge in dark limb.

Error in knowledge of star star-spot stability, on spectrometer CCD, when considering the SATU barycenter position (peak to peak value)

0.07 nm in UVVIS

0.015 nm in IR1

0.018 nm in IR2

Spectral stability knowledge in bright limb.

Definition as for dark limb

0.22 nm in UVVIS

0.025 nm in IR1

0.030 nm in IR2

Relative spectral accuracy

Stability of the wavelength associated with one detector pixel between any two occultations

1.5 nm in UVVIS

0.3 nm in IR1

0.3 nm in IR2

Dispersion direction

Angle between wavelength dispersion plane and tangent plane of earth limb

Tangential to earth limb within  $\pm 2$  deg.

Dispersion Stability

Spectral drift between any two pixels over one occultation. Mainly the stability of the each CCD position w.r.t. the others

0.12 nm in UVVIS

0.02 nm in IR1

0.02 nm in IR2

Relative dispersion accuracy

Spectral drift between any two pixels over instrument nominal lifetime. Mainly the stability of each CCD position w.r.t. the others

1.5 nm in UVVIS

0.3 nm in IR1 0.02 nm in IR1

0.3 nm in IR2 0.02 nm in IR2

Spatial extent of spectra

Spatial width (angle in the vertical direction) of the CCD binned lines

**Band**

Binned lines

UVIS arcsec

IR1 / IR2 arcsec

**Target (star)**

2 - 14

18-70 arcsec

13-52 arcsec

**Background**

3 - 19

24-96 arcsec

18-70 arcsec

Polarisation sensitivity

Relative difference in sensitivity to two perpendicular polarisation directions  $(P_1 - P_2) / P_1 - P_2$  in percent

<1% (Goal)

Linearity response

Maximum deviation of the response w.r.t. perfect linearity of any spectral element for a variation of any specific flux within a dynamic -ratio of 1 to 10, i.e. local linearity over each decade. Gain setting dependant

1%

**Actual Performance**

Visual magnitude range: max. -1.6 to min. 4.6 to 6.8 for stars with 30000 K and 3000 K temperature respectively

UV: 248 - 371 nm  
 VIS: 387 - 693 nm  
 IR1: 750 - 776 nm  
 IR2: 915 - 956 nm

0.72 / 0.89 nm in UVVIS (min / max typical)  
 0.12 / 0.14 nm in NIR (min / max typical)

0.314 nm in UV, 0.312 nm in VIS  
 0.0465 nm in IR1, 0.0571 nm in IR2

UVIS: 85% in 2.8 / 4.7 samples monochromatic (min / max typ)  
 NIR: 85% in 3.15 / 3.85 samples monochromatic (min / max typ)

0.04 nm in UVVIS  
 0.007 nm in IR1  
 0.008 nm in IR2

0.04 nm in UVVIS  
 0.011 nm in IR1  
 0.014 nm in IR2

0.017 / 0.20 nm in UVVIS (dark / bright limb typical)  
 0.005 / 0.05 nm in IR1(dark / bright limb typical)  
 0.06 / 0.01.83 nm in IR2 (dark / bright limb typical)

Tangential to earth limb within ±2 degrees (worst case)

<0.01 nm in UVVIS  
 <0.002 nm in IR1  
 <0.002 nm in IR2

0.04 nm in UVVIS  
 0.02 nm in IR1  
 0.02 nm in IR2

Separation	Band	Target (star)	Background	Separation
- 4	Binned Lines	2 - 14	3 - 19	1 - 4
20 arcsec	UVIS	11-74 arcsec	16-100 arcsec	5.3-21 arcsec
20 arcsec	IR1 / IR2	11-74 arcsec	16-100 arcsec	5.3-21 arcsec

< 1, 3, 7, 7% for UV/VIS/IR/PHOT respectively

UV : 0.27 - 0.48% depending on gain / limb  
 VIS : 0.36 - 0.5% depending on gain / limb  
 IR1 : <0.33%  
 IR2 : <0.34%

**Table 4.6 Instrument performance summary**

*(continued on next page)*

**Requirement description****Requirement**

Integration Time  
The time during which the detectors are collecting photo electrons.  
Dead time  
Dead time between consecutive integration's (transfer time)  
Start time of record precision  
Datation accuracy

0.5 sec  $\pm$  0.5 msec  
< 10 msec  
< 5 msec  
< 100  $\mu$ sec

**PHOTOMETERS**

The spectral bands  
Defined by the full-width half-maximum (FWHM) of the spectral response function

470-420 nm and 650-700 nm

Photometer instataneous FOV  
The photometer pixel FOV (each photometer sees 14 pixels in the vertical direction and 5 pixels in the horizontal direction)

> 60 arcsec vertically  
> 10 arcsec horizontally

Photometer spatial rejection  
The target energy in percent collected by the 14 x 5 photometer pixels

> 95% of spatial LSF within 26 arcsec

Sampling frequency  
The rate at which the detectors are transmitting measurement values.  
Dead time  
Dead time between consecutive integration's (transfer time)  
Start time of record precision  
Datation accuracy

1 kHz  
< 0.1 msec  
< 5 msec

Linearity response  
Maximum deviation of the response w.r.t. perfect linearity of any spectral element for a variation of any specified flux within a dynamic -ratio of 1 to 10, i.e. local linearity over each decade. Gain setting dependant

1%

**POINTING REQUIREMENTS**

Pointing stability  
Peak to peak LOS jitter during one integration = FWHM of the dynamic LSF

Better than 40 microradian peak-peak

Number of occultations per orbit

45 on average, i.e. approximately 920000 occultations during the 4-year mission

Detectable stars number of stars  
Assuming use of SATU-2

No Spec

Loss of tracking probability  
Probability of losing star tracking due to other reasons than a) programmed tracking duration exceeded, b) edge of total FOV exceeded, c) edge of tracking FOV exceeded.  
Valid for specified visual star magnitude range.

<10% in dark limb, <20% in bright limb

Angular coverage  
Azimuth angle with respect to the flight direction  
Elevation angle with respect to the flight direction

-10 deg. to +90 deg.  
62 deg. to 68 deg.

Tracking FOV  
Maximum possible LOS range of the pointing function during a single occultation

7 deg. azimuth  
5 deg. elevation

**Actual Performance**

0.498 sec ± 50 microseconds  
< 2 msec  
< 3 msec  
< 100 µsec

466-528 nm and 644-705 nm

> arcsec vertically / spatial direction  
> 50 arcsec horizontally / spectral direction

> 95% of spatial LSF within 26 arcsec

1 kHz  
< 0.1 msec  
< 5 msec

Phot-1 (blue): <2.8% measured  
Real performance is likely below 0.5%  
Phot-2 (red): <0.51%

Better than 40 microradian peak-peak

45 on average, i.e. approximately 920000 occultations during the 4-year mission

Bright limb: 180 stars (typical)  
Dark limb: 1450 stars (typical)

<1% in dark limb, <20% in bright limb

-11 deg. to +91 deg. (typical)  
61.7 deg. to 69 deg. (typical)

7.4 deg. azimuth  
6.5 deg. elevation

**Table 4.6 Instrument performance summary**

*(continued )*



# 5. Characterisation and Calibration

## 5.1 Introduction

The main advantage of the GOMOS operating principle is that of being inherently self-calibrating as far as its principal low-level product, the atmospheric transmission spectrum, is concerned. This is defined as the ratio between the measured spectrum of the star without atmospheric absorption (i.e. outside the Earth's atmosphere) and the measured spectrum of the star with atmospheric absorption. This means that the instrument is self-calibrating, assuming that the instrument response function does not change during one occultation of typically 30 seconds (which is most unlikely).

However GOMOS is, as far as the star signal is concerned, a slitless spectrometer, so any difference in the pointing-error history between the two spectra will result in a small relative spectral shift between the two. Because of this the two spectra are initially spectrally aligned using the pointing history data from the star acquisition and the tracking unit (SATU). This procedure ensures that the self-calibration remains valid.

Nevertheless, transmission spectra may, due to long-term thermal distortion and the "settling" of the optical bench, be shifted with respect to each other in the long term. The related spectral shift is not reflected in the SATU data and this calls for

the calibration and monitoring of parameters related to spectral assignment and for precise knowledge of the dispersion.

Furthermore, due to the method used to achieve the ozone vertical density profiles from the transmission spectra, the instrument's spectral resolution needs to be known. The spectral resolution is measured and reflected in the spectral rejection parameter and the instrument line-spread-function (LSF).

As far as the self-calibrating nature of the spectrometer is concerned, the radiometric response, transmission and instrument gain are not important, since any long term response changes are cancelled when calculating the transmission. However, the radiometric response is of interest for the photometer data and for the spectrometer when used as a photometer.

## 5.2 Definition of Calibration versus Characterisation

Calibration is the process of quantitatively defining the system response with respect to known, controlled signal inputs. The *calibration parameters* are the instrument parameters which are expected to change and which therefore require continuous scrutiny and monitoring. GOMOS has special observation

modes, which will be used for in-flight monitoring of several calibration quantities and which are also used during the on-ground calibration.

The *characterisation parameters* are determined by design or measurement at unit level and are assumed to be fixed. Monitoring of these parameters is still necessary, as a drift could indicate changes in the instrument's functioning.

### 5.3 Characterisation and Calibration Database

The GOMOS characterisation and calibration database defines 35 parameters, of which some will be used for science data correction and some for instrument performance monitoring. The main calibration and characterisation parameters are listed in Table 5-1.

All the data presented in the following discussion relate to the flight model (FM) data and have been measured in ambient conditions (20°C and ambient pressure in the laboratory), unless otherwise stated. The main parameters related to the spectrometer are listed below:

- spectrometer wavelength ranges (50% transmission edges)
- spectrometer wavelength dispersion (nm/pixel or nm/mm)
- spectrometer static line spread function (spectral and spatial)
- spectrometer radiometric uniformity
- spectrometer linearity
- spectrometer and photometer radiometric sensitivity (DN/ph/s/nm/cm<sup>2</sup>)

### 5.4 Ground Support Equipment

Several items of equipment have been developed to support the instrument on-ground characterisation and calibration:

- *source-pack*  
optical bench with a collection of optical spectral sources.
- *collimator*  
30 cm aperture collimator for simulation of star and background signal
- *calphot*  
absolute calibrated photometer for determination of collimator output flux

The source-pack consist of a transportable optical table with a number of spectral lamps (Ne, Hg, K/Ar and K) and a HeNe laser. A Jobin-Yvon monochromator is fed with a xenon lamp flux and is used as a medium resolution adjustable spectral source (FWHM  $\Delta\lambda=0.1$  nm).

The collimator simulates a star with adjustable spectral and photometrical characteristics (motorised star focus) A background signal can be superimposed on the star signal to simulate the Earth limb. The assembly is vacuum compatible. It will be extensively used during ambient, as well as thermal vacuum, tests.

The calibration photometer measures the input flux to the collimator. The specified accuracy is  $\pm 10\%$ . The detector is a Hamamatsu photo-multiplier tube with a InGaAs(Cs) photocathode. The spectral range is specified as 160 to 1040 nm.

<b>Parameter characterised</b>	<b>Comment</b>
Spectrometer wavelength ranges	Spectral band 50% transmission edges vs. CCD position
Spectrometer wavelength dispersion	For each CCD a dispersion look-up table
Spectrometer radiometric sensitivity	Spectral sensitivity (ph/s/cm <sup>2</sup> /nm/DN)
Spectrometer spectral uniformity	Pixel to pixel CCD uniformity maps
Spectrometer linearity	Detection chain response to full exposure range
Spectrometer IR vignetting	Instrument response variation at end of pointing range due to vignetting from optomechanical cover
Spectrometer static line spread function (spectral and spatial)	Semi-static (optical and detector MTF) line spread function. Also contains dynamic term from mirror control loop
Spectrometer direction of spectral dispersion	Spectrum rotation vs. pointing direction
Spectrometer dark current	CCD dark signal maps
Spectrometer dark current temperature dependency	CCD dark current doubling temperature
Photometer spectral bands	Spectral band 50% transmission edges
Photometer radiometric sensitivity	Photometer sensitivity (ph/s/cm <sup>2</sup> /DN)
Photometer response uniformity	CCD uniformity pixel map
Photometer linearity	Photometer response to a linear increasing flux
Photometer dark current	CCD dark signal maps
Photometer dark current temperature dependency	CCD dark current doubling temperature
SATU radiometric sensitivity	Photometric response of SATU
Instrument-external Sun stray light response	CCD stray light maps due to sun outside but close to line of sight (sun angle > 40 degrees)
Instrument-external Earth stray light response	CCD stray light maps due to Earth limb outside but close to line of sight
Instrument internal stray light response	Internal scattering CCD maps
SATU pointing shift with respect to background	SATU pointing shift due to limb gradient
SATU output versus wavelength shift	Pointing data (SATU) conversion factors
Polarisation sensitivity	Sensitivity to polarisation of extended source
Steering mirror reflectance vs. angle of incidence	For correction of photometer response

## 5.5 Wavelength Ranges, Assignment and Dispersion

The GOMOS ozone retrieval algorithm fits the wavelength assignment of the pixels in the transmission spectrum. It uses a first guess of the wavelength

assignment taken from the calibration database that includes, for each CCD, a wavelength look-up table.

Even though the environmental tests have shown that the wavelength assignment is very stable, it is likely

**Table 5-1 Main Calibration and Characterisation Parameters**

<b>Band</b>	<b>Measurement Half-maximum [nm]</b>	<b>Specification Half-maximum [nm]</b>
UV	242 - 382	250 - 375
Visible	385 - 693	405 - 675
IR1	749 - 777	756 - 773
IR2	916 - 956	926 - 952
Phot 2 'Blue'	468 - 528	470 - 520
Phot 1 'Red'	644 - 703	650 - 700

**Table 5-2 Spectrometer/Photometer spectral band-edges. The measurements show that the UV band is slightly shifted toward the shorter wavelength compared with the specification (250-375 nm), and also that the visible band is extended 18 nm toward the longer wavelength with a half-maximum at 693 nm (specification 405-675 nm). The photometer bands are both slightly larger than the specification**

to change due to the relatively harsh launch environment. Consequently the on-ground wavelength assignment cannot be assumed to be useful for in-orbit operation. An on-ground calibration is nevertheless important to assess the effect of the launch and will be useful for initial in-orbit instrument programming.

The wavelength range of each CCD is determined from a white spectrum covering the complete band. The measurements in Table 5.2 list the half-maximum values at the band edges. The measurement in the infrared band (IR2) is somewhat degraded by the strong variations in the transmission of the fibre used to couple the source to the collimator, to illuminate GOMOS. The IR2 band edge accuracy is consequently about  $\pm 1$  nm.

**Table 5-3. Spectrometer dispersion (from FM ambient test)**

From the table it can also be seen that all spectral bands are compliant

with the specifications and, since the GOMOS transmitted wavelengths can be programmed, this allows for the shift adjustment (but not extension) of spectral bands.

Spectral dispersion is unlikely to significantly change due to the launch environment or during the lifetime of the instrument. The spectral assignments and dispersion were deduced from measurements by several monochromatic lines using a monochromator from Jobin-Yvon. Table 5-3 lists the barycentre spot-positions of each wavelength, for each CCD. The final spectral assignment calibration, was performed in thermal vacuum using spectral lamps, with the same results as during the ambient test presented below.

From the spatial position column, it can also be seen that the spectrum is slightly rotated (of the order of  $0.1^\circ$ ). This small rotation, together

<b>Band</b>	<b>Wavelength (nm)</b>	<b>Spectral position (pixel number)</b>	<b>Spatial position (pixel number)</b>	<b>Dispersion (nm/pixel)</b>	<b>Mean dispersion (nm/mm)</b>
UV	280	558.06	79.99	0.314	15.70 $\pm$ 0.05
UV	370	844.82	79.46	0.313	
Visible	435	963.04	78.47	0.312	15.58 $\pm$ 0.05
Visible	675	192.45	79.01	0.310	
IR1	761	654.39	83.47	0.0466	2.32 $\pm$ 0.02
IR1	771	870.25	82.93	0.0464	
IR2	931	556.47	83.74	0.0574	2.85 $\pm$ 0.02
IR2	951	907.75	84.06	0.0569	

with the spatial line-spread-function (or spatial rejection), is the main contributor to the star-band binning width (presently set at 7 lines).

The spatial/spectral position accuracy was calculated to 0.2 pixel. The corresponding UV/visible dispersion accuracy is 0.001 nm/pixel and the IR1/IR2 dispersion accuracy 0.0005 nm/pixel. The corresponding value in nm/mm is found by dividing by the spectral direction pixel size (0.02 mm or 20  $\mu$ m).

## 5.6 Spectrometer Line Spread Function

The spectrometer line spread function (LSF) is a measure of the instrument's ability to resolve fine spatial or spectral details in the scene or the spectrum. Knowledge of the LSF is important in the GOMOS product algorithm because the reference transmission is based on an ideal instrument with higher resolution than the instrument can achieve. Prior to correlating the measured transmission with the reference, the reference spectrum needs to be convoluted with the LSF and re-sampled to reflect the real instrument resolution. The LSF is specified in terms of the rejection, defined as the width of the

symmetric integral of the line spread function, along either the spatial or the spectral direction containing 85% of the LSF area (or energy of the spectral line observed). The spatial rejection value is particularly important for setting the band-binning width (or number of rows per binned line).

The LSF has been measured at 18 wavelengths from 250 nm to 756 nm, and with model predictions performed for three wavelengths in the IR2 band from 926 to 956 nm. Three measured spectral LSFs are presented here in terms of the spectral rejection (85%) and spectral resolution (FWHM) as measured during the instrument thermal vacuum tests. The specified and measured spectral rejection and resolution are given in Table 5-4.

### 5.6.1 Contributors to systematic errors

There are three main contributors to the instrument LSF and the total instrument LSF is the convolution of the three:

- The *detector modulation transfer function* (MTF) is a measure of the ability of the detector to resolve the image focused onto the focal plane (the CCD). The primary contributor to the detector MTF is the pixel cross-talk, i.e. the fact that

**Table 5-4. Spectrometer spectral rejection (85%) and spectral resolution (FWHM). The value in pixels is found by dividing by the spectral sampling width (UVIS = 0.31 nm/pixel, IR1 = 0.05 nm/pixel and IR2 = 0.06 nm/pixel)**

Wavelength (nm)	Spectral Rejection		Spectral Resolution	
	Specification [nm]	Measured [nm]	Specification [nm]	Measured [nm]
254	1.4	1.48	1.2	0.89
375	1.4	0.89	1.2	0.74
405	1.4	0.87	1.2	0.72
675	1.4	0.95	1.2	0.75
756	0.19	0.18	0.2	0.12
926	0.19	0.18	0.2	0.14

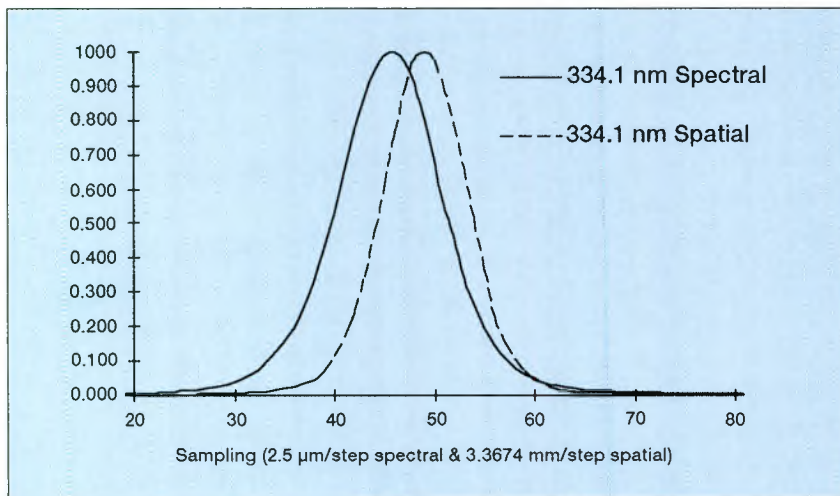


**Fig. 5-1 Static line spread function (Engineering Model Data). The full width half maximum (FWHM) of the two curves is 50.5 micron spectrally (2.5 pixels or 0.8 nm) and 53.9 micron spatially (2 pixels)**

photons falling on one pixel caused a response in neighbouring pixels.

- The *optical line spread function* is the ability of the optical system to resolve the spatial information of the scene. The major contributors are design, defocus and non-alignment due to thermal distortion. As far as optical design is concerned, the telescope aperture shape and imaging grating have a large influence on the defocussing, as well as the imaging of a curved spectrum onto a flat detector. Other less significant contributors include straylight and particle contamination of the optical surfaces. The static line spread function is in principle the convolution of the MTF and the optical LSF.
- The *dynamic line spread function* is the response of the detection system to a vibration of the optical axis. The main contributors are electronic noise in the steering-mirror control-loop and mechanical micro-vibrations from other moving mechanisms on Envisat such as reaction wheels and coolers. During the on-ground calibration the dynamic

components are, in addition to the control-loop noise, the acoustic and vibration environment coming from the test equipment (vacuum pumps, air-conditioning and other ambient noise-sources). During the on-ground measurements the dynamic contribution proved to be much smaller than first anticipated, partly due to the high stiffness of the pointing system, and can be expected to be a minor contributor to the total LSF.

Fig. 5-1 illustrates the static line spread function (convolution of detector MTF and optical LSF) as measured using a point-like monochromatic source of 334.1 nm.

### 5.6.2 Measurement method

The final LSF calibration measurement was performed in thermal vacuum with the instrument in spatial spread monitoring mode and with the pointing loop activated. The advantage of this set-up was that the instrument was in the same configuration and environment (apart from the 1g gravitational factor) as it will be in orbit.

Even though the acoustic or vibration environment will not be flight representative, the pointing loop control will effectively filter all mechanical noise below 5 Hz, while high frequency noise will be kept to a minimum, as the complete test set-up will be mounted on a seismic optical bench. As for long term effects such as moisture release, gravity, micro-setting and thermal effects, these are not expected to influence the results, due to the relatively short measurement time.

The test consists of the construction of the spot-shape curve by displacement of a point-like spot (monochromatic) on the CCD. The flux received over the

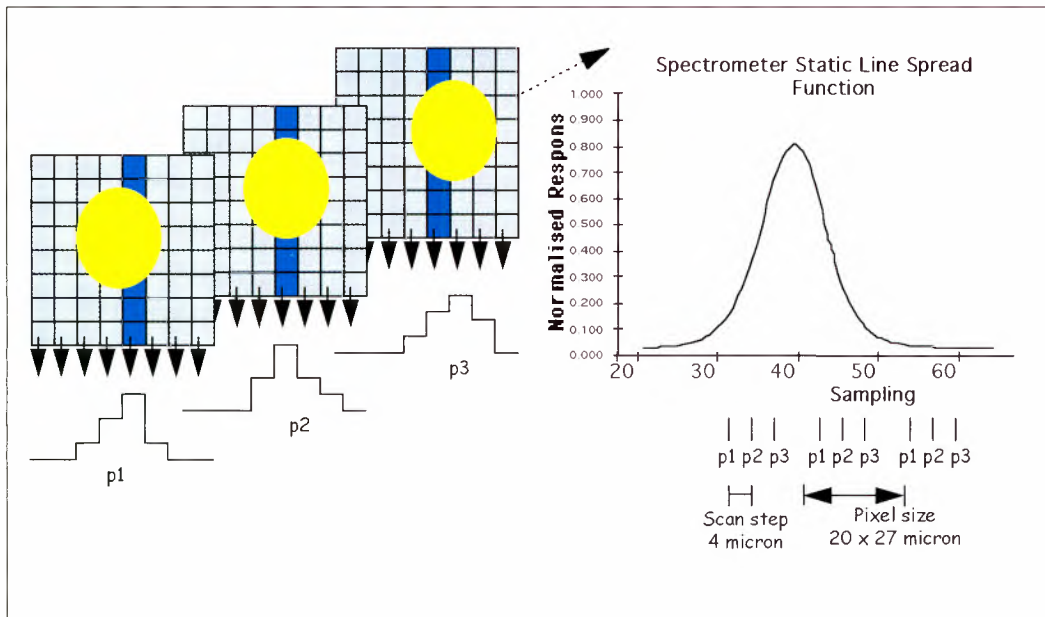


**Fig. 5-2 Line Spread Function measurement principle. When measuring the spatial LSF the spot is moved along the row (across the column) in steps of 2.5 micrometre (4 micron on the SATU). For each step-setting the 'course' LSF is read out through the column. For each position of the position a new LSF plot is created. From the resulting set a 'high resolution' LSF is created**

columns (or the lines) is measured as the spot is moved in 2.5-micron steps (1/5 of a pixel) across the spectrometer CCD. The spot is moved on the spectrometer CCD, not by physically moving the source (30 cm aperture collimator with a 10 micron pinhole at the focal plane), but by shifting the SATU tracking-window position between consecutive measurements. The pointing control reacts to the changed position-information by moving the steering front mirror such that the spot moves accordingly on the spectrometer. The line spread function measurement principle is shown in Fig. 5-2.

### 5.7 Spectrometer Radiometric Uniformity

The uniformity of the response of the individual pixels of a CCD must be known accurately, in particular for the scattered sunlight correction and pointing jitter correction.

One important reason for calibrating the spectrometer radiometric uniformity comes from the need to

remove the sky (scattered sunlight) signal. First, the signals in the three bands (star band, band of the sky above and below the star) are corrected for non-uniformity of the CCD. Second, the sky band signals are interpolated from the two sky bands to the star band, where it will be subtracted from the star band signal.

Due to pointing jitter during the occultation, a shift of the spectrum from one position on the CCD to another will give an apparent change in the signal, due to the non-uniformity. Jitter correction therefore needs both the CCD uniformity map and the pointing history from the star-tracker.

The CCD uniformity maps are created during the on-ground calibration using an extended uniform source. A corresponding in-orbit calibration will be difficult to achieve with the same accuracy because of the lack of uniform calibration targets in orbit. For example, the Earth's limb is not sufficiently uniform.

The on-ground uniformity calibration

will be performed in a thermally-controlled vacuum environment with the instrument in its 'uniformity monitoring' mode, using the collimator and a polychromatic and uniform source. The uniformity has already been measured in ambient conditions using a quartz lamp and a white screen (as part of the external Earth straylight test). The data presented here are the result of these measurements made in ambient conditions.

The uniformity is not likely to change due to the launch environment, as it is largely dependent on the CCD quantum efficiency uniformity. However, tests with earlier CCDs of different manufacture showed changes in uniformity on time-scales of days to months.

### 5.7.1 Definition of radiometric uniformity

The uniformity of spectral response is the measure of the relative difference between the average sky band response and the average target response to a uniform illumination. The measurements are performed with the instrument in its 'occultation' mode. The widths of the upper and lower sky bands are set to the same value as the star band.  $T$  is the average signal measured for a binned pixel in the star-target band and  $B_1$  and  $B_2$  the signal in the upper and lower sky band. Then, the radiometric uniformity is defined as:

$$uniformity = \left| \frac{T - B}{B} \right| < X\% \quad (5.1a)$$

$$B = \frac{B_1 + B_2}{2} \quad (5.1b)$$

where  $X$  is the specified uniformity.

### 5.7.2 Measurement of the uniformity map

The uniformity was measured using a white screen and a QTH lamp. The uniformity of the white screen was much better than 0.5%. A high flux (and hence small error-contribution, due to a large SNR) was ensured. The results of these measurements are given in Table 5-5.

## 5.8 Spectrometer Linearity

The GOMOS detection chain, from the CCD output amplifier to the analogue-to-digital converter, exhibits a very small but measurable non-linearity and is specified to be better than 1% over any 10:1 dynamic range. It will largely depend on the amplifier gain setting and will increase with the electronic gain.

A specific instrument mode for the calibration of linearity has been implemented and allows the user to observe a stable source using a programmable integration time from 0.25 to 10 sec.

Using the linearity mode with a stable extended source, the linearity was measured while illuminating each CCD over a wide area. Each measurement was averaged spatially over 200 pixels. The performance has been tested over a large dynamic range (wider than the star specified range). Different gains have been used to measure both CCD and ADC saturation levels.

The dynamic range covered whilst making the measurements spanned in the range 2100 to 568000 electrons for UV, 200 to 952000 electrons in VIS and 300 to 110000 electrons in IR.

Table 5-6 summarises the linear performance.

<b>Band</b>	<b>Uniformity specification</b>	<b>Uniformity measured</b>	<b>Accuracy</b>
UV	mean 1 %	mean 1.5% max 3.5%	< 0.5%
VIS	mean 1 %	mean 1% max 4.5%	< 0.3%
IR1	mean 3 %	mean 2% max 7.5%	< 0.5%
IR2	mean 9 %	mean 13% max 44%	< 2%

### 5.9 Instrument Radiometric Sensitivity

The radiometric sensitivity of the spectrometer, photometer and SATU (Star Acquisition and Tracking Unit) represent the conversion factors between the instrument flux in photons/s/cm<sup>2</sup>/nm at the instrument input and that at the instrument output in terms of digital number (DN). The spectrometer sensitivity is shown in Fig. 5-3.

Characterisation was performed under ambient conditions, as part of the last performance test prior to delivery of the instrument. The measurement at ambient has the advantage of being more accurate than if measured in vacuum but will nevertheless be verified against the thermal vacuum signal-to-noise measurements. In view of this, the calibration database will contain values from the ambient measurements as well as those from the vacuum.

The radiometric sensitivity will decrease throughout the life of GOMOS as the optical transmission is reduced, due to contamination and radiation of optical components.

The following test set-up was used:

- instrument in tracking ('occultation') mode
- collimator with monochromator illuminating the instrument aperture using a fluorine-tungstenhydrogen-molybdenum spectral source (e.g. 2.5 nm at 500 nm)
- 500 acquisitions recorded for each of the four UVIS detection module gains

Each acquisition set was recorded for the UV-visible chain for all 4 gains, while the IR spectrometer was recorded for the lowest gain (i.e. operation gain). Also the corresponding photometer and SATU (star-tracker) signals were recorded.

The source calibration accuracy is listed in Table 5-7, which also lists the spectral sensitivity as measured during the ambient measurement campaign. It represents the best knowledge of the instrument.

**Table 5-5. Uniformity values from ambient measurements using white screen and QTH lamp. The high values in the IR1 and IR2 bands are due to interference in the thinned CCD substrate. This is a typical feature of thinned CCDs**

**Table 5-6. Synthesis of linearity performance: The values indicated are the worst case non-linearity error over any 10:1 range (values for gain 8 are over the full range). Dark cells indicate that the measurement was not performed, because they are not used in normal operation of the instrument. Note that, during nominal operation for spectrometer IR1/IR2, only gain 1 will be used**

<b>Channel</b>	<b>Gain 1</b>	<b>Gain 2</b>	<b>Gain 4</b>	<b>Gain 8</b>
UV	0.27 %	0.45%	0.30 %	0.48 %
VIS	0.36 %		0.50 %	0.41 %
IR1	0.33 %			
IR2	0.34 %			

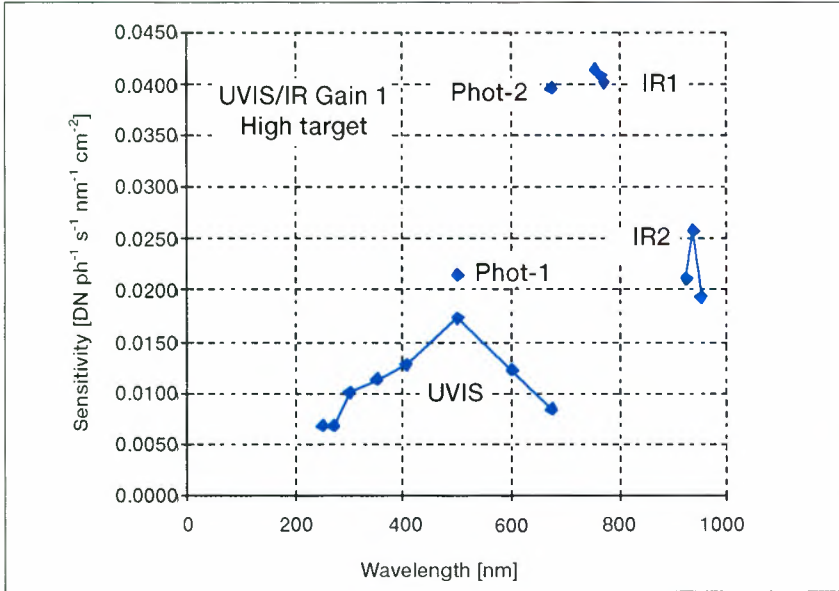


**Fig. 5-3 Spectrometer sensitivity (or gain) in DN/ph/s/nm/cm<sup>2</sup>. Note that the measured signal was first corrected for non-uniformity before calculating the gain. The curves presented are for UVIS and IR detection chain gain setting 1 with a high target flux**

**Table 5-7. Total radiometric sensitivity accuracy is given by adding up all error contributors. The UV-visible (spectrometer A) is calibrated for all four gain-settings using the low target flux. In addition to the error listed, the instrument signal-to-noise ratio must also be considered, although the effect will be much lower than the two main contributors listed. The high and low flux levels are defined in Table 5-8**

## 5.10 Instrument Signal-to-Noise Ratio

The signal-to-noise (SNR) was measured as part of the noise characterisation and is defined for each binned pixel (7 lines wide) in several wavelength bands. The SNR is defined as ratio between the (background subtracted) star flux and the standard deviation of the total measured signal over 500 acquisitions.

The SNR for GOMOS is specified for each wavelength band for a set of flux cases. The SNR measurements were conducted in thermal vacuum and performed at cold, nominal and hot operational temperature in order to validate the instrument's SNR models. The source used was a white xenon lamp. The fluxes used during these measurements were different than the

ones presented below. The values presented in Table 5-8 are based on a nominal instrument temperature (CCD temperature of about 12°C). Also, with the SNR model, the performance presented is that expected (typical) at the end of life (i.e. after 4 years in-orbit). Fig. 5-4 shows the ratio of the measured and specified signal-to-noise ratio.

## 5.11 In-flight Calibration

### 5.11.1 Introduction

The GOMOS measurements are in principle self-calibrating as far as the atmospheric transmission measurements are concerned. The transmission product is the ratio between two spectra, the star spectrum outside the atmosphere and the attenuated spectrum, acquired closely in time. It can be assumed that during one occultation sequence the change in the instrument's response function will be small, so that long-term instrument drifts cancel out and can be ignored.

Regarding the higher level products (geophysical parameters), the transmission product has to be transformed by a number of numerical procedures, each one made on the basis of specific assumptions. More importantly, the inversion algorithm is a nonlinear process, meaning that a small change in the transmission could have a large nonlinear impact on vertical density products.

Radiometric sensitivity accuracy	UVIS		IR1		IR2	
	Gain 1	Gain 8	LT	HT	LT	HT
Collimator source calibration [%]	3.9	5	6	4.4	8	6.3
Dark image subtraction error [%]	1		1		1	
Total (linear sum) [%]	4.9	6	7	5.4	9	7.3

SNR EOL	Spectral band	Star Flux <i>ph/s/nm/cm<sup>2</sup></i>	Sky Flux <i>ph/s/nm/cm<sup>2</sup>/nsr</i>	Typical	Specification
LOW TARGET NO LIMB (LTINL)	250-300 nm	1100	0	19.0	12 (target)
	310-375 nm	1100	0	30.6	13
	405-530 nm	1000	0	38.4	23
	540-600 nm	1000	0	28.1	12
	610-675 nm	700	0	20.3	12
	756-773 nm	1000	0	14.5	6
HIGH TARGET NO LIMB (HTINL)	926-952 nm	900	0	6.7	3
	250-300 nm	60000	0	248.8	150
	310-375 nm	60000	0	339.3	190
	405-530 nm	60000	0	405.1	190
	540-600 nm	50000	0	364.1	190
	610-675 nm	40000	0	260.5	150
HIGH TARGET BRIGHT LIMB (IMBL)	756-773 nm	30000	0	143.4	100
	926-952 nm	20000	0	73.3	40
	250-300 nm	60000	120	185.1	20
	310-375 nm	60000	10000	113.7	20
	405-530 nm	60000	10000	139.0	30
	540-600 nm	50000	3000	177.1	35
BRIGHT LIMB (IMBL)	610-675 nm	40000	1500	134.3	35
	756-773 nm	30000	0	83.6	70
	926-952 nm	20000	0	43.9	30

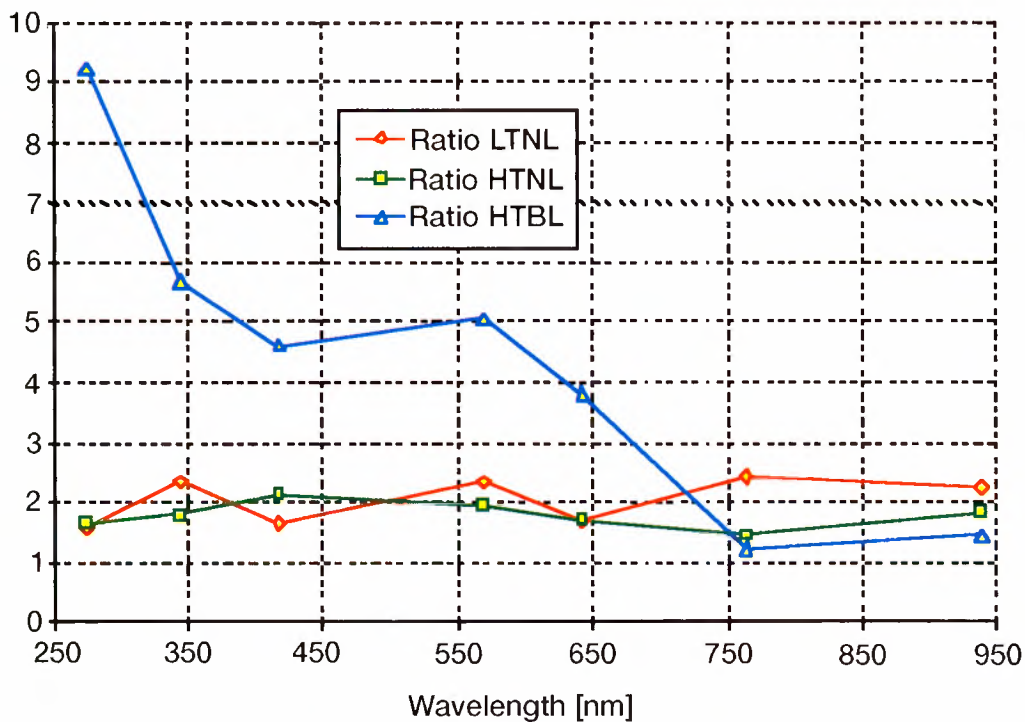


**Table 5-8. Instrument Signal-to-Noise Ratio predicted at end of life (4 years)**

**Fig. 5-4 GOMOS Signal to Noise Ratio for high and low target irradiance with dark sky and high target irradiance with bright sky radiance. As can be seen the signal to noise performance is more than a factor of two above the specification and for high targets stars in bright close to 10**

Calibration is the process of quantitatively defining the system response to known, controlled, signal inputs. GOMOS has several special observation modes, which are intended to enable the in-flight determination of several calibration quantities. This section considers how these quantities can be monitored from the normal flow of occultation data and from the use of GOMOS special operation modes.

#### a) Occultation Mode

The occultation mode provides several possibilities for in-flight calibration:

- The reference spectra (from each occultation) can be used both for long-term wavelength calibration and absolute radiometric calibration.
- The background spectra, particularly at high tangent heights (only Rayleigh scattering), can be used for long-term wavelength and relative radiometric calibration.
- The stellar spectra (with a tangent height above 40 km) can be examined by using cross-correlation to check for the shift and broadening determined from the SATU data.
- All the data can be examined for statistical consistency.

It is also important to note that in addition to the conventional star tracking there are other possibilities:

- fictitious star tracking, which follows the inertial trajectory of a hypothetical star,
- offset tracking, which follows a real star, but the SATU target point is offset so that the star remains out of the field of view of the slit.

#### b) Linearity Mode

A stable star target is acquired, locked on to and tracked outside the atmosphere several times using different integration times (0.25 to 10 sec). This mode is only possible by exploiting the binned operation and will thus generate the same spectrometer data as in occultation mode, but with the signal level varying by a factor of 40. The dynamic range can be further extended by using several stars of different brightness, such that their 1:40 dynamic ranges overlap. A linearity curve with integrated flux versus instrument output can then be generated. It will in all likelihood be necessary to use observations of the same star in successive orbits.

#### c) Uniformity Mode

An extended uniform target (the Earth limb is a reasonable good proxy) is imaged and a pixel map is obtained. The purpose is to take both binned and unbinned pictures to confirm (and update) flat field correction, to check for bad pixels and to confirm binning operation.

#### d) Spatial Spread Mode

The objective of this mode is to perform periodic monitoring of the instrument line spread function (which includes satellite jitter). A star (preferably with sharp spectral features, such as Sirius) is tracked above the atmosphere and a whole picture is taken to compare with the binned version. In this way the instrument function (spatial and spectral directions), including the effects of satellite jitter, can be observed directly and compared with the binned version.

### 5.11.2 The GOMOS calibration database

During the development of the algorithm for determining GOMOS level 1b data products (consisting mainly of transmission and stellar spectra), a number of correction parameters were identified. These include parameters such as, measurements of instrument gain (radiometric units per instrument digital output), linearity correction, biases, spectral wavelength assignment and spectral dispersion. Using the instrument modes explained above, these parameters are computed using the CALEX calibration processor (an integral part of the GOMOS Instrument Engineering Calibration Facility, IECF), which updates the calibration database. This database is an important input to the geophysical product processor and will need to be periodically updated.

In order to achieve this, an in-orbit calibration plan is being developed and will be executed and optimised during the Envisat commissioning phase. The primary objective is to selectively update the complete on-ground calibration data base during the commissioning phase. Of course, this will have to be performed in a highly interactive way, due to the difficulty of balancing, on one hand clearly defined and accurate calibrations made on ground and, on the other relatively uncontrolled in-orbit calibrations.

#### a) Verification of A/D converter

A histogram of the outputs from any one CCD, accumulated over several occultations, will be used to indicate deviations in the converter's transfer function, for example if one particular value  $n$  is under-represented with respect to values  $n-1$  and  $n+1$ .

#### b) Spectral Characteristics

By comparing stellar Fraunhofer lines with ground-based high-resolution spectra, one can verify the spectral point-spread-function and the absolute wavelength scale of the spectrometers, as well as the correspondence between the SATU star positions and the wavelength assignment of pixels. Such verification might be made systematically for all occultations at Level 1b.

#### c) Straylight

Measurements of straylight, external to the spectrometer, are almost impossible to conduct during ground calibration, as it is very difficult to construct a stray-light environment on the ground that simulates that in space. In order to generate look-up tables for data processing, a model has to be constructed after launch, using as input the measured light with solar spectral features derived from detector rows dedicated to the observation of the sky background (when observing above the atmosphere), together with the solar elevation and azimuth angles and the angles with the terminator on the Earth's surface.

The presence of straylight internal to the spectrometer is easy to detect at places and times when one would otherwise expect no light (e.g. in the ultraviolet at low altitude, or from stars which have no ultraviolet in their spectra). It can also be detected if any filling of Fraunhofer lines is observed (comparing equivalent widths of ground-based high-resolution spectra with those obtained in flight). At night, light from stars, spilling over into detector rows dedicated to the observation of sky background also determines internal straylight, when sufficient care is taken to exclude any other astronomical source.

#### d) Flat Fielding

Unlike stellar spectra, the spectral spread function of measurements of the bright sky in the upper and lower background bands is determined by the slit. Because the width of the spectrometer slit is equivalent to many pixels, spectra of the bright sky

are heavily smoothed. This allows confirmation that pre-flight measurements of pixel response non-uniformity are still correct. Because the spectra are not smoothed over a very large number of pixels, the exact values of any changes in pixel response non-uniformity may have to be deduced by iteration.

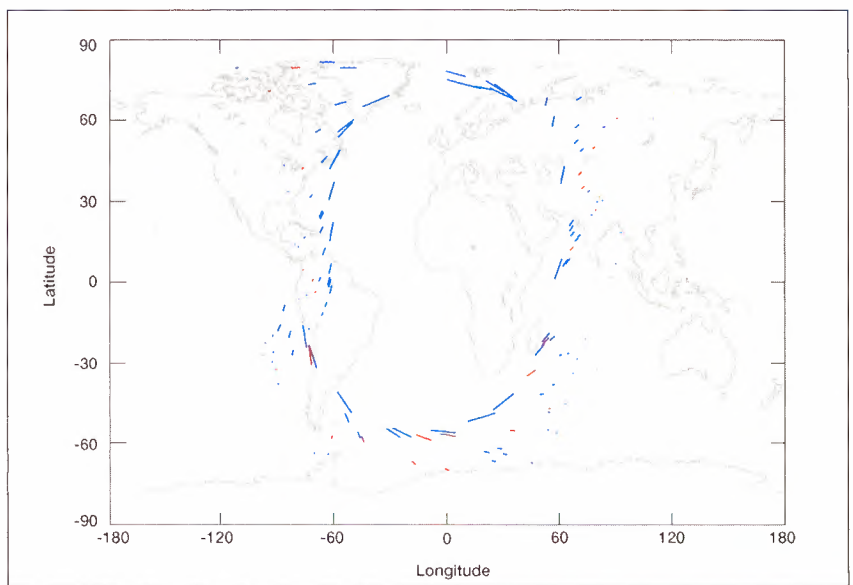
# 6. Mission Planning

## 6.1 Introduction

The advantage of the technique of stellar occultation – as opposed to solar occultation – is the large number of possible occultations per orbit. Stars are not evenly distributed in the sky, and this may lead occasionally, depending on the season, to poor coverage in certain regions and to an oversupply of possible occultations in other regions. In the latter case, decisions have to be made as to which star should be chosen among various alternatives. In fact, the number of star targets that GOMOS is able to track and measure is so large that selection of the optimal target will be required most of the time .

Since the quality of the retrieval of GOMOS data products depends on star parameters such as brightness and temperature, different occultations are of different merit for the various GOMOS data products. The purpose of the GOMOS mission planning is to use the freedom of selection to draw up measurement programmes that fulfil scientific user requirements in an optimal way while satisfying the constraints of the GOMOS instrument and the Envisat mission.

The GOMOS mission planning can be divided into three levels. The highest level is the mode selection level. Here decisions are made as to whether, during a given mission planning period, the monitoring mode, the occultation



mode or the wait mode is selected. The second level concerns mission planning inside the occultation and monitoring modes. The third and lowest level concerns the determination of low level instrument parameters, which will eventually be broadcast to the satellite and the instrument. In this chapter mission planning inside the occultation mode is discussed. GOMOS mission planning has previously been described by *Kyrölä and Tamminen, 1999*.

## 6.2 Motivation

Depending on the time of year there will be 150-250 stars that are bright enough for GOMOS to track and which will be in its field of view at

**Fig. 6-1 Possible occultations during one orbit in January. The green and red lines indicate the location and horizontal extension of the occultations. A selection performed for the mission objective “stratospheric ozone monitoring” selects the occultations marked in red. The green occultations are those not selected. The lines show the path of the tangent point from the moment of star acquisition to the loss of the star signal in the lower stratosphere. Long (oblique) occultations show a significant horizontal extension while short occultations are very localised**

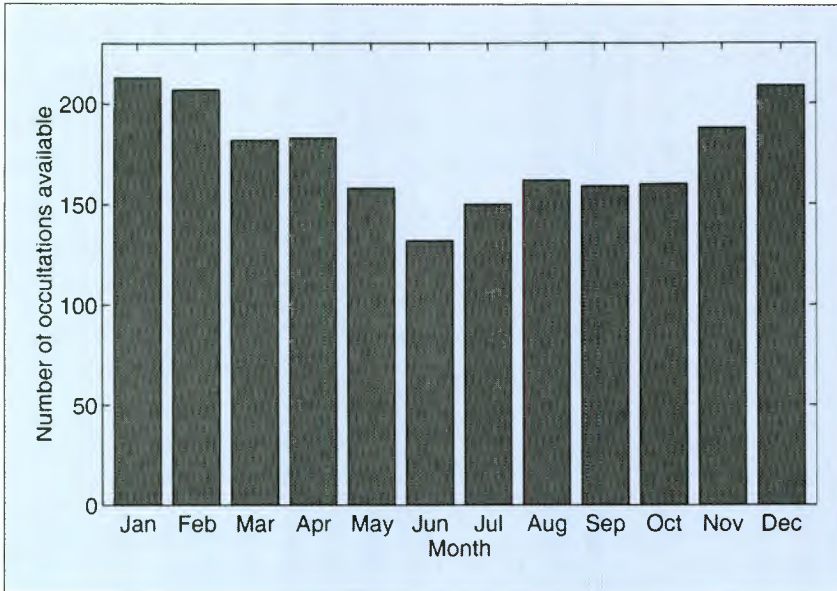
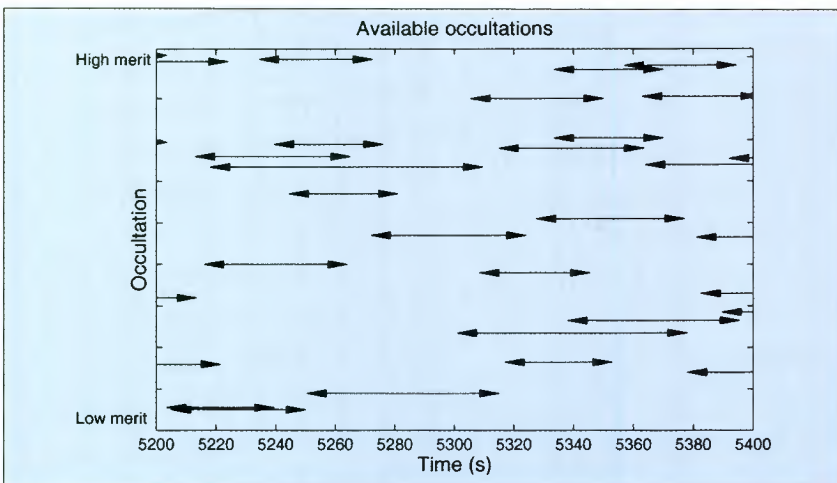


**Fig. 6-2 Monthly variations of the number of occultations available for GOMOS. (This preliminary estimate as well as subsequent results are published by the FMI LIMBO-simulator)**

**Fig. 6-3 An example of a 200 s. period from the Envisat orbit during March. Occultations are indicated by arrows in time. The vertical position indicates the merit value of the occultation with respect to ozone monitoring**



specific times during an orbit. The number of available occultations during one orbit is shown in the geographical map in Fig. 6-1. The monthly variation in the number of occultations available is shown in Fig. 6-2.

Since the possible star occultations often overlap each other in time, as shown in Fig. 6-3, not all the possible occultations can be observed. Instead, a number of alternative occultation sequences can be generated, each with different characteristics, for example with respect to the quality of ozone retrieval. This presents an opportunity to find an optimal sequence to satisfy the accuracy requirements of a specific mission objective.

### 6.3 Elements of the GOMOS Mission Planning

In order to carry out the GOMOS mission optimisation the different GOMOS mission objectives have to be accurately quantified. A phrase like 'stratospheric ozone monitoring' as a scientific objective cannot be used as such in the mathematical mission optimisation procedure. In order to quantify the objectives, specific sets of mission planning criteria are used, to which are assigned the values required to fulfil the mission objectives. These values constitute the data requirements. The mission planning tool is a routine which uses the list of available stars, along with the data requirements and instrumental constraints, to generate a measurement programme which satisfies the mission objectives in an optimum way. The main elements of the GOMOS mission planning are depicted in Fig. 6-4. They are discussed in more detail in subsequent sections.

## 6.4 Criteria characterising mission objectives

The *mission objectives* are presented in Chapter 2 and summarised in Fig. 2-10. The most important mission objectives are *stratospheric ozone monitoring* and *mesospheric ozone monitoring*. Each mission objective can be characterised by a set of criteria.

The realisation of a *mission objective* depends on the fulfilment of the corresponding set of *criteria* by which the objective is characterised. The mission planning criteria fall into three groups according to their scope.

### 1. Star-specific criteria:

- the accuracy of the retrieved geophysical parameter (e.g. ozone profile, temperature profile, etc.) for each constituent and altitude range

### 2. Occultation-specific criteria:

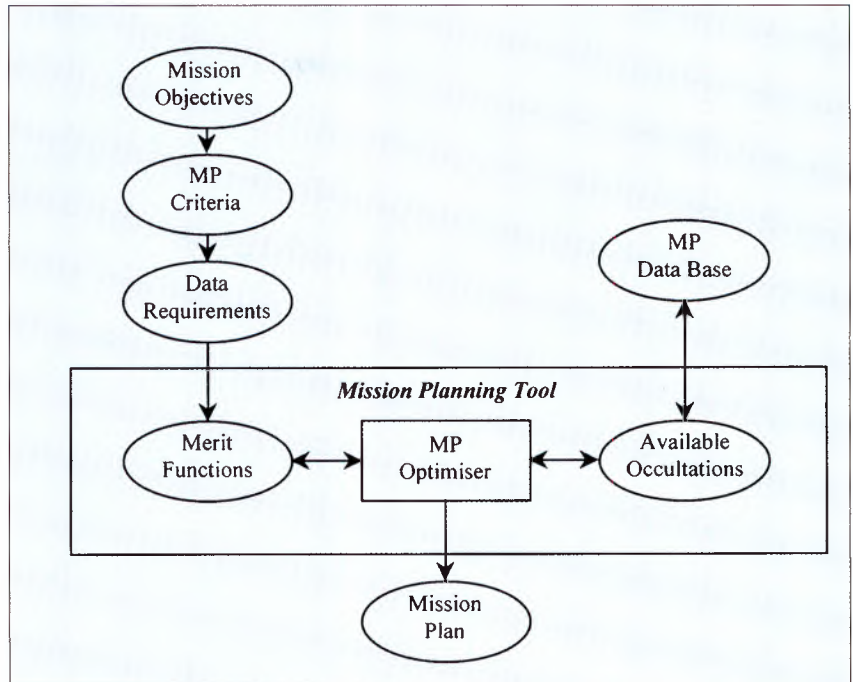
- occultation condition (dark limb, bright limb, terminator measurement)
- obliqueness (directly related to the duration of the occultation)
- local coverage

### 3. Occultation sequence-specific criteria

- global coverage

As an example, Table 6-1 shows the data requirements for the stratospheric ozone monitoring mission objective.

In general, each *criterion* is defined by its *target* and *threshold requirement*. For example, one criterion of the mission objective ‘stratospheric ozone



monitoring’ is ozone accuracy with the target requirement of 2% and the threshold requirement of 5%. A measurement fulfilling the target requirement is considered to be of highest scientific value. A measurement fulfilling the threshold requirement is considered to be of significant importance. A star would not be prioritised if it does not fulfil the threshold requirement. The reason for using a target requirement, rather than forcing the algorithm to find the absolute best star for the given criterion, is to provide flexibility for fulfilling other criteria as well.

**Fig. 6-4** Main elements of the GOMOS mission planning (MP)

The relative importance of each criterion is set by the *priority* assigned to it. According to Table 6-1, the ozone accuracy criterion has the highest priority, i.e. is more important than the other criteria in the mission objective (aerosol accuracy, air density accuracy etc.).

The global coverage criterion is incorporated through a global coverage parameter, as described later.

**Table 6-1 Data requirements for the stratospheric ozone monitoring mission objective. The first value in the requirement column indicates the accuracy, which is still considered as the best accuracy and the second value is the least acceptable accuracy. The priority column weights the different criteria against each other with respect to the mission objective**

<b>Stratospheric ozone monitoring with global coverage</b>		
<b>Criterion</b>	<b>Target and Threshold Requirement (<math>x_1</math> and <math>x_2</math> values)</b>	<b>Priority</b>
O <sub>3</sub> , line density accuracy 20-50 km	0.5%, 5%	1
H <sub>2</sub> O, vertical profile accuracy 20-35 km	30%, 70%	2
air density, line density accuracy 20-40 km	1%, 2%	2
aerosol, line density accuracy 15-20 km	5%, 40%	2

The data requirements listed in Tables 6-1 and 6-2 take into consideration the estimated product accuracies of GOMOS and will be reviewed after analyses of the true product accuracies, which will be estimated during the first six months of the Envisat mission, the commissioning phase. The tables reflect only which altitude range and which product accuracy will be the driver for the star selection. Each occultation will, in general, cover the whole altitude range from about 130 km down to the tropopause region and will also be used to produce the other data products aside from those listed in the tables.

### 6.5 Mission Planning Tool

Merit functions are mathematical functions which quantify the mission planning criteria and indicate their relative importance with respect to

the mission objective. They enable the merit of an occultation to be determined with respect to the mission objective. The value  $m$  of the merit function ( $0 \leq m \leq 1$ ) is equal to one if the criterion is perfectly satisfied by the occultation and zero if it is not satisfied at all.

Each mission planning criterion (accuracy, local coverage, duration, and diurnal condition) has its own merit function, which is derived from the data requirements. For simplicity, each criterion is characterised by the following generic merit function with five free parameters (see Equation 6.1).

The shape of the function is monotonic, either ascending or descending, with a maximum equal to one. The parameters  $x_1$  and  $x_2$  determine the width of the transition region from the target values ( $x_1$ ) for the associated criterion (merit near 1)

$$m(x) = b_1 + \frac{b_2 - b_1}{1 + \exp\left(-\left(x - \frac{x_1 + x_2}{2}\right) \frac{|x_1 - x_2|}{H}\right)} \quad (6.1)$$

### Chemistry of the lower and middle stratosphere

Criterion	Target and Threshold Requirement ( $x_1$ and $x_2$ values)	Priority
O <sub>3</sub> , line density accuracy 20-35 km	2%, 10%	1
NO <sub>2</sub> , line density accuracy 20-35 km	10%, 30%	2
NO <sub>3</sub> , line density accuracy 25-35 km	20%, 40%	2
H <sub>2</sub> O, vertical profile accuracy 20-35 km	30%, 50%	2
aerosol, line density accuracy 15-20 km	5%, 40%	2

**Table 6-2. Data requirements for chemistry in the lower stratosphere**

to the threshold value ( $x_2$ ). (See the example given in Table 6-1 and merit function examples discussed below). The parameters  $b_1$  and  $b_2$  are the best and worse possible merit values and associated with the parameters  $x_1$  and  $x_2$ , respectively.  $b_1$  is always equal to one, while  $b_2$  is set to reflect the priority of the criterion, as explained later. The parameter  $H$  is a scaling parameter, which determines the slope between  $b_1$  and  $b_2$ . It has to be selected so that  $m(x_1) \approx b_1$  and  $m(x_2) \approx b_2$ . An appropriate value is  $H=10$ . Mission planning would be a nearly trivial exercise if only one requirement at a time had to be considered, e.g. ozone accuracy. Instead, occultation sequences have to be planned for mission objectives containing more than one criterion (for example as given in Tables 6-1 and 6-2). Within one mission objective different criteria can have different priorities. For example, the mission objective 'stratospheric chemistry (lower and middle stratosphere)' necessitates measurements of ozone, NO<sub>2</sub>, NO<sub>3</sub>, H<sub>2</sub>O and aerosol, each with their respective target and threshold requirements, as listed in Table 6-2.

However, not all have the same priority; ozone has the highest priority, while aerosol has the lowest.

For a priority-1 criterion (e.g. criterion 'O<sub>3</sub> accuracy' of objective 'stratospheric ozone monitoring') the parameter  $b_2$  is set to 0; for a priority-2 criterion (e.g. 'aerosol accuracy') it is set to 0.3. The respective values of  $b_2$  have been determined after assessing the relative importance of the different criteria for the respective mission objectives. An example is shown in Fig. 6-5. In this example, ozone has the highest priority and target and threshold accuracy requirements of  $[x_1, x_2] = [5\%, 10\%]$ . Aerosol has priority 3 ( $b_2 = 0.5$ ) and target and threshold accuracy requirements of  $[x_1, x_2] = [20\%, 100\%]$ .

The principle of how a merit function attaches a specific value to an occultation is illustrated schematically in Fig. 6-6. The total merit of each occultation is obtained by combining the merit values from the various criteria (accuracy, coverage, duration, and diurnal

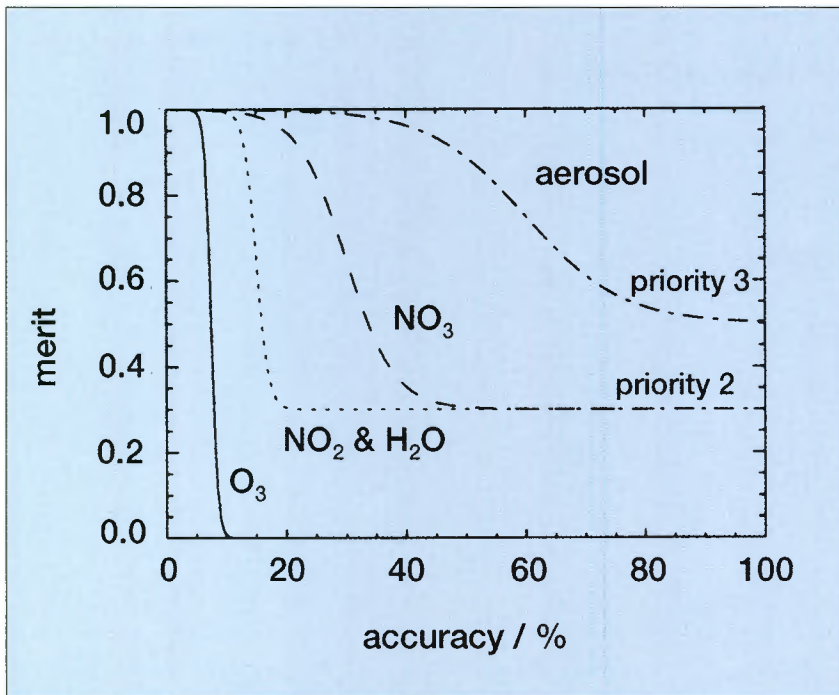


Fig. 6-5 Example for generic merit functions

condition). Among the several possible ways of combining them the following was chosen:

$$M = \sqrt[n]{m_1 \dots m_n} \quad (6.2)$$

This approach avoids prioritising a star if a mission planning criterion of first priority is not fulfilled, even if criteria of lower priority are perfectly fulfilled.

The merit of a sequence of occultations can then be obtained simply by adding all the merits associated with the occultations in the sequence:

$$B = \sum_i M_i \quad (6.3)$$

The sum extends over all the occultations in the sequence. This does not yet incorporate the global coverage merit, which cannot be derived from individual occultations. This is due to the fact that the global coverage merit is not intrinsic to the parameters associated with the occultation but rather depends on the distribution of tangent point locations. The goal is to seek a uniform distribution of occultations over the globe. By the very nature of polar orbits, an occultation can usually be repeated once each orbit at the same latitude, thus achieving uniform coverage. This means the question reduces to one of identifying a uniform distribution of occultation merit with latitude. The concept of *entropy* is used for measuring the latitudinal distribution of the occultations. The global coverage merit is denoted by *S* (irrespective of how it is calculated).

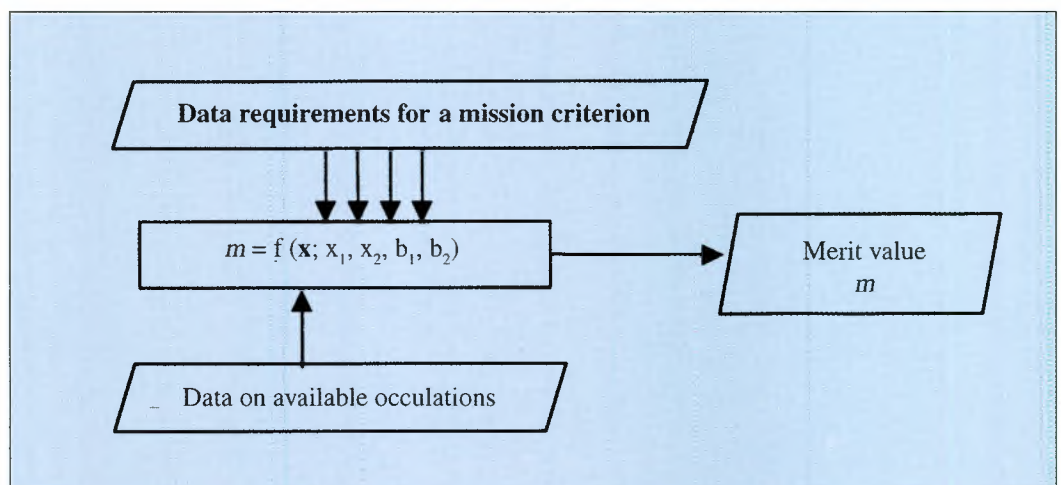


Fig. 6-6 The principle of the merit function

Method	Number of stars	Merit M
Available occultations	182	46.6
Occultations selected on first-come basis	44	9.3
Best ozone merit (a=0)	41	17.8
Best global coverage (a=1)	41	12.7
Global coverage and ozone merit (a=0.5)	41	17.3

**Table 6-3 Enhancement of measurement programme by the optimised selection**

The total merit of an occultation sequence,  $F$ , is thus obtained by combining the sequence merit  $M$  and the global coverage merit  $S$ :

$$F = (1 - a)B + aS \quad (6.4)$$

where  $B$  is as defined in Equation (6.3). Through the parameter  $a$ , the relative emphasis of the merit of the occultation sequence  $B$  and the global coverage merit  $S$  can be adjusted. The parameter  $a$  is set to zero for mission objectives which do not include the global coverage criterion.

The total merit  $F$  can now be calculated for every possible occultation sequence. The objective of the optimisation algorithm is to find the sequence with the highest total merit  $F$ . This task is more difficult than it may appear because the number of possible sequences increases in an explosive way as the duration of the mission planning window increases. A special technique has been developed to handle this problem.

## 6.6 Results

Table 6.3 gives an example of how the use of an optimising algorithm leads to a more efficient measurement programme for GOMOS. Here, the focus is on how to obtain the best possible ozone measurement accuracy and global coverage. Four cases were chosen for comparison: (1) stars were

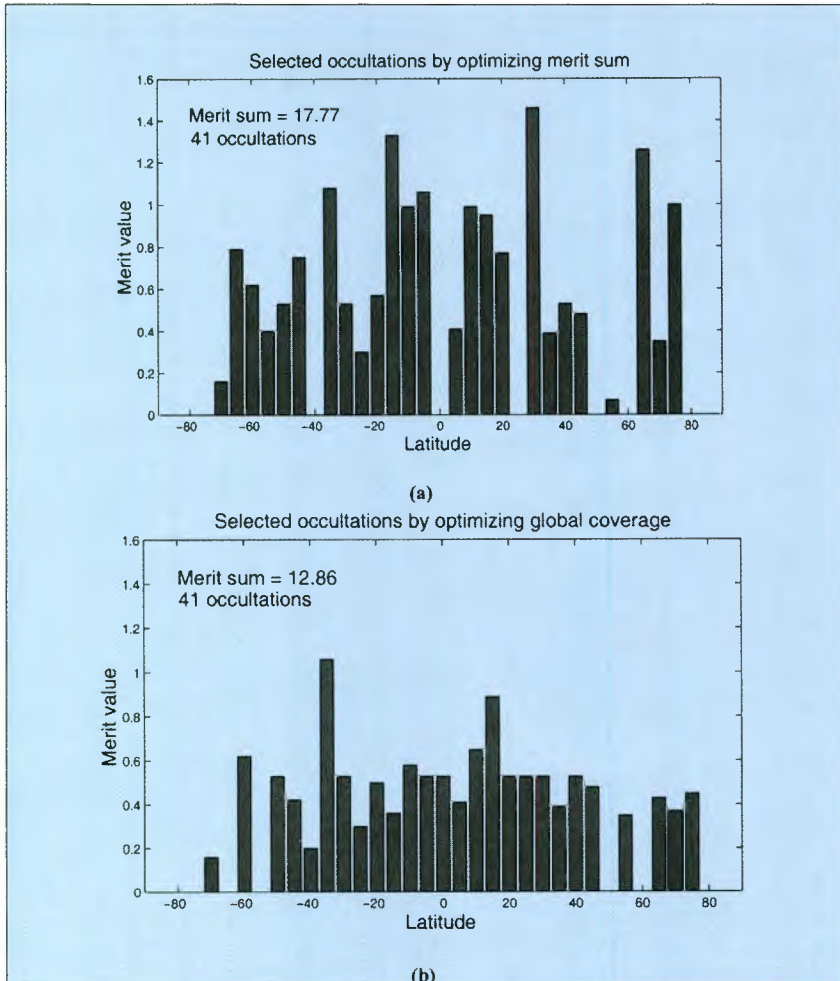
selected according to their entrance into the instrument's field of view as the satellite progresses along the orbit ('blind selection'); (2) stars were selected in order to maximise the ozone accuracy merit  $M$ ; (3) stars were selected to maximise the global coverage merit  $S$ ; (4) stars were selected to maximise the total merit  $F$  with  $a=0.5$ .

The results show that by using a technique of optimal selection, the total merit can be doubled compared to a 'blind selection'.

Fig. 6-7 gives an example of how the latitude distribution can change depending on whether (a) the merit sum (parameter  $B$  in Equation 6.4) or (b) the global coverage (parameter  $S$  in Equation 6.4) is maximised.

## 6.7 Summary

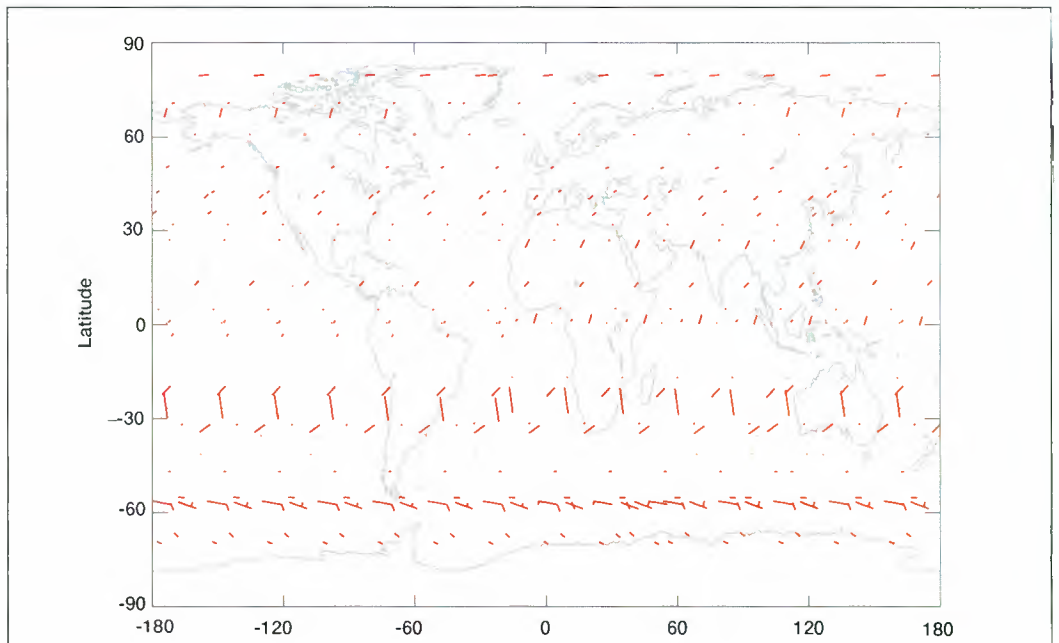
The primary mission objective of GOMOS is to monitor ozone in the stratosphere on a global scale. The multitude of suitable stars makes it possible to seek an optimal selection of occultations in order to maximise the global coverage, the accuracy of the retrieved geophysical parameters, as well as other requirements. An example of the global coverage obtainable with GOMOS using an optimal selection of stars is shown in Fig. 6-8. The mission planning also provides the opportunity to consider other mission objectives in a manner such that the interference with the



main objective is minimal. In summary it can be said that a considerable enhancement of the GOMOS mission can be achieved using the optimising mission planning technique described here. An essential element in the mission planning is the selection and updating of the mission objectives and the planning of observation periods in which to focus on particular mission objectives.

**Fig. 6-7** The upper plot (a) shows an occultation sequence selection with an optimised total merit, disregarding the global coverage. The second plot (b) emphasises the global coverage. This leads to a much more even distribution of occultations over latitude, but to a lower merit sum

**Fig. 6-8** Full global coverage is achieved with 15 consecutive orbits. This figure shows the selected occultations for the mission objective "stratospheric ozone monitoring." The lines show the path of the tangent point from the moment of star acquisition to the loss of the star signal in the lower stratosphere



# 7. Scientific Data Processing and Data Products

## 7.1 Introduction

The GOMOS data processing consists of two major steps. The raw data (Level 0 data) are processed in the Level 0-1b processing, creating the Level 1b data, which are the localised calibrated transmission spectra and photometer fluxes and the background spectra. From this, the Level 1b-2 processing calculates the Level 2 data products consisting of the atmospheric constituent profiles, which are the vertical and line density profiles of  $O_3$ ,  $NO_2$ ,  $NO_3$ ,  $O_2$ ,  $H_2O$ , air density, aerosols, temperature and turbulence. Furthermore, the Level 1b-2 processing outputs the recomputed transmission spectra, corrected for scintillation and dilution effects. The tangent height range of the Level 2 data products is 15-100 km, the elevation range is  $+62^\circ$  to  $+68^\circ$  and azimuth range is  $+90^\circ$  to  $+190^\circ$  (with respect to flight direction).

The link between the constituent densities and the spectra measured by the spectrometers is the horizontal transmission function. From the measurements it can be expressed as the ratio between a stellar spectrum observed through the atmosphere and one measured outside the atmosphere. If the measurement is made through the limb illuminated by the Sun, the scattered sunlight must first be eliminated from the occulted spectrum. Moon, auroral, and other emissions may also add background radiation to the spectrum.

The concept of the transmission function is central to both the GOMOS instrument concept and the GOMOS data processing scheme. Transmission provides in principle information that is free of calibration factors. The property of self-calibration is the most important advantage of any occultation instrument.

The main inputs to the GOMOS processing are the spectrometer (UV-visible and IR) and photometer data plus the occultation and photometer recording times and auxiliary data (e.g. satellite location, mirror position).

The GOMOS data retrieval processes are not totally independent of external data. In particular, meteorological (ECMWF) data will be used for ray tracing calculations and temperature-dependent cross sections. This meteorological information can optionally be replaced by the atmospheric information retrieved from GOMOS measurements during an iterative retrieval procedure.

## 7.2 Level 0-1b Processing

The main goal of the GOMOS Level 0-1b processing is to estimate a set of horizontal transmission functions  $T_{obs}(\lambda)$  using data measured by the GOMOS spectrometers. This so-called full transmission function will serve

as basic data for the Level 1b-2 processing.

In an idealised setting the Level 0-1b processing would be a series of simple operations. For each stellar exposure one could calculate the atmospheric transmission as a ratio between the counts  $N_{occ}$  measured through the atmosphere at a given tangent altitude and the reference stellar counts  $N_{ref}$  measured above the atmosphere:

$$T_{obs}(\lambda) = \frac{N_{occ}}{N_{ref}} \quad (7.1)$$

In the real world, the following instrumental effects will have to be taken into account in particular, causing deviations from an ideal situation:

- optical deformations from instrument input aperture onto the detector surface
  - spreading of the image in the spatial dimension,
  - changes in the orientation of the optical axis.
- non-perfect efficiency of the detector
- accumulation of dark charges and the addition of read-out noise
- electronic gain in the amplifiers

All these are connected with the characteristics of the instrument. If any of these effects act in the same way on the occultation signal and on the reference signal and can be represented as multiplicative effects,

they will cancel out. Otherwise corrections have to be used in order to remove the distorting effects.

Besides the instrumental effects there are a few atmospheric phenomena which obscure the identification of the transmission function. These are the following:

- radiation generated in the atmosphere and entering the FOV of the instrument. for the specific wavelength ranges of GOMOS the following sources are expected:
  - solar or lunar light scattered one or more times,
  - auroral lights,
  - natural emissions (continuum and lines).
- straylight
- cosmic rays

Solar light scattered in the atmosphere will dominate over the stellar light when GOMOS is looking at the daylight side of the Earth (bright limb) whereas it can be ignored in the night side (dark limb). In the bright limb condition the solar background must be estimated and separated from the stellar signal, in order that the occultation processing can be continued. The solar signal removed will, however, constitute an important data product in itself.

Taking all these effects into account makes forward modelling a relatively complicated task. After several simplifications the signal counts  $N$  (for a binned pixel column  $m$  during one integration time) can be calculated as:

$$N(m, \Delta t) = F \left( \sum \left( \iint_{\Delta t} Q(m, n, \lambda) W(\lambda, \lambda') T_{atm}(\lambda', l(\lambda, t)) I_{star}^o(\lambda') d\lambda' dt + N_{bg} + N_{dc} \right) + N_{read} \right) \quad (7.2)$$

Process	Content
Datation	All data will be tagged with time.
Wavelength assignment	The small oscillations in the GOMOS and the spacecraft pointing make the image of the star wander on the detector surface. This will change the wavelengths that each detector pixel will see. The information from the star pointing system will make it possible to correct this perturbation.
Geolocation	The needed geolocation for measurements. Calculated from orbit data, earth geoid model and atmospheric model.

**Table 7-1 Pre-processing in level 1b**

Here  $F$  represents all the elements in the amplification chain,  $Q$  is the quantum efficiency for pixels,  $W$  is the instrument function,  $T_{atm}$  is the atmospheric transmission and  $I_{star}^0$  the original star spectrum. The remaining terms are due to the background radiation, dark current and read-out noise. The sum goes over the binned pixels.

Level 1 data are distinguished into Level 1a and Level 1b. The Level 1a data are Level 0 data, assorted and filtered by some low-level quality checks. The first data product of interest to the user is the Level 1b product.

Level 1b processing consists of several steps, listed in Tables 7-1 and 7-2. The data input and output are summarised in Fig. 7-1. The processing can be divided into pre-processing common to all data and the processing of data from various sub-instruments.

During preprocessing of the data, the wavelength assignment and the calculation of the geolocation are carried out. In the wavelength assignment a nominal assignment is produced but there is also a step where the possible wavelength shift is

**Fig. 7-1 Level 0-1b data processing: data providers, main processing modules, external data suppliers**

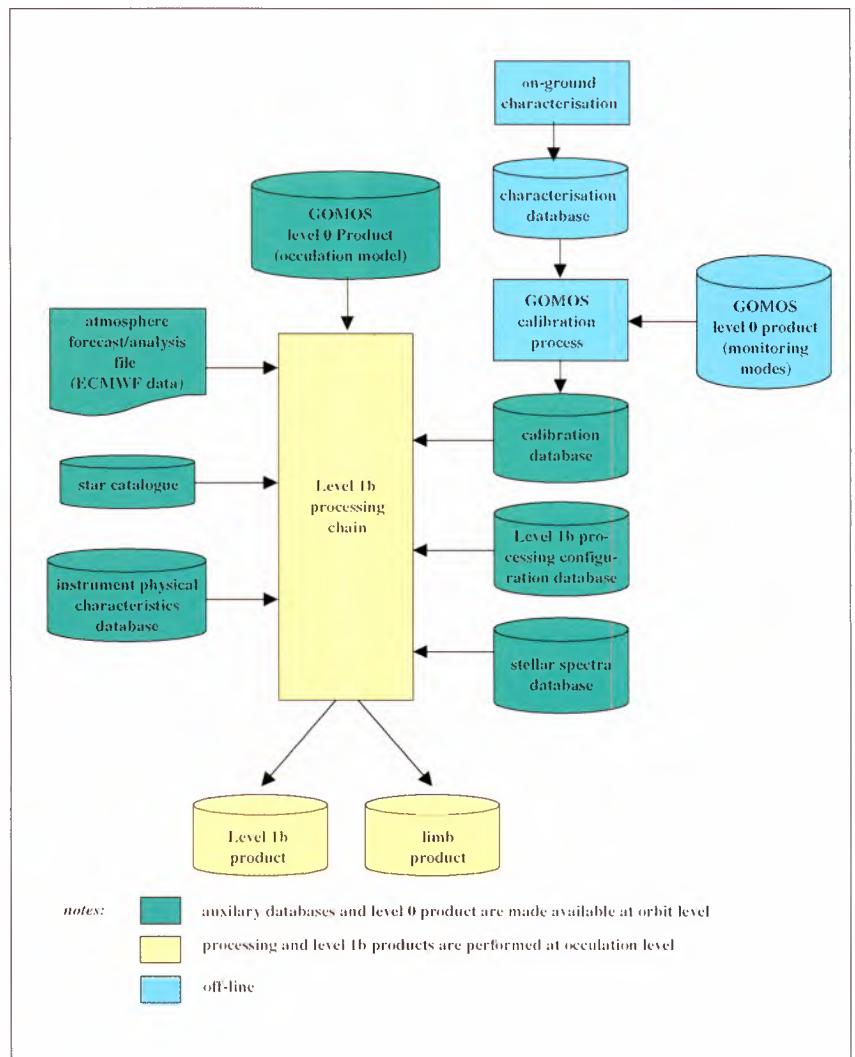


**Table 7-2 Level 1b processing for spectrometer**

<b>Process name</b>	<b>Content</b>
Saturated samples	Saturated samples are screened, flagged and removed from processing.
Bad pixels	<p>CCD pixels that do not respond normally will be flagged and removed.</p> <p>Instead of removing, new data will be generated for bad pixels.</p>
Cosmic rays	CCD pixels hit by cosmic rays will be temporary or permanently damaged. The abnormal values in the spectra can be detected with some probability and data from these pixels will be replaced using median filtering.
Dark charge correction	CCD detectors generate dark charge electrons. By ground and in-flight measurements the average amount of dark charge can be estimated on a pixel-by-pixel basis and this average can be removed from the measured signals. Optionally, dark current can be estimated from GOMOS measurements.
Internal and external straylight	Straylight may potentially disturb the measurements and it will be removed from signals as completely as possible.
Vignetting	This operation is applied only for spectrometer B.
Central background estimation	The two-dimensional nature of the CCD detector means that we can estimate background signal relatively accurately.
Star signal	At this stage the background contribution is subtracted from the central signal leaving only the star occultation signal. The flat field (modified by scintillations) correction is also applied.
Slit correction	This will correct the optical transmission modifications if the image of the star is shifted near the edge of the slit in the focal plane.
Reference star spectrum	The measurements above a predefined altitude level are interpreted to be samples representative of the original star spectrum. This means that all absorptive and scattering effects are considered to be negligible. From a set of n measurements the reference spectrum is defined as an average. This reference spectrum will be one of the side products of the GOMOS mission.
Transmission	This is the final step in the level 1b processing of the spectrometers. The ratio of two quantities are determined and this ratio is interpreted to represent the full transmission function for this measurement. An estimate for the corresponding variance vector is also calculated.

determined. This is based on the analysis of the star tracker data. During the determination of the geolocation, ray tracing calculation is performed. The atmospheric data needed for this calculation come from meteorological data or from atmospheric models.

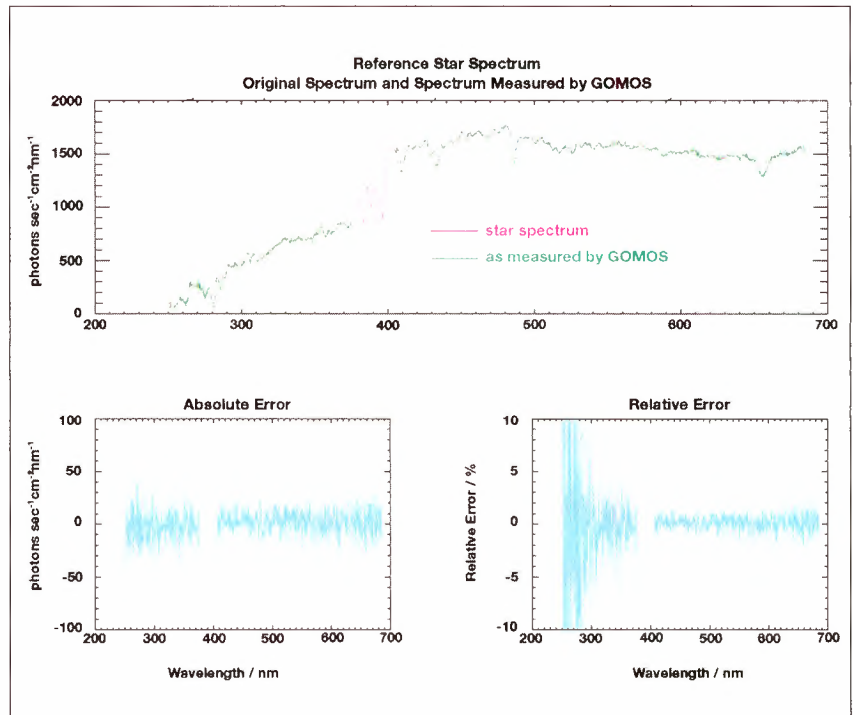
There is a distinction between the near real time (NRT) processing and the off-line processing. NRT processing uses the ECMWF forecast for the lower part of the atmosphere and the atmospheric model MSIS90 for the upper part. In off-line processing the meteorological analysis replaces the meteorological forecast. It must be remembered that GOMOS itself will measure atmospheric characteristics such as neutral density and temperature but these are produced only during Level 1b-2 processing. Therefore some initial atmospheric data are needed to start the retrieval process.

The instrument-specific Level 0-1b data processing also accounts for instrumental effects. These include the identification of saturated samples, the bad pixel processing and the elimination of cosmic ray effects. Very important steps concern the estimation and removal of dark current and the atmospheric background signal from the central CCD-band, which is the detection area for the stellar signal. Both the dark current and the background can be estimated from the pixels on which no stellar signal falls. The dark current can also be estimated from calibration data.

### 7.3 Level 1b Data Product

Table 7-3 lists the main level 1b products from GOMOS.

A typical spectrum of a star with magnitude 2 is shown in Fig. 7-2.



The flux in the two photometers during one occultation sequence is shown in Fig. 7-3. An example of the major Level 1 product, the atmospheric transmission spectra, is shown in Fig. 7-4.

The *reference star spectrum* is obtained by averaging the first five spectra obtained during the occultation. It will be used to calculate the atmospheric transmittance and, as a mission spin-off, can contribute to creating a stellar data base.

The *full transmission spectra* are obtained by dividing each spectrum by the reference star spectrum. It is described as 'full' because it is the actual measured transmission, not corrected for refraction effects (dilution, scintillation, chromatic refraction) or for variable point-spread-function. Each spectrum is resampled on the wavelength pixel grid of the reference spectrum before calculating the transmission. The spectrum

**Fig. 7-2 Example of a star spectrum: the original spectrum and the spectrum as measured by GOMOS. The two lower plots show the absolute and relative statistical errors of measurement. the star magnitude is 2 and the star temperature is 6400 K**

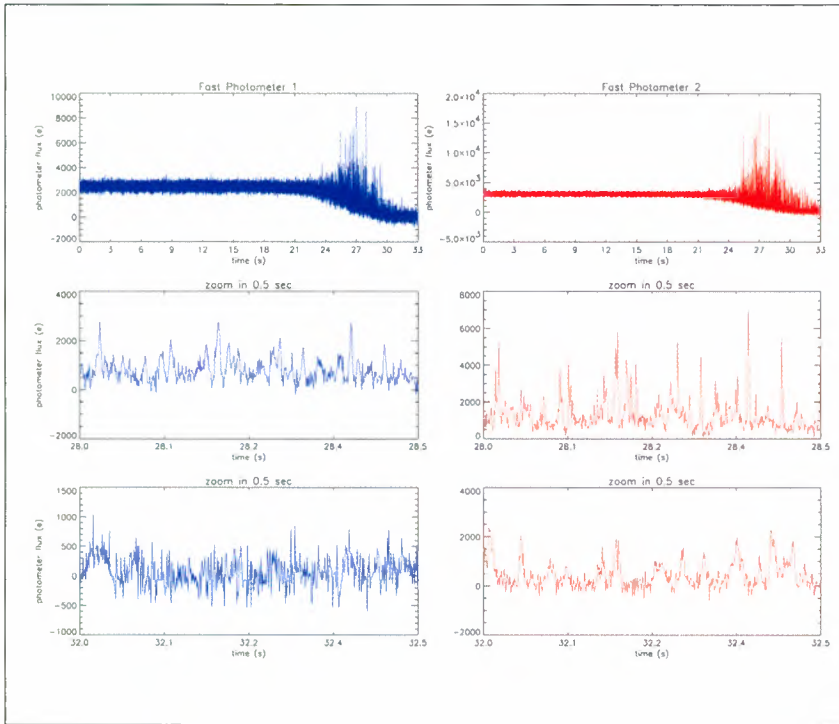


**Fig. 7-3 Photometric flux.** The small inhomogeneities on the atmospheric temperature field cause individual, originally parallel light rays to travel along slightly differing routes. When these rays emerge from the atmosphere they will create a light field having a structure which varies rapidly in space. GOMOS will see this as a field fluctuating rapidly in time. Although a nuisance for the stellar signal analysis, the fluctuating field can be used for a high resolution analysis of the atmospheric temperature field

covariances are computed from the analysis of the signal-to-noise ratio.

The *central background estimate* is the estimated background contribution to the total signal in the central band.

This signal was subtracted from the measured stellar signal during the occultation in order to get the pure stellar signal without background (atmospheric straylight) contamination.

The *photometer flux* data (given in electrons) are used to quantify and correct for atmospheric scintillation.

Further Level 1b data are the wavelength assignment, the calculated geolocation and limb spectra measured with the two extra bands (above and below the star image) of the CCD spectrometers.

All products issued from Level 1b are accompanied by error estimates. These estimates assume Gaussian error statistics and disregard modelling errors.

### 7.4 Level 1b-2 Processing

GOMOS Level 0-1b data processing produces a set of the full

Product	Unit	Potential application
Reference star spectrum	electrons	Astronomy GOMOS processing GOMOS calibration
Geolocated and calibrated transmission spectra	dimensionless	GOMOS level 2
Geolocated development calibrated limb spectra	electrons	GOMOS higher order product
Photometer flux	electrons	GOMOS level 2 GOMOS higher order product development

**Table 7-3 Main level 1b products**

transmission functions for the occultation. Before they can be used to retrieve trace gas densities two physical effects must be considered. These are refractive dilution and scintillation modulation. After these have been eliminated the reduced transmission function is obtained. For an occultation measurement the reduced horizontal transmission function (often expressed as extinction) is definitely an important scientific product.

Modelling the reduced transmission by using Beer's law and applying spectral inversion methods produces tangential column densities of different contributors to the extinction. As external data absorption and scattering cross-sections for the constituents which affect the signals are required. The atmospheric temperature is an important parameter for the calculation of temperature-dependent cross-section. In the vertical inversion knowledge of the measurement geometry is used to invert the line densities into vertical profiles of the constituents.

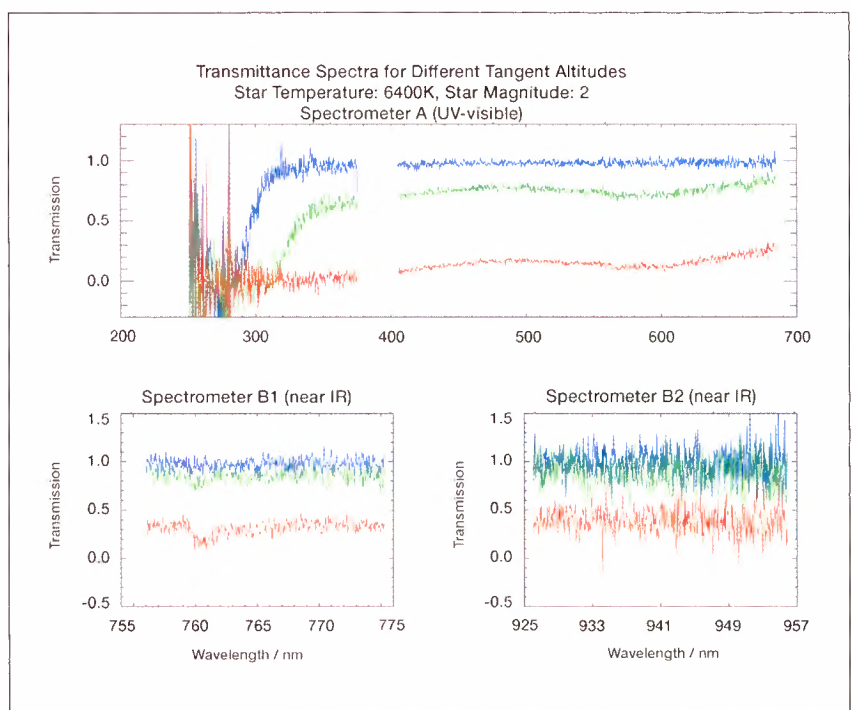
Three basic inversion schemes have been considered. All assume spherical symmetry of the atmosphere and evaluate individual, rather than several consecutive, occultations.

In the first scheme, transmission data from every tangent height are inverted to line densities for different constituents (spectral inversion). For every constituent, the collection of line densities at successive tangent heights is converted to vertical densities. By dividing the atmosphere into discrete layers the well known 'onion peeling' method can be used. The second scheme first calculates the vertical profile of the wavelength-dependent extinction. Using the cross-sections the vertical profile can

then be converted to vertical profiles of the constituents. The third method starts from the transmissions from all tangent heights and inverts the constituent densities in one step. Details are given in *Sihvola, 1994*.

The present GOMOS processing scheme relies on the first method, i.e. spectral inversion followed by vertical inversion. This method has been chosen for two reasons. The first is a significant reduction in the amount of data, which must be handled at a time. The 'spectral first' approach contributes to the fast reduction in size of data. In order to take into account the coupling effects between spectral and vertical problems, the processing makes use of an iterative approach. The second reason is related to the observation geometry of GOMOS. The result of the spectral inversion is atmospheric column densities along the line-of-sight of the instrument (line density), i.e. the data product corresponds to the observation geometry. The line

**Fig. 7-4 Transmission spectra at several tangent heights. Blue = 50 km, green = 34 km, red = 21 km). The vertical transmission function describes the important atmospheric transparency, which is of crucial importance for the biosphere**



densities might also be more useful for assimilation of GOMOS measurements into atmospheric models, if the model can simulate GOMOS observation geometry.

Further information on the level 1-2 processing can be found in **Kyrölä, 1999**.

#### 7.4.1 Preparation of the inversion process

The Level 1b product, which is input to the Level 1b-2 processing, is processed in such a way that it contains only the effects of atmospheric extinction (absorption and scattering) and refraction. It can be assumed that the full transmission can be written as a product:

$$T_{atm} = T_{abs} T_{scin} T_{ref} \quad (7.3)$$

The refractive dilution  $T_{ref}$  can be estimated from the ray tracing calculation. The scintillation modulation  $T_{scin}$  will be estimated by using data from the fast photometers. If these effects are not removed from the transmission they will increase the errors in the aerosol and neutral density retrievals. There is also an optional stage for chromatic refraction correction (the second possibility resides inside the spectral inversion).

#### 7.4.2 The spectral inversion module

The purpose of this module is to extract information about the atmosphere using the spectral dimension of the transmission data. From these data the horizontal column densities of the constituents are

retrieved. The treatment is divided into two parts depending on whether it concerns the data from the UV-visible spectrometer or the IR spectrometer. This division is necessary because the forward calculation of the IR spectrometer wavelength region data is computationally demanding and is done beforehand by using a large 'look-up' table. The UV-visible spectrometer wavelength range allows a relatively fast calculation. The two data sets are inverted separately but information exchange occurs at a later stage.

The UV-visible spectrometer data inversion may be done in a nonlinear or a linear way. The nonlinear method is the most favourable approach as it retains the original normal distribution of the transmission data noise. In the linear case the logarithmic function distorts the noise which may cause bias if not corrected. Details can be found in **Kyrölä et al., 1993**.

The observed transmission can be modelled as (see equation 7.4 below):

where  $L$  represents the collection of light trajectories  $l$  where each trajectory depends on wavelength (chromatic refraction) and time (movement of satellite during the integration time), and  $\tau$  is the optical depth:

$$\tau(\lambda, l(\lambda, t)) = \sum_j \int_{s \in l(\lambda, t)} \rho_j(s) \sigma(\lambda, T(s)) ds \quad (7.5)$$

Equation (7.4) is approximated into a still more practical form by moving time and wavelength integration into the optical depth function and also

$$T_{abs}(\lambda, L) = \frac{1}{\Delta t} \int_{\Delta t} \int W_{gen}(\lambda, \lambda') e^{-\tau(\lambda', l(\lambda, t))} d\lambda' dt \quad (7.4)$$

making an approximate expansion of the chromatic refraction.

Various methods are available for the introduction of cross-sections into the calculation. These can be absolute or differential. The global spectral inversion scheme uses the whole spectral range whereas in the step-by-step method a single constituent is retrieved from a restricted wavelength range.

The temperature dependence of the cross-sections makes the spectral inversion of Equation (7.5) impossible without further approximation. The straightforward method is to use the tangent (or any other fixed) point temperature which decouples spectral and spatial parts. In the GOMOS processing this is done for the first round of spectral inversion but the approximation is improved by exploiting the 'effective' cross-section concept (see below). The optical depth is written as

$$\tau = \sum_j N_j \sigma_j^{eff}(\lambda) \quad (7.6)$$

where

$$N_j(l) = \int_{s \in l(\lambda, t)} \rho_j(s) ds \quad (7.7)$$

is the column density and the 'effective' cross-section is

$$\sigma_j^{eff}(\lambda, l(\lambda, t)) = \frac{\int_{s \in l(\lambda, t)} \rho_j(s) \sigma(\lambda, T_s) ds}{\int_{s \in l(\lambda, t)} \rho_j(s) ds} \quad (7.8)$$

The 'effective' cross-section is a weighted mean cross-section where the weights are the constituent densities. Because of the implicit nature of the 'effective' cross-sections the processing architecture includes

an iteration loop from the vertical inversion (see below) back to the spectral inversion.

Absorption and scattering cross-sections constitute the heart of the GOMOS Level 2 spectral inversion. The Rayleigh cross-section is quite accurately known and many of the absorptive cross-sections have been measured to adequate accuracy. An important fact is that many of the absorptive cross-sections depend on temperature, which adds a complexity to the spectral inversion. The aerosol cross-sections are less well known. In GOMOS processing either a simple Ångström law is assumed or the aerosol cross-section is taken to be a polynomial of wavelengths where the polynomial coefficients are unknowns.

The nonlinear inversion problem defined by Equations (7.4) - (7.8) is solved for the UV-visible spectrometer measurements by the well-known Levenberg-Marquardt algorithm. The algorithm provides estimates for the line densities and their errors. *A priori* trace gas profiles are presently not being used for the retrieval.

The IR spectrometer measures the density of O<sub>2</sub> in the 756-773 nm band and H<sub>2</sub>O in the 926-952 nm band. The calculation of the transmission function is computationally very demanding. Therefore, a different retrieval algorithm is applied, which uses pre-calculated reference transmission spectra for various integrated densities of O<sub>2</sub> and H<sub>2</sub>O. Transmission spectra of O<sub>2</sub> and H<sub>2</sub>O are pre-calculated and tabulated for atmospheric models covering various seasons and latitudes. The retrieval of O<sub>2</sub> and H<sub>2</sub>O finally consists of a fit of the measured to the tabulated model transmittances.

### 7.4.3 The vertical inversion module

The column densities produced by spectral inversion are inherent quantities, which should vary rather smoothly as a function of height. Therefore the Level 2 processing includes an optional smoothing stage before the vertical inversion.

In this module the set of horizontal column densities is converted to vertical profiles. First a general layer structure is generated for the atmosphere and a coverage vector is calculated for every constituent. This is a collection of tangent heights at which the spectral inversion module has been shown to be able to produce column densities for the constituent in question.

For the vertical inversion two approaches have been considered. The first solution uses a 'generalised onion peeling' method, employing the well known 'onion peeling' method for the case where the number of layers is equal to the number of measurements. In cases where more measurements are available than layers, a least-squares solution is first used inside each layer and then the ordinary 'onion peeling' method is used. The second solution, the so-called polynomial inversion, is an attempt to include the variation of the constituent profiles inside each layer in the solution. The polynomial method with a linear variation of the constituent densities inside each layer will be used in the GOMOS ground segment. The stepwise linear profiles will be taken to be continuous.

In the method used in the GOMOS ground segment the local densities are approximated by a linear function of altitude between two consecutive GOMOS measurements:

$$\rho(z) = \frac{(z_{j-1} - z)\rho(z_j) + (z - z_j)\rho(z_{j-1})}{z_{j-1} - z_j} \quad (7.9)$$

The problem can be transformed into a matrix equation:

$$A\rho = N \quad (7.10)$$

where  $A$  is (a relative complicated) kernel matrix. The line densities are the result of an integration in time and should be adapted to the 'instantaneous' expression that has been derived (because the linear system is only valid for instantaneous line densities). To pass from integrated to instantaneous data a Taylor expansion is used:

$$\bar{N}_j = N_j + \frac{(\Delta t)^2}{24} \frac{\partial^2 N_j}{\partial t^2} \quad (7.11)$$

These contributions can be summarised into matrix form and the vertical inversion consists of solving the following linear system:

$$\bar{N} = K\rho \quad (7.12)$$

This matrix equation is solved by standard methods. The covariance matrix will also be produced.

### 7.4.4 Level 1b-2 processing loops

In the vertical inversion, density profiles and a new temperature profile are produced. Initially, temperature profiles given by ECMWF and MSIS90 model are used. GOMOS data provide several possible sources for a new temperature profile, most obviously the Rayleigh scattering from the UV-visible spectrometer and the  $O_2$  data from the IR spectrometer. Neutral density can be derived from Rayleigh

scattering using the ideal gas law and assuming hydrostatic equilibrium. Similarly, neutral density can be derived from the O<sub>2</sub> data assuming a constant mixing ratio and temperature according to the ideal gas law. These two estimates must be assimilated together with weights according to their reliabilities (covariances). These new data are used, after a quality check, in the calculation of the effective cross-sections and the spectral and vertical inversions are carried out again. It has been shown that this iterative process over spectral and vertical inversions improves the final results significantly. It is therefore routinely applied with one or two iterations.

A second iteration loop is available to repeat the ray-tracing calculation with the newly retrieved GOMOS atmosphere followed by another retrieval iteration. Fig. 7-5 depicts the Level 1b-2 processing architecture.

Rayleigh extinction and O<sub>2</sub> absorption are not the only possibilities for generating temperature from GOMOS measurements. Small-scale vertical structures in the atmosphere induce scintillations in the signal of the blue and red photometers, which are slightly shifted in time due to the chromatic difference in the refractive bending of the light. The computation of the time delay between the two signals can be used to determine the total bending angle of the light and, using the Abel integral, the vertical profile of index of refraction, which is proportional to atmospheric density. A high vertical resolution (100-200 metres) temperature profile can be derived from the density profile, using the hydrostatic equation.

## 7.5 Level 2 Data Products

The main Level 2 data products are listed in Table 7-4. The data products

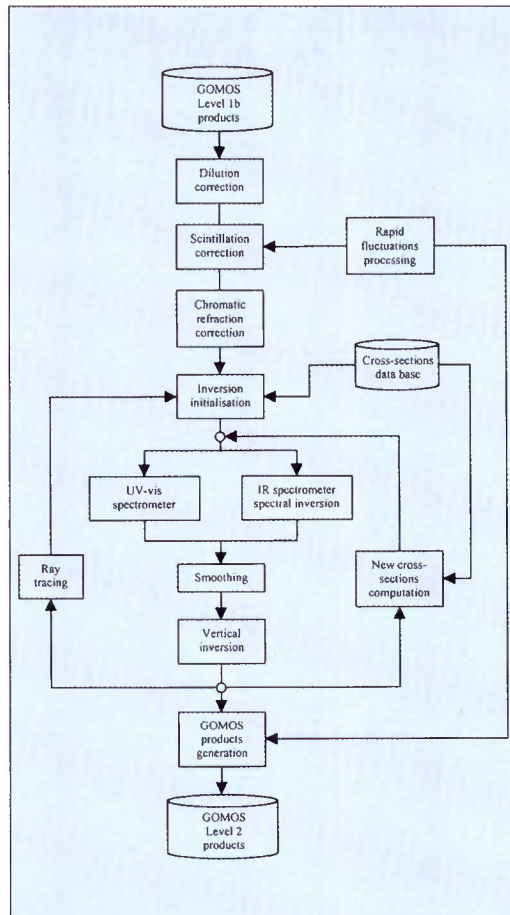


Fig. 7-5 GOMOS Level 1b-2 processing architecture (after Kyrölä, 1999)

also contain error estimates, which are calculated throughout the processing chain and propagated to the final data products.

The *line densities* are the results of the spectral inversion procedure. These line densities may be directly used, for example in data assimilation systems, to create higher-order data products.

The *vertical density profiles* are the results of the vertical inversion. Vertical profiles derived from long-lasting (oblique) occultations have to be used with care as they have a large geographical extent. Occultations in polar regions can easily extend through several local time zones.

**Table 7-4 Main level 2 GOMOS products**

<b>Product</b>	<b>Unit</b>	<b>Potential application</b>
O <sub>3</sub> , NO <sub>2</sub> , NO <sub>3</sub> , H <sub>2</sub> O, air horizontal column densities	1 molec/cm <sup>2</sup>	Higher order GOMOS products Monitoring of trends
Aerosol extinction and polynomial extinction coefficients	1 molec/km 1 molec/(km nm <sup>2</sup> )	Aerosol research Atmospheric chemistry research
O <sub>3</sub> , NO <sub>2</sub> , NO <sub>3</sub> , H <sub>2</sub> O, O <sub>2</sub> , air vertical density profiles	1 molec/cm <sup>3</sup>	Atmospheric chemistry research Monitoring of trends
GOMOS produces profiles for T and density	K 1 molec/cm <sup>3</sup>	GOMOS processing Atmospheric research
Turbulence product: High resolution T and density	K 1 molec/cm <sup>3</sup>	Atmospheric dynamics research
Meteo product		Meteorological applications

The *turbulence product* (high-resolution temperature and density vertical profiles) is derived basically from the time delay of the signal between the peaks of the red and blue fast photometer.

The *Meteo product* consists of extracted profiles with reduced spatial resolution for near-real-time dissemination to meteorological users.

## 7.6 Characteristics of GOMOS Products

Regarding the data products from GOMOS some special features of the measurement principle (stellar occultation) and the instrument itself must be kept in mind. The following are the most important:

1. *Accuracy of the retrieved product depends strongly on the star used in occultation:* For ozone, to take an important example, hot stars provide good accuracy for ozone at high altitudes whereas cool stars

are more suitable for O<sub>2</sub> and H<sub>2</sub>O measurements in the IR. The accuracy also depends strongly on the visual magnitude of the star used. The precision of the retrieval also depends on straylight, i.e. dark limb or bright limb condition. The expected precisions of retrieved ozone profiles are shown in Fig. 7-6. The magnitude and star temperature limits of the GOMOS target stars are determined using an instrumental technique (star tracker). This has been shown to give useful retrieval accuracies for ozone. For other trace gases the useful limits are much narrower.

2. *Retrieval coverage and accuracy is geographically uneven:* this is a consequence of the points discussed above, the limited number of stars and their uneven distribution. Another contributing factor is that measurements in daylight give lower accuracy than night-time measurements. This means that for ozone a quite good global coverage can be achieved but for other minor gases the

coverage will be more sporadic. This is in contrast to instruments measuring atmospheric emission, e.g. MIPAS.

3. *The altitude limits of the measurements range from the lower stratosphere to about 100 km: the lower limit of the ozone retrieval may vary according to the aerosol content of the lower stratosphere. For other minor gases the useful altitude range is much smaller.*

4. *The vertical resolution of the GOMOS measurements can be described by weighting functions, as shown in Fig. 1-2. Most of the signal comes from near the tangent altitude. The tangent altitude itself moves about 1.7 km during the occultation (in the aft direction). For long oblique occultations movement of the tangent point is considerably smaller but the horizontal component of the movement is correspondingly larger.*

5. *The horizontal extent of the measurement varies from occultation to occultation: the direct occultation ray covers about 15 degrees in latitude and during very oblique occultation the tangent point moves considerably in the direction of the latitude.*

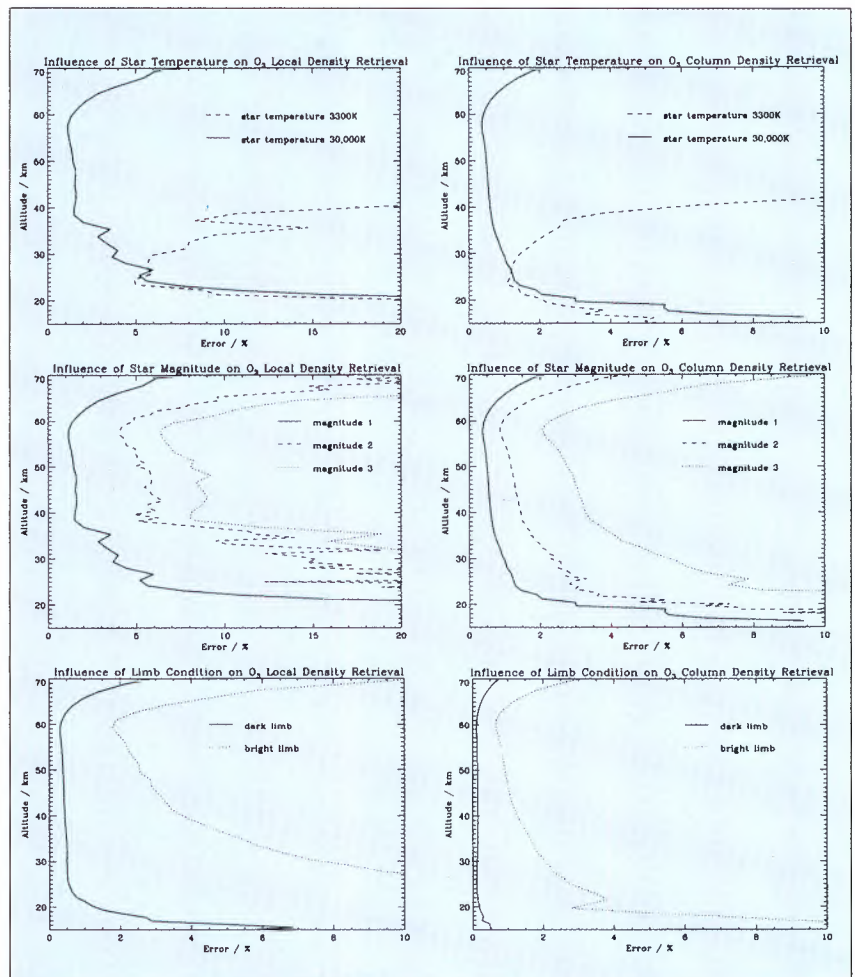


**Fig. 7-6 Preliminary estimate of the precision of ozone local density and ozone line (or line of sight column) density retrievals. Upper plots: influence of star temperature; middle plots: influence of star magnitude; lower plots: influence of limb condition (stray light)**



# 8. GOMOS Validation

The validation of GOMOS data products will start during the commissioning phase of Envisat and continue through the whole lifetime of the instrument. The Envisat validation is largely dependent on the Principal Investigators of the accepted proposals, who will contribute to the validation of Envisat data products, submitted in response to the 1998 Envisat 'Announcement of Opportunity' (AO).

Envisat is scheduled for launch in mid- 2001 and a validation plan has been established to provide early results during the six month Commissioning Phase, as well as longer-term validation during the mission lifetime. A validation team has been set up by ESA, which consists mostly of the Principal Investigators of accepted AO proposals. First validation results will be analysed at the end of the Commissioning Phase, before Envisat products are released to a wider public.

## 8.1 Internal Consistency of GOMOS Measurements

### 8.1.1 Measurements at the same place

There will be certain occultation geometries in which the same geographic location can be observed on successive orbits using different stars. Comparison of the different

observations will help confirm that corrections for solar stray-light and vignetting are accurate, although the effects of variations in viewing angle must be taken into account.

### 8.1.2 Comparison of temperature derivations

Atmospheric temperature will be derived from GOMOS measurements in the following three ways:

- from the O<sub>2</sub> profile density,
- from the Rayleigh extinction of stellar light,
- from the scintillations observed with the two photometers.

Verification of the consistency of these methods is important for the evaluation of each algorithm and for evaluating error budgets.

Theoretically, it could also be possible to derive temperature information from the following:

- from the Rayleigh scattering of sunlight into the background bands,
- from the O<sub>3</sub> temperature-dependent cross-section in the ultraviolet,
- from the curve of mean dilution.

However, these information sources will not be used routinely for temperature information as the effect of the temperature on these parameters is not as significant as on the first three listed above. It might also be possible to retrieve temperature via refractivity measurements, which would require very accurate knowledge of mirror pointing and spacecraft attitude.

### 8.1.3 Comparison of ozone derivations

Ozone absorbs at both ultraviolet and visible wavelengths. Values will be retrieved separately in both parts of the spectrum from both stellar and bright-limb measurements and from both absolute and differential (DOAS) spectra. All eight values will be of high accuracy in the middle stratosphere (30 km), so a meaningful comparison between values will be possible. Differences in absolute values will indicate inconsistencies between the ultraviolet and visible cross-sections, or errors in aerosol retrievals which differ in their effects in the UV and in the visible, or errors in internal straylight which again differ between the UV and the visible. Differences in differential stellar values will point to errors in the spectral transfer function – the ultraviolet bands have much finer structure than the visible – so that errors in assumed spectral resolution will affect the ozone retrieved from ultraviolet spectra more than the ozone from visible spectra. Differences between stellar and bright-sky values will point at errors in the radiative transfer code used to calculate bright-sky paths and radiance. Differences between the absolute DOAS stellar values will point at errors in the aerosol characterisation deduced from the absolute spectra.

### 8.1.4 Self-consistency check of $\text{NO}_2$ , $\text{NO}_3$ and $\text{O}_3$

The self-consistency of GOMOS  $\text{NO}_2$ ,  $\text{NO}_3$ ,  $\text{O}_3$  measurements can be checked by using the reaction equations:



hence

$$\frac{d[\text{NO}_3]}{dt} = k_1[\text{NO}_2][\text{O}_3] - k_2[\text{NO}_2][\text{NO}_3] \quad (8.3)$$

where  $k_1$  and  $k_2$  are temperature dependent.

In the lower stratosphere,  $\text{NO}_3$  goes rapidly to steady state:

$$\frac{d[\text{NO}_3]}{dt} = 0 \quad (8.4)$$

Hence a consistency check in the lower stratosphere is to see that

$$k_1[\text{O}_3] = k_2[\text{NO}_3] \quad (8.5)$$

In the upper stratosphere, Equation (8.3) has an equilibrium time of several hours. So consistency of GOMOS measurements with Equation (8.3) might be checked explicitly. Unfortunately the signal-to-noise ratio of the  $\text{NO}_3$  measurement (based on a single occultation) is poor, and several occultations at successive times during the night at the same location will be rare. Hence Equation (8.3) can only be checked in an averaged sense, or via an assimilation scheme.

No other consistency checks are obvious from GOMOS data alone.

## 8.2 Geophysical Validation

### 8.2.1 Introduction

Validation is the process of assessing the quality of data products by independent means. The main operational GOMOS products to be validated are in particular the vertical profiles of O<sub>3</sub>, NO<sub>2</sub>, NO<sub>3</sub>, O<sub>2</sub>, H<sub>2</sub>O, temperature and aerosol extinction coefficients and spectral parameters. Non-operational data products must also be validated, but this has a lower priority.

The GOMOS data product accuracy will vary with altitude, occultation geometry, temperature and visible magnitude of the occulted star and the spectrum of the star. This means that validation results obtained by observing the occultations of a specific star cannot be considered representative of all stars.

### 8.2.2 Campaign activities

It is planned to devote the first six months after the launch of Envisat to the commissioning of the instruments. During this phase the functionality of the instruments and the whole observing system will be tested, calibrations will be performed and the first data products will be produced. The validation of the geophysical products will start as soon as the Level 0-1b processing has been successfully tested and Level 2 products can be produced with preliminary confidence. After the commissioning phase the mission will start its operational mode.

ESA is coordinating the geophysical validation activities for Envisat. These activities will last beyond the end of

the commissioning phase, in fact during the whole lifetime of Envisat, albeit at a reduced level. The larger data set that is so obtained will allow the statistically significant identification of errors that could not previously be distinguished from random noise. In addition, the large set of regular, continuous data points so obtained, will contribute to long-term instrument performance analyses and modelling.

### 8.2.3 Independent sources of correlative data

Before scientific investigations of trends and of agreements with model predictions are carried out using GOMOS measurements, it is essential to conduct campaigns to confirm the validity of the atmospheric parameters measured by GOMOS by comparison with measurements of the same parameters from other sensors. Different classes of observation techniques will be used for this validation.

A common problem for all validation measurements will be to measure the variables as simultaneously as possible in space and time with GOMOS. Furthermore, the vertical resolution and horizontal smearing of the measurements will vary markedly between validating instruments. Two strategies will be applied to overcome this problem:

1. The GOMOS mission planning has to try to make GOMOS measurements as close as possible to those of the validating instruments. This will be easiest for ground-based instruments, which are observing 24 hours a day, but it will be more difficult for balloon campaigns.
2. The GOMOS data could be assimilated into atmospheric

chemistry-transport models, which can calculate (via their atmospheric models) the state of the atmosphere on the exact location and time of the validating instrument.

**a) Other instruments on Envisat**

The instruments MIPAS and SCIAMACHY will each measure, amongst other parameters, O<sub>3</sub>, NO<sub>2</sub>, aerosol and temperature. MERIS and AATSR may also provide relevant information, for example measures of aerosol properties. Comparisons with GOMOS data will start during the commissioning phase.

In general, the measurements will neither take place simultaneously nor be collocated. SCIAMACHY will measure only during the day, while the best GOMOS measurements are at night. Collocated measurements of GOMOS and MIPAS can only be achieved when GOMOS acquires stars in the same direction as the MIPAS field-of-view.

Since none of the three Envisat chemistry instruments, GOMOS, MIPAS and SCIAMACHY, are yet validated

individually, the comparison of the data products can only be used for consistency checks and will be valuable for error exploration, but cannot really validate GOMOS products.

**b) Other spaceborne instruments**

Comparison of products from different satellite instruments is particularly useful for global validation, since a large range of observation parameters (latitude, longitude, solar zenith angle, cloud presence etc.) can be covered in a short time. Table 8.1 lists satellite sensors that produce data products that will be useful for GOMOS validation.

Of these instruments, those with good vertical resolution and with O<sub>3</sub>, NO<sub>2</sub> or aerosol products of comparable accuracy to GOMOS are POAM-III and SAGE-3 (O<sub>3</sub>, NO<sub>2</sub>, aerosol), HIRDLS (O<sub>3</sub>, NO<sub>2</sub>) and MLS (O<sub>3</sub>, BrO). Validation activities with these instruments will be continued as long as possible.

**c) Instruments on aircraft**

Aircraft provide more control (than any other platform) on the selection of

**Table 8-1 Satellite sensors available for comparison with GOMOS (aer = aerosol)**

Spacecraft	Agency / Country	Date	Instrument	Spectral region	Technique	GOMOS gases measured
ADEOS-2	NASDA	1999	ILAS-2	IR, near IR	solar occultation	O <sub>3</sub> , NO <sub>2</sub> , aer, O <sub>2</sub>
ODIN	Sweden	1999	OSIRIS SMR	UV-vis sub-mm	limb sunlight limb emission	O <sub>3</sub> , NO <sub>2</sub> , aer O <sub>3</sub>
SPOT-4	CNES/NRL	1998	POAM-III	UV-vis	solar occultation	O <sub>3</sub> , NO <sub>2</sub> , aer
ERS-2	ESA	1995	GOME	UV-vis	nadir sunlight	O <sub>3</sub> , NO <sub>2</sub>
METEOR	RKA	2000	SAGE-3	UV-vis	solar occultation	O <sub>3</sub> , NO <sub>2</sub> , aer
EOS-CHEM	NASA	2003	HIRDLS EOS-MLS	IR sub-mm	limb emission limb emission	O <sub>3</sub> , NO <sub>2</sub> , aer O <sub>3</sub> , BrO

air volume that is observed by the instruments they carry. The flight path can even be flexible enough to make *in-situ* and remote sensing instruments on board sample the same air mass during a single flight.

Although less suitable for inexpensive routine operation, such platforms offer advantages during campaigns, since observation strategies can be adapted at short notice, even during the course of a measurement.

Payloads can be installed on various aircraft that have been adapted for atmospheric measurements. Aircraft foreseen to participate in the validation campaigns include the Russian M-55 Geophysica, the NASA ER-2 and DC-8, the German DLR Falcon and Transall and the Dutch Cessna Citation.

#### **d) Balloon-borne measurements**

Balloon-borne *in-situ* sensors provide vertical profiles of very good vertical resolution throughout the stratosphere, as required for the validation of GOMOS. However, careful planning is needed to ensure collocation of a stellar occultation with a balloon flight.

Regular ozone sonde balloon flights should be a prime target for ozone validation up to 30 km altitude. A chemiluminescent NO<sub>2</sub> sensor is available in Japan, but is large and heavy. Although a small balloon-borne NO<sub>2</sub> sonde has been developed in Canada, it is as yet untested in its stratospheric version. Balloon-borne frost point hygrometers have been flown by French and British groups, and would provide important contributions to the validation of GOMOS H<sub>2</sub>O measurements. A new low-cost frost-point hygrometer is being developed in the UK.

The Wyoming aerosol sonde, which provides the size-spectrum of number density, can be used for GOMOS stratospheric aerosol measurement validations. Meteorological radiosondes provide air pressure and temperature as a function of altitude. From these quantities, using the known altitude dependence of the oxygen volume mixing ratio (VMR), it is possible to calculate the O<sub>2</sub> profile, to be used for validation of GOMOS O<sub>2</sub>. In addition, the temperature values can be directly compared to temperature values from GOMOS.

Balloon-borne remote sensors can also provide good vertical resolution, though this varies from sensor to sensor. In particular, instruments that can measure during ascent have excellent vertical resolution, and for this reason SAOZ-balloons may be the only practicable system to validate GOMOS NO<sub>2</sub> measurements. In fact they have a better vertical resolution than GOMOS. Lille sensors BALLAD and BOCCAD measure aerosol phase functions.

The AMON balloon-borne sensor is particularly relevant as it exploits the stellar occultation method similarly to GOMOS. This is essential for the validation of NO<sub>3</sub> profiles and of night-time profiles of OCIO, as these cannot be measured by any other current sensors. During an occultation, the balloon is much closer to each tangent point than Envisat. Thus errors in the refraction calculation induce a much smaller error in tangent altitude in AMON than in GOMOS.

Balloon-borne *in-situ* instruments will be limited to the flight altitude of the balloons in the lower stratosphere. Upper stratospheric and mesospheric GOMOS measurements can only be validated by remote sensing instruments.

### *e) Ground-based instruments*

Several techniques provide stratospheric measurements, which can be used for comparison, with the limitation that these techniques - except lidars - are generally very limited in vertical resolution:

- spectroscopy of sunlight scattered from the zenith sky (SAOZ network and others, measuring O<sub>3</sub>, NO<sub>2</sub>, OClO, BrO): these measurements are of total column, plus profiles of NO<sub>2</sub> and O<sub>3</sub> (using Umkehr-Dobson measurements).
- spectroscopy of stars in the UV-visible and of the Sun in the UV (Dobson and Brewer net works): these measure O<sub>3</sub> to high accuracy. This is now the internationally accepted standard.
- microwave spectro-radiometers observing thermal emission from the atmosphere (NDSC network) measuring O<sub>3</sub>: profiles are measured day and night, although with a coarse vertical resolution compared to GOMOS. The lowest part of the stratosphere (below about 12 km) can usually not be observed.
- infrared spectrometers observing the Sun (NDSC network), measuring O<sub>3</sub> and NO<sub>2</sub> as well as many non-GOMOS gases: profiles are now being measured with the same coarse vertical resolution as microwave sensors, but with an opposite, upper altitude limit of about 35 km, imposed by the width of the infrared lines becoming Doppler- rather than pressure-broadened. Both heterodyne and Fourier-transform spectrometers are used. Clear skies and dry atmospheres are needed.

- lidars (NDSC network), measuring aerosols, temperature and O<sub>3</sub>: profiles are measured with excellent vertical resolution. Clear skies are needed and measurements must usually be made at night. Aerosol extinction and backscatter can be retrieved independently on lidars with Raman channels.

Most of these ground-based instruments (and many sondes) are now grouped in the international Network for the Detection of Stratospheric Change (NDSC). The NDSC observation sites cover a wide range of latitudes and longitudes. Several instruments record data every possible day. For those instruments that measure continuously, no planning effort is required (except for fast processing) for comparisons with GOMOS. The GOMOS mission planning has only to consider their location for specific localised occultations.

NDSC holds frequent inter-comparison campaigns, which focus on particular gases or instrument types. Inter-comparison with NDSC measurements guarantees a comprehensive validation, because:

- NDSC instruments use techniques and algorithms that are different from GOMOS,
- Most NDSC instrument scientists are independent of GOMOS; a high, uniform level of data quality is guaranteed through strict, network-wide quality control procedures

### **8.2.4 Analyses using models**

#### *a) Temperature analyses*

All GOMOS temperature retrievals will

be compared with the output of ECMWF, allowing the determination of the bias, error and domains of excellence. ECMWF analyses include data from radiosondes and temperature-sounding satellites assimilated into the forecast from the previous analysis, so they are inherently collocated.

By the time of Envisat, a more complete assimilation research product for numerical weather prediction (NWP) may be available, which includes more stratospheric levels. This might be a useful tool to compare Envisat measurements with atmospheric models and NWP analyses.

#### *b) Interpolation using chemistry data assimilation models*

Data assimilation is a technique for combining observations and theoretical models. Model quantities are forced towards observations, without using forcing gradients (in time or space) that are unreasonable according to the physics or chemistry of the model. In principle, the forced values are the weighted mean of the observations and the model predictions. The assimilation mode requires the tuning of the weights according to the perceived errors of measurement and model. The procedure has been successfully used in meteorology for more than a decade, but chemical assimilation is hardly beyond an experimental stage.

In order to assimilate chemistry measurements, a general circulation model (GCM) can be used for the longer-lived products ( $O_3$ , total reactive nitrogen), but it becomes more difficult to insert other gases with shorter photochemical lifetimes. It eventually becomes imperative to use a chemistry-transport model (CTM), where the transport of gases is

specified from the wind fields and the temperatures from meteorological analyses. The transport calculations are decoupled from the chemical calculations. Trajectory models, in which transport and chemistry are also decoupled, can also be used for assimilation.

Assimilation could be a helpful tool for comparing GOMOS with other instruments. The simplest application could be to use the assimilation for interpolating measurements in time and space in order to match GOMOS with other instruments. More sophisticated applications could include the assimilation of observations from several different instruments, excluding GOMOS, in order to compare with individual GOMOS constituent profiles. Perhaps one of the most ambitious applications would be to derive species, which are not directly measured, but retrieved from the model chemistry, driven by the assimilation of measured species data. However, this would require thoroughly validated assimilation tools and chemistry models.

#### **8.2.5 Activities of the Envisat validation team**

For the coordination of the Envisat validation activities, validation teams have been established with ESA convenors. For the three chemistry instruments, GOMOS, MIPAS and SCIAMACHY, the Atmospheric Chemistry Validation Team (ACVT) has been created. The teams will have the following tasks:

- review and update the validation plan,
- perform validation rehearsal,
- generate calibration/validation requirements,

- perform correlative measurements or provide services with atmospheric models (e.g. data assimilation),
- perform validation analysis,
- report results.

A data storage facility for the validating instruments will be established at the Norsk Institutt for Luftforskning (NILU) in Norway. NILU will provide access to correlative measurements from sensors onboard satellites, aircraft, balloons (and ships for other Envisat instruments), as well as from ground-based instruments (and underwater devices for other Envisat instruments) and numerical models, such as that of ECMWF.

### 8.3 Discussion and Conclusions

GOMOS uses stellar occultation for measurements of the stratospheric composition. This technique is new and therefore particular care must be taken in the selection of the data retrieval techniques. Amongst the large variety of different retrieval techniques successfully employed for other satellite instruments, a method has been chosen that accounts in particular for the limb-sounding geometry utilising basically the 'onion peeling' method.

In addition to the official Level 1b and Level 2 GOMOS data product, scientists are working on the

production of higher order GOMOS products, such as stratospheric ozone maps, total ozone maps and turbulence products. The use of data assimilation techniques is being studied.

As for any other new instrument, there is a clear need for in-flight calibration and validation. The necessity, principles and methods of calibration and validation for GOMOS have been explained. GOMOS is a unique instrument, hence investigation of its error sources is a task that cannot fully rely on routine methods, and will require a coordinated effort by many scientists and engineers. Since GOMOS measurements are sensitive to a variety of observation parameters (including stellar properties) it is important to acquire many coincident observations with independent instruments, in order to arrive at an assessment of GOMOS end-to-end performance that is representative under most conditions.

Both calibration and validation must continue beyond the commissioning phase, since the statistical significance of calibration and validation results will increase with the number of measurements, and new systematic errors may develop during the instrument lifetime. The calibration and validation results will have direct consequences on the evolution of the data-processing algorithms used in the ground segment.

## 9. Concluding Remarks

This report presents an overview of GOMOS, one of the three atmospheric composition sounding instruments onboard Envisat. Envisat will be Europe's largest Earth observation mission to date, to be launched in the summer of 2001.

Envisat will fly in a polar orbit at a mean altitude of about 800 km with a repeat cycle of 35 days. The local equator crossing time in the descent mode will be 10 am. Flight operations will be controlled from ESOC, Darmstadt, Germany. ESRIN, Frascati, Italy, will provide the interface to the users. More information can be found in *ESA 1998a* and on the Envisat web page <<http://envisat.estec.esa.nl>>. A full listing of all the products, which are planned to be made available shortly after the end of the commissioning phase, will be found in *ESA 1998b*.

The primary objective of GOMOS is the monitoring of stratospheric and mesospheric ozone for trend observations. GOMOS will be able to detect linear ozone trends of the order of 0.1% per year, which would contribute to the long-term monitoring of the ozone layer. The instrument will measure ozone in the UV and visible frequency band at 250 to 675 nm (Huggins band and Chappuis band). As secondary objectives, GOMOS will also observe NO<sub>2</sub> and NO<sub>3</sub>, important species within the nitrogen chemistry family. NO<sub>2</sub>, NO<sub>3</sub> and aerosol extinction will be observed in the UV-visible band,

where also OCIO and BrO are possibly detectable. Air density will be derived from Rayleigh scattering and O<sub>2</sub> measurements. Water vapour and O<sub>2</sub> will be measured in the near infrared. Temperature profiles will be retrieved from O<sub>2</sub> density measurements and Rayleigh extinction and, with very high vertical resolution, from the analysis of the scintillation signal measured with two fast photometers.

GOMOS will exploit the stellar occultation technique to measure line densities and vertical profiles of ozone and other atmospheric constituents with a vertical resolution of 1.7 km or better and an accuracy for ozone concentration of up to 1%. The instrument is highly complementary to the two other composition sounding Envisat instruments, MIPAS and SCIAMACHY.

Most of the time there is more than one observable star in the instrument's field of view, which necessitates a selection of the star sequences with the highest scientific value. A concept using merit functions and entropy has been developed to find the best compromise between geophysical product accuracies and global coverage for alternative star observation sequences. Different mission objectives can be mathematically described and the optimal combination of occultation sequences can be derived. This approach makes it easier to address the various

mission objectives, with minimal interference to the main objective. A considerable enhancement of the GOMOS mission will be possible using the optimising mission planning.

Data processing mainly involves calculating the atmospheric transmittances and geophysical parameters. The retrieved geophysical parameters are column densities along the line-of-sight and vertical profiles. Both the transmittance spectra and the geophysical data products will be made available to the users.

The GOMOS data products will undergo extensive validation activities with other satellite, ground-based and air-borne instruments, also exploiting data assimilation techniques.

Looking further to the future it is important to note the increasing concerns over the human impact on the environment in general and on

the climate and ozone problem in particular. Human activities are causing damage directly to the environment and have significant long-term impacts in particular related to climate. These concerns are reflected in the list of priority issues identified by the Inter-Governmental Panel on Climate Change (IPCC) which includes topics such as the sources, sinks and concentrations of greenhouse gases, the Earth's radiation balance, ecosystem dynamics and the role of aerosols.

In partial response to this, the Member States of the European Space Agency have not only approved the Envisat mission, but, in addition, have supported the formulation of a long-term strategy for Earth Observation, which envisages a series of research and/or demonstration missions called the Earth Explorer Missions. More information on these missions, including their research objectives, can be found in **ESA 1998c**.

# References

## *Atreya et al., 1976*

Atreya, S.K., T.M. Donahue, W.E. Sharp, B. Wasser, J.F. Drake, G.R. Riegler, Ultraviolet stellar occultation measurements of the H<sub>2</sub> and O<sub>2</sub> densities near 100 km in the Earth's atmosphere, **Geophys. Res. Letters**, 3, 607-610, 1976.

## *Bertaux, 1999*

Bertaux, J.L., GOMOS Mission objectives, ESAMS'99 – in Proceedings European Symposium on Atmospheric Measurements from Space, **WPP-161**, European Space Agency, Noordwijk, The Netherlands, 1999.

## *Engel and Schmidt, 1999*

Engel, A., U. Schmidt, An Estimate of the Trend of the Stratospheric Chlorine Loading Based on *In-situ* Balloon-borne Observations, **SPARC Newsletter**, 13, July 1999.

## *ESA, 1998a*

Envisat Mission, Opportunities for Science and Application, **SP-1218**, European Space Agency, Noordwijk, The Netherlands, 1998.

## *ESA, 1998b*

Envisat Mission, Product Summary Overview, **SP-1221**, European Space Agency, Noordwijk, The Netherlands, 1998

## *ESA 1998c*

Earth Explorer: The Science and Research Elements of ESA's Living Planet Programme, **SP-1227**, European Space Agency, Noordwijk, The Netherlands, 1998

## *ESA 2000*

Envisat MIPAS – An Instrument for Atmospheric Chemistry and Climate Research, **SP-1229**, European Space Agency, Noordwijk, The Netherlands, March 2000.

## *Evans et al., 1998*

Evans, S.J., R. Toumi, J.E. Harries, M.P. Chipperfield, and J.M. Russell, Trends in Stratospheric Humidity and the Sensitivity of Ozone to These Trends, **J. Geophys. Res.**, 103, 8715-8725, 1998.

## *Frederick, 1984*

J.E. Frederick, Measurement Requirements for the detection of ozone trends, Ozone Correlative Measurements Workshop, **NASA Conf. Pub. 2362**, Appendix 3, 1984.

## *Gretchko et al., 1981*

Gretchko, G.M., A.S. Gurvich, Y.V. Romanov, S.V. Sokolovskiy and M.S. Tatarskaya, Layered temperature structure of the atmosphere from refraction measurements made on the Salyut 6 orbiter, **Isv. Atmos. Ocean. Phys.** 17(2), 87-91, 1981.

## *Gretchko et al., 1997*

Gretchko, G.M., A.S. Gurvich, V. Kan, A.I. Pakhomov, Ya.P. Podvyaznyi and S.A. Savchenko, "Observations of atmospheric turbulence at altitudes of 20-70 km", **Trans. Russ. Acad. Sci., Earth Sci. Sect.**, 357A(9), 1382-1385, 1997. (English translation).

## *Hays and Roble, 1968*

P.B. Hays and R.G. Roble, Stellar

spectra and Atmospheric Composition, **J. Atmos. Sci.**, 25, 141, 1968.

**Holton et al., 1995**

Holton, J.R., P.H. Haynes, M.E. McIntyre, A.R. Douglass, R.B. Rood and L. Pfeister, Stratosphere-troposphere exchange, **Rev. Geophysics**, 33, 403-439, 1995.

**Kyrölä et al., 1993**

Kyrölä, E., E. Sihvola, M. Tikka, Y. Kotivuori, T. Tuomi, and H. Haario, Inverse Theory for Occultation Measurements 1. Spectral Inversion, **J. Geophys. Res.**, 98, 7367-7381, 1993.

**Kyrölä et al., 1999**

Kyrölä, E., GOMOS ATBD-Level 2, ESAMS '99 – European Symposium on Atmospheric Measurements from Space, **WPP-161**, ESA, 1999.

**Kyrölä and Tamminen, 1999**

Kyrölä, E. and J. Tamminen, GOMOS mission planning, ESAMS'99 – in Proceedings European Symposium on Atmospheric Measurements from Space, **WPP-161**, European Space Agency, Noordwijk, The Netherlands, 1999.

**Nedoluha et al., 1998**

Nedoluha, G.E., R.M. Bevilacqua, R.M. Gomez, D.E. Siskind, B.C. Hicks, J.M. Russell, B.J. Connor, Increases in middle atmospheric water vapor as observed by the Halogen Occultation Experiment and the ground-based Water Vapor Millimeter-wave Spectrometer from 1991 to 1997, **J. Geophys. Res.**, 103, 3531-3543, 1998.

**Oltmans and Hofmann, 1995**

Oltmans, S.J. and D.J. Hofmann, Increase in lower-stratospheric water vapour at a mid-latitude site from 1981 to 1994, **Nature**, 374, 146-149, 1995.

**Riegler et al., 1976**

G.R. Riegler, J.F. Drake, S.C. Liu and R.J. Cicerone, Stellar occultation measurements of atmospheric ozone and chlorine from OAO-3 1976, **J. Geophys. Res.**, 81, 4997, 1976.

**Riegler et al., 1977**

G.R. Riegler, S.K. Atreya, T.M. Donahue, S.C. Liu, B. Wasser, J.F. Drake 1977, UV stellar occultation measurements of nighttime equatorial ozone, **Geophys. Res. Letters**, 4, 145, 1977.

**Sihvola, 1994**

Sihvola, E., Coupling of spectral and vertical inversion in the analysis of stellar occultation data, Licentiate of philosophy thesis, University of Helsinki, Geophysical publications, FMI, 38, 1994.

**Smith and Hunten, 1989**

G.R. Smith and D.M. Hunten, Study of Planetary Atmospheres by Absorptive Occultations, **Rev. Geophysics**, 28, 117, 1989.

**SORG, 1996**

SORG, Stratospheric Ozone 1996, Sixth report of the United Kingdom Stratospheric Ozone Review Group, U.K. Department of the Environment, 1996.

**SPARC/IOC/GAW, 1998**

SPARC/IOC/GAW, Assessment of Trends in the Vertical Distribution of Ozone, Edited by N. Harris, R. Hudson and C. Phillips, SPARC Report No.1, WMO Ozone Research and Monitoring Project Report No. 43, May 1998.

**Théodore, 1998**

Théodore, B., Simulation de la scintillation lors de l'occultation d'étoiles par l'atmosphère terrestre. Application à la restitution du profil de température, Thèse de l'Université Paris VII, Paris, April 1998.

**Thomas, 1991**

Thomas, G.E., Mesospheric clouds and the physics of the mesopause region, **Rev. Geophysics**, 29, 553-575, 1991.

**WMO, 1985**

Atmospheric Ozone 1985, World Meteorological Organization Global Ozone Research and Monitoring Project, Report No. 16, 1985.

**WMO, 1990**

Report of the International Ozone Trend Panel: 1988, World Meteorological Organization, Global Ozone Research and Monitoring Project, Report N° 18, Geneva, 1990.

**WMO, 1998**

Scientific Assessment of Ozone Depletion; 1998, World Meteorological Organization, Global Ozone Research and Monitoring Project - Report N°. 44, Geneva, 1998.





**European Space Agency**  
**Agence spatiale européenne**

*Contact: ESA Publications Division*  
c/o ESTEC, PO Box 299, 2200 AG Noordwijk, The Netherlands  
Tel. (31) 71 565 3400 - Fax (31) 71 565 5433